SPATIAL OPTICAL ORTHOGONAL FREQUENCY-DIVISION MULTIPLEXING

SPATIAL OPTICAL ORTHOGONAL FREQUENCY-DIVISION MULTIPLEXING FOR INDOOR VISIBLE-LIGHT COMMUNICATION SYSTEMS

BY

MOHAMMED MOSSAAD, B.Sc., M.Sc.

A THESIS

SUBMITTED TO THE DEPARTMENT OF ELECTRICAL & COMPUTER ENGINEERING

AND THE SCHOOL OF GRADUATE STUDIES

OF MCMASTER UNIVERSITY

IN PARTIAL FULFILMENT OF THE REQUIREMENTS

FOR THE DEGREE OF

DOCTOR OF PHILOSOPHY

Doctor of Philosophy (2021) McMaster University

(electrical & computer engineering) Hamilton, Ontario, Canada

TITLE:	Spatial Optical Orthogonal Frequency-Division Multiplexing for Indoor Visible-Light Communication Systems
AUTHOR:	Mohammed Mossaad B.Sc., M.Sc. (Electrical and Electronic Engineering) Alexandria University, Alexandria, Egypt
SUPERVISOR:	Dr. Steve Hranilovic
NUMBER OF PAGES:	xxii, 148

Lay Abstract

Visible-light communications (VLC) is an emerging technology that exploits the increasingly widespread use of light-emitting diodes (LEDs) for indoor lighting, and modulates the optical power output of the LED for data transmission.

Among the various modulation techniques that have been proposed for VLC, orthogonal frequency-division multiplexing (OFDM) offers high data rates, resistance to channel impairments, and simple channel estimation and equalization. However, OFDM signals suffer from a high peak-to-average power ratio (PAPR) which degrades the efficiency of the power amplifier in the transmitter and hinders the communication performance.

In this thesis, a new multiple-LED modulation technique, termed spatial optical OFDM (SO-OFDM), is proposed to reduce the PAPR. Using a frequency-to-space mapping, SO-OFDM divides the wideband high-PAPR OFDM signal into multiple narrowband low-PAPR signals and assigns each signal to a group of LEDs. Spatial summing of the transmitted signals occurs at the receiver allowing for the use of a conventional OFDM receiver. Several variations of SO-OFDM are introduced and are shown, using simulations, to reduce the PAPR, combat non-linear distortion (NLD), and improve the bit-error rate (BER) performance at high signal-to-noise ratios (SNRs), typical of VLC systems.

Spatial optical OFDM is also applied to a practical scenario where its PAPR reduction capability is used to improve the overall capacity of a proposed system that integrates power-line communication (PLC) and VLC.

A low-complexity variant of SO-OFDM, that uses square-wave carriers and simplifies the transmitter design by eliminating the need for digital predistortion (DPD) and digital-to-analog converters (DACs) is also proposed, and tested experimentally.

Abstract

Radio frequency (RF) spectrum congestion motivates the search for alternative communication techniques to complement radio systems. Visible light communications (VLC) is an emerging technology that exploits the recent and ever-growing increase in the usage of energy-efficient light emitting diodes (LEDs) to imperceptibly modulate the optical power output of LEDs to enable communication and augment RF networks.

Orthogonal frequency-divison multiplexing (OFDM) has been proposed as a modulation scheme for VLC due to its high spectral efficiency, ease of channel estimation and equalization, resistance to inter-symbol interference (ISI) and frequency-selective fading, efficient implementation using the Fast Fourier Transform (FFT), and compatibility with RF and power-line communication (PLC) standards that use OFDM.

One of the major drawbacks of conventional OFDM techniques is the high peak-to-average power ratio (PAPR) of OFDM signals. The peaks of the OFDM signals are clipped due to the limited dynamic range of the LED, which translates the high PAPR of the OFDM signal into non-linear distortion (NLD). This signal distortion causes bit-error rate (BER) performance degradation, especially at high optical signal-to-noise ratios (SNRs) typical of indoor VLC scenarios.

In this thesis, a new family of modulation techniques, termed spatial optical

OFDM (SO-OFDM), is proposed with the aim of reducing the PAPR of conventional DC-biased optical OFDM (DCO-OFDM) by making use of the large number of LEDs typically available in indoor lighting settings. Each LED group signal is a narrowband signal consisting of a small number of subcarriers, and thus has a smaller PAPR than the original OFDM signal.

Firstly, SO-OFDM is introduced and its two key concepts of frequency-to-space mapping and spatial summing are explained. Frequency-to-space mapping is achieved by allocating a subset of OFDM subcarriers to each LED. Each LED group signal is a narrowband signal consisting of a small number of subcarriers, and thus has a smaller PAPR than the original OFDM signal. Several design variations of the subcarrier assignment to LEDs are introduced and are shown through simulations, to reduce PAPR, and NLD noise due to clipping, and improve the BER performance at high SNRs as compared to DCO-OFDM. In addition, luminous efficacy is identified as an important lighting design parameter that is impacted by modulation. Relative luminous efficacy is defined as the ratio of the luminous efficacy of a modulated LED to that of an LED driven by a DC signal, and is introduced as a metric to assess the impact of modulation on LED lighting. Relative luminous efficacy links communication parameters such as signal variance to lighting design requirements.

Secondly, a low-complexity amplify-and-forward (AF) scheme is proposed for an integrated power-line communication/visible-light communication (PLC/VLC) where SO-OFDM is used for the VLC link. Frequency translation of the incoming PLC signal is used to increase the usable bandwidth of the LED. The use of both frequency translation and SO-OFDM leads to capacity gains over DCO-OFDM in the high SNR regime.

Finally, a low-complexity variant of SO-OFDM, termed square-wave SO-OFDM (SW-SO-OFDM), is proposed. Square-wave SO-OFDM uses square-wave carriers instead of sinusoidal waves to modulate a single OFDM subcarrier signal per LED. By using square-wave carriers, SW-SO-OFDM eliminates the need for digital-to-analog converters (DACs), digital predistortion (DPD), and the FFT operation. Square-wave SO-OFDM is also shown, through simulations, to achieve BER performance gains over SO-OFDM and DCO-OFDM. In addition, an experimental demonstration of SW-SO-OFDM with 64 QAM modulation on subcarriers is described.

To Lanah

You gave me the strength to make it through another day, every day, to fight, until the end.

Acknowledgments

I would first like to thank my supervisor, Dr. Steve Hranilovic, for all his help and support during my Ph.D. journey. His uncompromising commitment to the originality and quality of our research output has continuously pushed me out of my comfort zone to become the best researcher that I can be.

Next, a big thank you to my family. My mother, Dr. Maha El Gharbawy, and my father, Dr. Salah Mossaad, have provided me with unconditional love, encouragement, support, and direction over the years. Without them being there for me, I wouldn't have reached this far in my academic achievement. My brothers Moustafa and Omar have been an essential part of my support network here in Canada.

To my daughter Lanah: No words could express how blessed I am to have you in my life, smart girl. You gave my life meaning and purpose when I was in my darkest hour, and my world was falling apart. You gave me the strength to pick myself up, to continue to fight, to survive. While I am not sure I would recommend you to follow in my footsteps and do graduate studies, I will always support you and guide your steps in life.

I am grateful to Dr. Lutz Lampe, our research collaborator from the University of British Columbia, for his valuable insights that helped enrich the work presented in this thesis. I am thankful to my supervisory committee members, Dr. Tim Davidson

and Dr. Shiva Kumar, for their insightful discussions during my supervisory meetings. I would also like to thank all my current and former colleagues at the FOCAL lab, with special thanks to Kaichen Su and Warren Pawlikowski for their contribution to the research.

Thank you to all the wonderful staff at McMaster University. Special thanks to Cheryl Gies, the Graduate Administrative Assistant of the Department of Electrical & Computer Engineering, Rachel Gibbs from the Student Wellness Centre, Kaitlin Kellogg, and Tim Cameron from Student Support & Case Management.

I want to take this opportunity to thank Dr. Jordan B. Peterson for his life-changing book "12 Rules for Life: An Antidote to Chaos" and his lectures, talks, and interviews that I was able to watch on YouTube. They completely transformed my outlook on life while I was navigating the rough seas of my Ph.D. journey.

Finally, thank you to Juventus FC, EA Sports' FIFA, and Netflix for providing me with the necessary dose of entertainment so that I could refresh before I continue working. Special thanks to the greats of Egyptian and Arab music: the late Sayed Darwish, the father of Egyptian popular music, Fairuz, Amr Diab, and Mohamed Mounir. Their music has kept me company while I was working alone for long hours.

Contents

List of Figures

List of Tables

Abbreviations

ACE	Active Constellation Extension
ACO-OFDM	Asymmetrically-Clipped Optical OFDM
AF	Amplify-and-Forward
AI	Artificial Intelligence
AWGN	Additive White Gaussian Noise
BDM	Bit-Division Multiplexing
BER	Bit-Error Rate
CCDF	Complementary Cumulative Distribution Function
CLT	Central Limit Theorem
CM	Cubic Metric
CP	Cyclic Prefix
CSK	Color-Shift Keying
C-SW-SO-OFDM	Coordinated SW-SO-OFDM

DAC	Digital-to-Analog Converter
DCO-OFDM	DC-biased Optical OFDM
DF	Decode-and-Forward
DFT	Discrete Fourier Transform
DJ	Double-Jump
DLC	Digital-to-Light Converter
DPD	Digital Pre-Distortion
DSP	Digital Signal Processing
FFT	Fast Fourier Transform
FOV	Field-of-View
FPGA	Field-Programmable Gate Array
FS	Fourier Series
FS-DCO-OFDM	Frequency-Shifted DCO-OFDM
FSK	Frequency-Shift Keying
FS-SO-OFDM	Frequency-Shifted SO-OFDM
ICI	Inter-Carrier Interference
IDFT	Inverse Discrete Fourier Transform
IFFT	Inverse Fast Fourier Transform

IM/DD	Intensity Modulation/Direct Detection
IoT	Internet of Things
ISC	Iterative Signal Clipping
ISI	Inter-Symbol Interference
KKT	Karush–Kuhn–Tucker
LED	Light-Emitting Diode
LFSR	Linear-Feedback Shift Register
LPTV	Linear and Periodically Time-Varying
LoS	Line-of-Sight
LTE	Long Term Evolution
MIMO	Multiple-Input/Multiple-Output
M-PAM	M-ary Pulse Amplitude Modulation
NLD	Nonlinear Distortion
NLoS	Non-Line-of-Sight
OFDM	Orthogonal Frequency-Division Multiplexing
OOK	On-Off Keying
OOSC-FDMA	Overlapped Optical Single-Carrier FDMA
OSC-FDMA	Optical Single-Carrier FDMA

OSNR	Optical Signal-to-Noise Ratio
O-SO-OFDM	Overlapped Spatial Optical OFDM
QAM	Quadrature-Amplitude Modulation
QoS	Quality of Service
PA	Power Amplifier
PAPR	Peak-to-Average Power Ratio
pc-WLED	Phosphor-Converted White LED
PD	Photodetector
PLC	Power Line Communication
PM	Precoding Matrix
PPM	Pulse Position Modulation
PSD	Power Spectral Density
PSK	Phase-Shift Keying
PTM	Pulse Time Modulation
PTS	Partial Transmit Sequence
RC	Raised-Cosine
RF	Radio Frequency
RLE	Relative Luminous Efficacy

RMS	Root Mean Square
SC-FDMA	Single-Carrier FDMA
SDR	Signal-to-Distortion Ratio
SFN	Single-Frequency Network
SLM	Selected Mapping
SNDR	Signal-to-Noise-and-Distortion Ratio
SNR	Signal-to-Noise Ratio
SO-OFDM	Spatial Optical OFDM
SP	Spatial Processing
S/P	Serial-to-Parallel
SSLM	Symmetric Selected Mapping
SW-SO-OFDM	Square-Wave SO-OFDM
TI	Tone Injection
TR	Tone Reservation
U-SW-SO-OFDM	Uncoordinated SW-SO-OFDM
VLC	Visible-Light Communication

Chapter 1

Introduction

Over the past two decades, the "wireless revolution" has touched every aspect of human life and resulted in an explosive demand for wireless connectivity. The most recent emerging and fast-growing technologies such as big data, artificial intelligence (AI), Internet of Things (IoT), and cloud computing are putting even more demand on network infrastructure and resources, most notably the radio frequency (RF) spectrum [1, 2]. Meanwhile, due to their superior energy efficiency, longer lifespan, and lower carbon footprint, light-emitting diodes (LEDs) have transformed the lighting industry, largely replacing incandescent and fluorescent light bulbs [3]. Visible-light communication (VLC) systems exploit the wide availability of illumination LEDs to enable communications by imperceptibly modulating the optical power output of the LEDs to transmit data in the visible spectrum to complement RF networks [4].

1.1 Visible Light Communication: Advantages and Signaling Design

Visible light communications offers many advantages over RF networks. The spectrum range available for VLC (400-800 THz) is three orders of magnitude more than that available for RF communication (30 Hz-300 GHz) [5, 6, 7]. The current VLC technology enables data rates as high as 10s of Gbit/s, two orders of magnitude higher than fast broadband RF connections [5, 8]. Moreover, the spectrum in visible light bands is unlicensed worldwide. Signal security is improved in VLC systems since visible light radiation is contained by opaque boundaries [9]. A major advantage of VLC systems is energy efficiency since LED devices provide a higher lumen output per input electrical Watt than any other illumination technology [10]. Perhaps the most significant advantage of VLC is that it comes at a small fraction of the cost of Wi-Fi for indoor connectivity solutions. This is due to the fact that VLC relies on existing lighting infrastructure where the LEDs serve the dual purpose of lighting and communication [2, 11]. Despite these advantages, VLC systems are limited in range, and maintaining a good communication performance at low dimming levels poses a challenge to signaling design [2].

Since LEDs are non-coherent light sources, VLC is restricted to intensity modulation/direct detection (IM/DD), where the information signal directly modulates the LED's light intensity, rather than the phase. A photodetector (PD) is used at the receiver to convert the received optical power into an electrical signal [12]. Intensity modulation requires the signal to be real and non-negative. Moreover, the average amplitude of the light signal is restricted due to eye-safety regulations of the

International Electrotechnical Commission (IEC) [13].

Accordingly, several modulation techniques compatible with IM/DD have been proposed. Single-carrier approaches include on-off keying (OOK), M-ary pulse amplitude modulation (M-PAM), and pulse position modulation (PPM). A recent trend has been to consider multi-carrier modulation techniques, such as orthogonal frequency-division multiplexing (OFDM) [2, 14], given their robustness against inter-symbol interference (ISI) and ease of channel equalization compared to single-carrier techniques. This is particularly crucial for modern multimedia applications requiring high data rates for a reasonable quality of service (QoS) [15]. Variable PPM, OOK, and color-shift keying (CSK) have been adopted in the IEEE 802.15.7 standard, with data rates ranging from 11 kbit/s to 96 Mbit/s, and dimming support functionality [14, 16]. However, OOK is not a suitable candidate to meet the increasing high-speed demands of indoor VLC networks and is practical only for low-data-rate links [2].

1.2 Orthogonal Frequency Division Multiplexing for Visible Light Communication

Orthogonal frequency-division multiplexing uses multiple orthogonal subcarriers that are close-spaced and overlapping in the frequency domain. In this thesis, the spectral efficiency of OFDM is defined as the data rate per unit bandwidth and measured in bits/s/Hz. Hence, OFDM can better exploit the limited bandwidth of LEDs [17]. Moreover, OFDM offers robustness against multipath effects and ISI, design flexibility by using dynamic subcarrier allocation, ease of implementation using the Inverse Fast Fourier Transform/Fast Fourier Transform (IFFT/FFT) algorithm,

and ease of channel estimation and equalization [18, 19, 20]. For these reasons, OFDM has spurred the interest of the VLC research community and has been studied through theoretical analysis, simulations [21, 22], and experiments [23, 24], and found its way to commercial applications [25, 26].

Real and non-negative OFDM signals are required to modulate the light source intensity directly. A common method to achieve this is to impose a Hermitian symmetry structure on the OFDM subcarriers to get a real signal in the time domain and then to add a DC bias and clip any negative-going portions of the signal to get a non-negative signal. This technique is called DC-biased Optical OFDM (DCO-OFDM). Since the added DC bias does not carry information, the optical power efficiency of DCO-OFDM is reduced. Another technique called Asymmetrically-Clipped Optical OFDM (ACO-OFDM) that does not require DC biasing is also commonly used to solve the power efficiency problem. In addition to the Hermitian symmetry requirement, only the odd subcarriers are modulated for ACO-OFDM. In this case, it was shown in [27] that the clipping noise falls on the unmodulated even subcarriers. However, the improvement in optical power efficiency comes at the expense of a halved spectral efficiency for ACO-OFDM compared to DCO-OFDM [20]. These two signaling schemes and other OFDM-based VLC techniques are described and compared in [20], where it is shown that, despite its lower optical power efficiency, DCO-OFDM offers a higher spectral efficiency and lower complexity than the other techniques. Therefore, in this thesis, DCO-OFDM is the benchmark conventional optical OFDM signaling scheme of choice that the proposed schemes are compared to.

The main drawback of optical OFDM is the high peak-to-average power ratio (PAPR) of OFDM signals, which reduces the efficiency of LED drivers, leads to

signal distortion, and bit-error rate (BER) performance degradation. The high PAPR problem of OFDM and PAPR reduction techniques are discussed in detail in Sec. 1.3.

1.3 High Peak-to-Average Power Ratio in OFDM Systems: Overview and Reduction Techniques

An OFDM frame consists of the superposition of multiple orthogonal subcarrier signals. For a large enough number of subcarriers, a common approximation for the distribution of the time-domain OFDM signal samples approaches a Gaussian distribution, given the central limit theorem (CLT) [28]. This means the OFDM signal has a high PAPR that increases as the number of modulated subcarriers increases. Due to its detrimental effects on power amplifier (PA) efficiency in RF systems, the high PAPR problem of OFDM has been extensively studied and numerous PAPR reduction techniques have been proposed [29].

The simplest PAPR reduction technique is amplitude clipping and filtering [30]. However, it suffers from in-band distortion that cannot be filtered out. Other techniques that are distortionless include coding, partial transmit sequence (PTS) [31], selected mapping (SLM) [32], interleaving [33], tone reservation (TR) [34], tone injection (TI) [35], and active constellation extension (ACE) [36]. However, these distortionless techniques require more processing, which adds to the complexity of the system, and either require more transmit power or incur a data rate loss, or both. Another technique named clustered OFDM is used in RF systems where it divides the OFDM subcarriers into smaller "clusters" or blocks that are transmitted using

separate antennas. Since each cluster has a smaller number of subcarriers, this results in a smaller PAPR. However, since each cluster requires a PA, this approach is deemed costly for most RF applications [29]. In contrast, for VLC transmitters, PAs can be replaced by more efficient and simple DC/DC converters [37]. Moreover, in luminaires, the analogy of the multiple antennas required for clustered OFDM already exists in the form of multiple LEDs. Therefore, clustered OFDM is well-suited for OFDM-based VLC systems. In fact, clustered OFDM inspired Spatial Optical OFDM (SO-OFDM), the signaling design technique that is introduced in this thesis.

For VLC systems, the high PAPR of OFDM signals aggravates the nonlinearity problem of LED devices. The relation between the LED input electrical power and optical power output is nonlinear and for large peaks, the LED operates in the nonlinear region of the optical power versus current characteristics. While this can be mitigated by using digital pre-distortion (DPD) [38], large signal peaks that go beyond the LED operating range are clipped, causing nonlinear distortion (NLD) of the optical signal [39].

Several PAPR reduction techniques have been proposed for VLC systems using OFDM. Companding techniques include μ-law companding [40] and exponential companding [41]. Another technique is DFT-spreading which is similar to single-carrier FDMA (SC-FDMA) adopted as the uplink multiple access scheme in 3GPP Long Term Evolution (LTE) [42]. Cubic metric (CM) reduction is based on the ACE technique used in RF communication [43]. Pilot-assisted PAPR reduction is based on the SLM technique used in RF communication [44]. Other PAPR reduction techniques include symmetric selected Mapping (SSLM) [45], precoding matrix (PM) techniques [46], and constrained clipping [47]. Finally, another approach is to use a combination

PAPR reduction technique	Drawbacks
Companding (μ-Law [40], Exponential [41])	Companding transform at the transmitter, BER increase, and signal distortion.
DFT-Spreading [42]	Extra FFT at the transmitter and extra IFFT at the receiver.
Cubic Metric Reduction [43]	IFFTs at the transmitter, projection, and cubic metric calculation and selection.
Pilot-Assisted PAPR Reduction [44]	IFFTs and phase sequence selection at the transmitter and side information detection at the receiver.
Symmetric Selected Mapping (SSLM) [45]	IFFTs and phase sequence selection at the transmitter and side information detection at the receiver.
Precoding Matrix (PM) [46]	Precoding at the transmitter and deprecoding at the receiver.
Constrained Clipping [47]	FFT and distortion mitigation at the transmitter.

Table 1.1: Drawbacks of PAPR reduction techniques used in OFDM-based VLC systems.

of the aforementioned PAPR reduction techniques (e.g. combining clipping and PTS [48] and combining precoding and companding [49]).

However, PAPR reduction comes at the expense of an increased computational complexity, signal distortion, and BER increase. These drawbacks are summarized in Table 1.1 for the aforementioned techniques. Moreover, conventional PAPR reduction techniques fail to exploit the favorable aspects of VLC systems, such as the availability of multiple LEDs for communication, the lack of spectrum regulations, and the fact that LEDs have a low-pass frequency response which filters out out-of-band emissions.

1.4 Integration of Power Line and Visible Light Communications

In common with VLC, power line communication (PLC) uses existing infrastructure (the electrical power grid for PLC) to provide broadband access [50]. Furthermore, the IEEE 1901 Broadband Over Power Lines Standard [51] adopted OFDM for its PHY layer, which allows for the seamless integration between broadband PLC and OFDM-based VLC systems [52, 53]. The integration of PLC and VLC networks presents itself as a natural low-cost solution allowing for the extension of the reach and range of applications of the Smart Grid, especially in radio-hostile and/or radio-congested environments [54].

Proposals for PLC/VLC integration include [53]:

1. Multiple-input/multiple-output (MIMO) [55], where the PLC network connecting all LEDs in a room, serves as a backbone network that coordinates the transmission of the LEDs, in either a broadcast fashion, or a cooperative MIMO scheme.

2. Relaying [56], where the integrated PLC/VLC system is treated as a two-hop communication system with transmission in the power line considered the first hop, indoor VLC transmission considered the second hop, and LED lights acting as a relay.

Relaying techniques can be classified into decode-and-forward (DF) where the incoming power line signal is demodulated, decoded, then re-modulated and re-coded before VLC transmission, and amplify-and-forward (AF) where simple analog processing (e.g. filtering, amplification, and adding a DC bias) is applied to the PLC

signal, including noise, before VLC transmission [53].

Experimental demonstrations of integrated PLC/VLC systems using AF relaying have been conducted [52, 57] showing the possibility of reliable indoor broadband transmission at data rates on the order of 10s of Mbps, while requiring only minor modifications to existing power line and lighting infrastructure. Another simple design for the PLC/VLC module is using a phase-locked loop to demodulate a frequency-shift keying (FSK) power line signal and convert it to an OOK signal that is compatible with IM/DD requirements in the VLC subsystem [58]. An example of more complex DF PLC/VLC module is a bit-division multiplexing (BDM) scheme providing data communication and navigation in a single-frequency network (SFN) structure [59].

Despite these recent efforts in PLC/VLC integration, many design possibilities remain overlooked. For instance, to the best knowledge of the author, PAPR reduction for OFDM-based VLC subsystems in integrated PLC/VLC systems has not been discussed. Moreover, the AF PLC/VLC modules described in previous works are limited to basic analog processing such as amplification, DC biasing, and clipping the signal to fit in the dynamic range of the LED. It is possible, however, to use other analog processing techniques, such as filtering and frequency translation to cater to the needs of VLC. For example, it is possible to use filtering and frequency translation to assign portions of the incoming PLC signal spectrum to VLC OFDM subcarriers with favorable signal-to-noise ratio (SNR), e.g., using a water-filling algorithm [60]. Finally, the availability of multiple LEDs for indoor VLC was exploited to serve multiple users in VLC MIMO schemes. However, the multiple LEDs could also be used in a coordinated fashion to improve the optical signal quality, e.g., by reducing PAPR and NLD and improving the SNR of the VLC subsystem. This can be achieved by

using signaling design techniques that, unlike conventional techniques, allow different LEDs to be modulated by different signals. In general, little literature in the area of PLC/VLC integration has been published to date. Therefore, PLC/VLC integration is a promising future research area, especially as both PLC and VLC technologies mature and become more widespread.

1.5 Thesis Vision

Given the status of research in VLC solutions and signaling design in recent years, summarized in the previous sections, this thesis creates a vision, and makes contributions based on this vision, to guide future research directions, and help design and popularize practical, cost-effective, energy-efficient, and eco-friendly indoor VLC systems.

The thesis vision can be stated in the following three points:

1. Low complexity and low cost: VLC should be regarded and kept as an inexpensive complement to RF communication (e.g., Wi-Fi). Building complex and costly VLC systems defeats the purpose of VLC in exploiting existing and ubiquitous solid-state lighting infrastructure and providing communication at a low additional cost.

2. Lighting is the primary function of the LED lights, and VLC functionality is a secondary function: The lighting function should be prioritized, and the impact of communication on the lighting function should be minimal. For example, the impact of VLC on dimming support, energy efficiency, and luminous efficacy should be minimized. Moreover, flickering should be kept within the permissible,

and safe limits and the target illuminance on a surface should be achieved. Ideally, these lighting design parameters should first be specified and taken into account in the VLC system design. The design should then be tested, and these parameters should be measured and verified against the initial lighting design requirements before implementation and widespread manufacturing and commercialization.

3. Consideration of the intrinsic properties of VLC channels in system design: The same designs and techniques (e.g., PAPR reduction techniques, use of spectrum masks, sine-wave carriers, etc) cannot simply be imported from RF communication without verifying their compatibility with VLC systems. One key difference between RF and VLC is that the channel effects in indoor VLC systems are not as detrimental as the channel effects in typical wireless RF channels, where frequency-selective fading is large. Also, the availability of multiple LEDs and the high SNR of typical indoor scenarios should be considered in signaling design. In fact, given the simple channel equalization provided by OFDM, this thesis focuses the signaling design goals on reducing NLD and PAPR, since NLD is the dominant source of noise for high optical power transmission. Signaling design in this thesis also exploits the multiple LEDs available in typical VLC systems while keeping the design simple and cheap.

1.6 Thesis Outline

This thesis introduces a novel signaling design paradigm for OFDM-based indoor VLC systems to fulfill the vision outlined in Sec. 1.5 and circumvent the drawbacks of

conventional OFDM techniques pointed out in Secs. 1.1–1.3. The goal is to combine PAPR reduction and improved communication performance at high SNR with low complexity and low cost while satisfying lighting design constraints. Furthermore, this new signaling design is applied in a practical PLC/VLC relaying scenario to reduce the PAPR of the VLC OFDM signal and improve overall system capacity. Finally, with the aim of further reducing the VLC transmitter complexity, a low-complexity variant of the proposed design is presented and demonstrated experimentally.

This thesis is written following regulations for a "sandwich" format. In addition to the Introduction, it contains three self-contained chapters. Each chapter consists of an abstract, an introduction, a body, a conclusion, and necessary appendices. The references from all chapters are compiled in the bibliography list at the end of the thesis. The organization of the thesis is as follows:

In **Chapter 2**, a new modulation technique named Spatial Optical OFDM (SO-OFDM) is proposed, taking into account and making use of the features of indoor VLC systems [61]. In particular, the following four characteristics of VLC were observed and considered in signaling design:

1. Given a minimum required brightness level in lighting standards (e.g., 400 lx at the desktop height in the EN 12464-1 standard [62]), the optical SNR at the receiver is high ($\sim$ 60 dB as reported in [63]). This implies that the dominant source of noise is the NLD noise due the clipping of the transmitted signal, rather than the receiver noise. Hence, the main design goal of SO-OFDM is to reduce the PAPR and NLD clipping noise, leading to BER performance gains at high SNRs.

2. Practical VLC deployment scenarios use 10s to 1000s of LEDs for a standard

5 m × 5 m × 3 m room [12, 64]. Conventional VLC modulation methods, including OFDM-based techniques such as DCO-OFDM, drive all LEDs by identical signals. For the proposed SO-OFDM, however, LEDs are divided into groups, with a different "group" signal driving the LEDs in each group. This provides more signaling design flexibility.

3. Since LEDs are noncoherent light sources and have a wide spectral width, the optical power signals from all LEDs sum constructively at the receiver [2, 64]. This spatial summing of intensities is the key concept behind SO-OFDM. Moreover, the channel gains and delays between LEDs and and the receiver are assumed to be identical throughout this thesis since the difference in path lengths from each LED to the receiver is typically on the order of a few centimeters. However, the assumption of equal gains and delays between LEDs and receiver is not essential to SO-OFDM since different gains and delays between LEDs and receiver can be compensated using cyclic prefix (CP) and channel estimation and equalization techniques.

4. Adding a modulated VLC signal current to the DC current that normally drives the LED reduces the luminous efficacy of the LED. That is, a modulated LED produces fewer output lumens of luminous flux per Watt of electrical power consumed by the LED, as compared to an unmodulated LED that is used solely for lighting. The maximum tolerated luminous efficacy loss is specified by the lighting design requirements. Then the VLC signal parameters, such as signal standard deviation and clipping levels, are designed to ensure the luminous efficacy loss remains within tolerable limits.

Based on these four characteristics, SO-OFDM divides the LEDs into groups, and

each LED in a group is modulated by the same filtered subset of OFDM subcarriers. The idea is to reduce the number of OFDM subcarriers assigned to each LED group and thereby reduce PAPR and NLD noise. The simplest form of SO-OFDM, named SO-OFDM with subcarrier mapping, maps each subcarrier to exactly one LED group. Another variation, named Overlapped SO-OFDM (O-SO-OFDM), allows assigning scaled subcarrier data to more than one LED group. The group signals add up constructively at the receiver PD to realize a DCO-OFDM signal, allowing for a conventional OFDM receiver to be used. This implies that SO-OFDM does not add any extra complexity burden on the receiver side.

Other variations of SO-OFDM are also introduced in **Chapter 2**, and all SO-OFDM variations are compared to DCO-OFDM and SC-FDMA in terms of the complementary cumulative distribution function (CCDF) of the PAPR, BER performance, clipping distortion noise power, and signal-to-distortion ratio (SDR). Detailed analyses of the BER of SO-OFDM variations and luminous efficacy are also provided. The luminous efficacy is computed using a Gaussian model for the OFDM signal, and plotted as a function of both the signal standard deviation and clipping levels.

An important parameter that determines the effectiveness of SO-OFDM as a PAPR reduction technique is the number of LED groups G. In **Chapter 2**, the choice of G in practical systems is discussed. The factors that are taken into consideration when choosing G are the optical SNR at the receiver, the maximum allowed BER (determined by the forward error correction limit, for example), and transmitter hardware complexity. A good strategy is to choose the smallest possible G that achieves the target BER at practical optical SNR values in order not to overly increase the transmitter hardware complexity.

In **Chapter 3**, SO-OFDM is applied to a practical PLC/VLC integration scenario. Amplify-and-forward relaying is used where an all-analog processing module adds a DC bias to the incoming PLC signal to make it suitable for IM/DD. By keeping the incoming PLC signal in its analog form, all-analog processing avoids the use of analog-to-digital and digital-to-analog converters as well as digital signal processing (DSP) components, and thus provides a simpler and cheaper AF module design. Since the PLC signal occupies the frequency band from 2 to 28 MHz in the IEEE P1901 standard [51] and white-light LEDs have a low-pass frequency response of phosphor-converted white LEDs with a 3-dB bandwidth of a few MHz, frequency down-conversion of the PLC signal by 2 MHz is performed by the AF module in order not to waste the portion from 0 to 2 MHz. Spatial optical OFDM is used for VLC transmission with the purpose of reducing the PAPR and NLD due to clipping. Frequency-shifted SO-OFDM (FS-SO-OFDM) is compared to DCO-OFDM in terms of the CCDF of the PAPR and the overall capacity of the combined PLC/VLC system.

In **Chapter 4**, square-wave SO-OFDM (SW-SO-OFDM), a novel lower complexity variant of SO-OFDM using square-wave carriers instead of sinusoidal carriers, is proposed. A key limitation with SO-OFDM is that in order to realize a significant reduction of PAPR, a large number of transmit chains is required. Each transmit chain requires DACs, DPD, and IFFT operation.

Square-wave carriers are better suited for VLC systems since the VLC spectrum is free and out-of-band emissions are allowed. Square waves are simpler to generate using digital electronics compared to sinusoidal waves. Moreover, it is shown in **Chapter 4** that, among all periodic carriers constrained between two clipping levels, square waves have the largest fundamental component in the Fourier Series (FS)

expansion.

Using binary-level signaling restricts data symbols to a constant magnitude. To allow for multi-level signaling, a generalization of SW-SO-OFDM, named coordinated SW-SO-OFDM (C-SW-SO-OFDM), is proposed, where the binary-level transmission of pairs of LEDs is coordinated to construct multi-level signals after spatial summing at the receiver. An experimental proof-of-concept of C-SW-SO-OFDM is described, where 64-QAM data is transmitted over a distance of 1 m at a signaling rate of 130.2 ksymbols/sec, resulting in a data rate of 781.2 kbps.

In addition to analysis and BER simulations to compare the proposed SW-SO-OFDM and C-SW-SO-OFDM to DCO-OFDM, a new method for computing the LED luminous efficacy for the case of a single modulated OFDM subcarrier per LED group is presented. Since the Gaussian model is not accurate for an OFDM signal having a small number of activated subcarriers, a time-domain approach is followed by computing the time averages of luminous flux and electrical power consumption by the LED over one OFDM symbol, rather than the statistical averages used in **Chapter 2**.

Chapter 5 concludes the thesis and outlines the potential research avenues that could be motivated by this work and extend it.

1.7 Description of Contributions to Publications

This thesis has been prepared in the "sandwich thesis" format. Chapters 2 has been published in a journal [61]. Chapter 3 has been published at an international conference [65]. Chapter 4 is currently under preparation for submission to a journal. This section describes the contribution of each of the co-authors to the work.

Chapter 2: **Visible Light Communications Using OFDM and Multiple LEDs**

Authors: Mohammed S. A. Mossaad, Steve Hranilovic, and Lutz Lampe

The idea of SO-OFDM came up during supervisory meetings between Mohammed Mossaad and Dr. Steve Hranilovic who encouraged Mohammed to follow this research direction. Mohammed Mossaad then proceeded to formulate the indoor VLC system model, develop the system block diagram, and carry out all analyses and simulations in this paper. He also plotted all graphs and did all the writing of this paper, while receiving feedback and suggestions from Dr. Hranilovic. Once a draft of the paper was completed, Dr. Lutz Lampe reviewed the paper and provided his feedback and suggestions and Mohammed Mossaad continued to edit the paper based on this feedback, while Dr. Hranilovic helped with the final editing the of the paper and guiding the research. This work was presented in part in [66]. The material in this chapter was published in *IEEE Transactions on Communications* (Volume: 63, Number: 11, Pages: 4304-4313, November 2015) [61].

Chapter 3: **Amplify-and-Forward Integration of Power Line and Visible Light Communications**

Authors: Mohammed S. A. Mossaad, Steve Hranilovic, and Lutz Lampe

This research topic was planned as a research collaboration between Dr. Steve Hranilovic and Mohammed Mossaad with research focus on VLC on one side, and Dr. Lutz Lampe with research focus on PLC on the other side. Mohammed Mossaad set out to study

PLC standards, signaling, and channel modeling, and laid out the details of the PLC subsystem used in this paper. Mohammed then proceeded to design the AF module for PLC/VLC integration and the signaling and channel modeling for the VLC subsystem. He then performed all the analysis and simulations, obtained all the graphs, and did all the writing of the paper. Dr. Hranilovic reviewed the paper draft, helped with the final editing, and provided guidance through feedback and suggestions to improve the paper. Dr. Lutz Lampe reviewed the paper and provided comments and suggestions, especially for the PLC subsystem, in the initial phase of problem layout as well as before the paper submission. The material in this chapter was published in the *Proceedings of the 2015 IEEE Global Conference on Signal and Information Processing (GlobalSIP)* (Pages: 1322-1326, December 2015) [65].

Chapter 4: **Square-Wave Spatial Optical Orthogonal Frequency-Division Multiplexing**

Authors: Mohammed S. A. Mossaad, Kaichen Su, Warren Pawlikowski, Steve Hranilovic, and Lutz Lampe

The idea of this paper was motivated by the need for lower complexity transmitters for SO-OFDM, and was put forward during the review process of [61] by Mohammed Mossaad and Dr. Steve Hranilovic. Mohammed then set up the system model, and performed the analysis and simulations pertaining to SW-SO-OFDM, and presented his work to Dr. Steve Hranilovic and Dr. Lutz Lampe. The idea of C-SW-SO-OFDM came up during this presentation to extend the signaling capability to multi-level QAM constellations. Mohammed then performed the analysis and

simulations for C-SW-SO-OFDM and designed the communication parameters, such as QAM constellation size, OFDM subcarrier frequency, and OFDM symbol duration, for the experimental demonstration of C-SW-SO-OFDM. Mohammed then gave these design parameters to Kaichen Su and Warren Pawlikowski, who implemented it in hardware. In particular, Kaichen Su programmed the field-programmable gate array (FPGA) to generate the binary-level signal waveform data from the linear-feedback shift register (LFSR) and the synchronization signal. Warren Pawlikowski and Kaichen Su designed and implemented the current driver, and Kaichen Su conducted the experiment by driving the LEDs using the output signal of the current driver, receiving the optical signal using a PD, and capturing the electrical output signal of the PD using a digital oscilloscope. He then provided Mohammed Mossaad with the captured oscilloscope data including the time axis, the received signal, and the synchronization signal. Mohammed then demodulated the signal offline using MATLAB and produced the received constellation diagram and the time-Domain waveforms of C-SW-SO-OFDM. Mohammed Mossaad performed all the analysis and simulations for this paper, and obtained all the graphs. Mohammed also did all the writing of the paper except for the part of Section 4.5 that describes the hardware implementation of the experiment. The initial draft of this part was written by Kaichen Su, and later edited and modified to its present form by Mohammed Mossaad for inclusion in the paper. Dr. Steve Hranilovic provided feedback and research guidance throughout the different stages of this work and helped in editing the final draft of the paper. Dr. Lutz Lampe reviewed the final draft of the paper. The material in this chapter is in preparation for submission to a journal.

Chapter 2

Visible Light Communications Using OFDM and Multiple LEDs

In this chapter, the problem of high PAPR in OFDM-based indoor VLC systems is addressed, as discussed in Secs. 1.2 and 1.3. Spatial optical OFDM is proposed as a PAPR reduction technique exploiting the multiple-LED architecture and the spatial summing property of indoor VLC channels. Several SO-OFDM techniques are proposed and can be broadly classified into SO-OFDM with subcarrier mapping and overlapped SO-OFDM. Spatial optical OFDM techniques are compared against conventional DCO-OFDM in terms of the PAPR reduction capability and the BER performance. In accordance with the thesis vision outlined in Sec. 1.5, which prioritizes the lighting function of the LED lights, the relative luminous efficacy of the LED is introduced as a parameter that links the communication and lighting systems design by quantifying the effect of LED modulation on its luminous efficacy.

The work in this chapter appeared in *IEEE Transactions on Communications* (Volume: 63, Number: 11, Pages: 4304 – 4313, November 2015) [61]. IEEE owns

the copyright of the material in this chapter and it is permitted to be re-used in the thesis.

Abstract Visible-light communication (VLC) systems leverage solid-state illumination devices to create high-speed communication links. Orthogonal frequency-division multiplexing (OFDM) has been considered for these intensity-modulated/direct-detection (IM/DD) optical channels, however, it suffers from high peak-to-average power ratio (PAPR). Moreover, the implementation of linear, power-efficient, high-current, wideband drivers is challenging. In this paper, the concept of *spatial summing* is developed where wideband, high PAPR OFDM signals are partitioned into many low-PAPR narrowband signals that are transmitted from multiple LEDs. The signals from different LEDs are allowed to sum in space before being detected by a conventional OFDM receiver. Spatial optical-OFDM (SO-OFDM) is proposed in which filtered subsets of carriers are emitted by each LED. In addition, low-PAPR optical single-carrier FDMA (OSC-FDMA) is developed where different collections of LEDs act as virtual users in a multiple-access scheme. The different variations of SO-OFDM and OSC-FDMA are compared to conventional DC-biased optical (DCO) OFDM and are shown to achieve lower PAPR and more robustness to LED nonlinearities leading to error rate performance gains at high signal-to-noise ratios.

2.1 Introduction

Orthogonal frequency division multiplexing (OFDM) has been adopted in a large variety of communication standards due to its robustness to channel impairments, simple equalization, and efficient implementation using the fast Fourier transform (FFT). Recently, there has been a growing interest in applying OFDM to optical communication systems, including optical fiber and optical wireless communications [67]. A particularly difficult challenge in applying OFDM techniques to visible light

communication (VLC) optical wireless systems is the need for wideband high current drivers which can accommodate the large peak-to-average power ratio (PAPR) of OFDM. In this work, the multiple light-emitting diodes (LEDs) present in VLC-enabled illumination fixtures are exploited to mitigate the PAPR problem of OFDM.

Information is transmitted on VLC links by imperceptibly modulating the intensity of the luminary and measuring the instantaneous received optical power with a photodiode. These intensity modulated/direct detection (IM/DD) links require that all emitted signals be non-negative and constrained in the mean, i.e, average brightness. One approach to make OFDM compatible with IM/DD links, termed DC-biased optical OFDM (DCO-OFDM), is to add a fixed bias to the time-domain signal and clip negative excursions. However, the high PAPR of OFDM coupled with the non-linearity of the LED itself has been noted as a key challenge for VLC OFDM systems [68, 69]. The nonlinear characteristics of the LED can be partially compensated using digital pre-distortion (DPD) [70], however, the dynamic range of the LED is still limited. There are a wide array of techniques in the literature to improve the PAPR of OFDM signaling [71], however, they do not explicitly take into account the illumination constraints of LED luminaries. In [72] optimization of the scaling and bias level for DCO-OFDM VLC communications is given, however, no explicit linkage between communications system performance and the illumination function of the luminary is provided. We share the view that the primary purpose of a luminary is to provide illumination and data communication, via VLC , is a secondary function [12, 63]. Therefore, in this work illumination requirements are considered a priority over communication constraints in VLC system design.

In this paper, the *spatial summing* of the intensities of multiple LEDs in a given

luminary is used to mitigate the OFDM PAPR problem for VLC. Most lighting fixtures include multiple LEDs that are modulated by identical signals in conventional VLC systems. In contrast, in this work a wideband high PAPR OFDM signal is partitioned into a series of narrowband emissions which modulate the output intensity of groups of LEDs. The signals from each LED group are allowed to sum in free-space during propagation and a standard OFDM receiver is used at the receiver. In particular, we propose *spatial optical-OFDM* (SO-OFDM) where filtered subsets of carriers are emitted by each LED group. In the simplest form of SO-OFDM, each LED group is assigned a different OFDM subcarrier. In this case, the time-domain OFDM signal of each group is a sinusoidal signal with a PAPR of 3 dB. More generally, each LED group can be assigned a linear combination of OFDM subcarriers. In addition, low-PAPR *optical single-carrier FDMA* (OSC-FDMA) is also developed where different collections of LEDs act as virtual users in a multiple-access scheme. A key difference of OSC-FDMA over the version proposed for radio links [73] is that it is possible to coordinate amongst these virtual users in a given fixture to further reduce PAPR from each LED group.

Since LED luminaries are installed for their energy efficiency, a focus of this work is to link VLC OFDM system design to practical features of luminary design. Modulating the LED for VLC incurs a loss in the *luminous efficacy* [lm/W] of the luminary [74]. In contrast to earlier work on OFDM for VLC, we explicitly link the parameters of the designed communication systems to the luminous efficacy loss incurred due to VLC. In addition, the efficiency of the drivers used in VLC must be considered as a component in the overall efficiency of the luminary. Line drivers used in wideband OFDM applications (e.g., DSL) are of the push-pull type (e.g. class AB) or, more

recently, class G with maximum efficiency below 50% [75]. Since SO-OFDM and OSC-FDMA signals are narrowband, more efficient tuned amplifiers, such as class E, having efficiencies of 85% or higher [76] can be used. This is particularly important for VLC systems using high-brightness LEDs, where RF power amplifiers are used to boost the modulated signal to achieve high output power levels [37]. Thus, SO-OFDM and OSC-FDMA exploit spatial degrees of freedom to simplify VLC system design and maintain the high energy-efficiency of the luminary.

The idea of spatial summing in VLC has been mentioned in related ways in the literature. Spatial summation of signals from multiple LEDs has been proposed to remove the need for an electrical digital-to-analog converter (DAC) [77, 78]. Mesleh *et al.* [79] used spatial summing of signals from different LEDs to implement an iterative signal clipping (ISC) technique to reduce clipping distortion. Spatial modulation based on PPM was developed by Popoola *et al.* [80] to increase the data rate. Zhang *et al.* [81] use power imbalances between different transmitters in a spatial modulation OFDM scheme. Furthermore, the concept of spatial summing was mentioned for OFDM in parallel in [82], however, no analysis, system designs or performance results were provided. In parallel with our earlier work [66], Dong *et al.* [83] presented the concept of spatial summing applied only to the case of a single sub-carrier per LED. A VLC system based on SC-FDMA and spatial summing has been recently and independently proposed in [84]. We extend this idea in this paper to the more general case of overlapped optical SC-FDMA in Sec. 2.4.

The remainder of this paper is organized as follows. In Section 2.2, the spatial-summing VLC system model is introduced, and the impact of modulation on the luminous efficacy of the LED is quantified. Spatial optical OFDM is presented and

analyzed in Section 2.3. A tight approximation for the bit-error rate (BER) is provided and used to guide design. Section 2.4 extends theory from radio system to develop OSC-FDMA for VLC systems. The immunity to LED nonlinearity and the BER performance of the various signaling schemes presented in this paper are compared in Section 2.5. The paper concludes in Section 2.6 with suggestions for future work.

2.2 Spatial Summing VLC System Model

2.2.1 Spatial Summing OFDM Transmitter Architecture

Figure 2.1 presents a block diagram of the spatial summing OFDM transmitter architecture. The spatial summing transmitter consists of L LEDs divided into G groups. The number of LEDs in the g-th group is denoted by L_g where $g \in \{1, \ldots, G\}$. Each LED group has a bias current, I_{bias}, and a separate line driver sinks modulation current into each series connected branch. Thus, all LEDs in a group are modulated by the same signal. The emitted intensities from each LED group sum in space and are distorted by the channel as described in Sec. 2.2.2.

For each frequency-domain OFDM frame, the corresponding transmitted bits are mapped to constellation symbols using Gray labeling and chosen uniformly from a unit-energy square quadrature-amplitude modulation (QAM) constellation. The resulting frame $X_{\text{D}}[k]$ (of length N_{D}) is input to the spatial processing (SP) block, which produces the time-domain OFDM symbols, $x_g[n]$ (of length N), for each of the LED groups. The definition of the spatial processing block depends on the technique and is described in detail in Secs. 2.3 and 2.4. The time-domain symbols $x_g[n]$ are

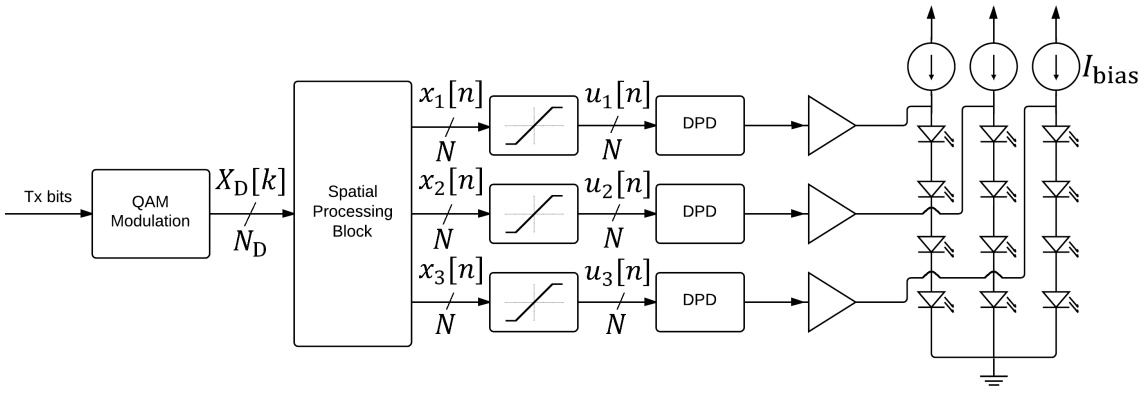

Figure 2.1: Architecture of spatial summing OFDM transmitter with $L = 12$ LEDs divided into $G = 3$ LED groups.

subject to hard-clipping to limit their dynamic range to that of the line driver. Let $I_{\mathrm{u}} > 0$ and $I_{\mathrm{l}} < 0$ denote the upper and lower current clipping levels and $(I_{\mathrm{u}} - I_{\mathrm{l}})$ as the *dynamic range* of the driver. Note that $x_g[n]$ is the time-domain OFDM signal before the addition of DC bias and has a zero mean. Therefore, the lower clipping level I_{l} is negative. Digital pre-distortion (DPD) is applied, as in [70], to linearize the response of the LED group around I_{bias} within the dynamic range. The DPD is added in order to make later analysis precise, but may be omitted in practical implementations depending on the severity of the nonlinearity.

Generally, a DAC and a DPD are required in each transmit chain. However, there are special cases where these hardware requirements are relaxed. For example, in the case of one independent data-carrying subcarrier per LED group ($N_D = G$), each LED can be driven by a sinusoidal source generated from a simple oscillator. Section 2.3.3 presents other simplified spatial summing architectures.

2.2.2 Indoor VLC Channel Model

In general, the channels between different LEDs and the receiver will not be identical. Consider that the LEDs in a fixture are modelled as having a Lambertian emission pattern and that the line-of-sight path is assumed to dominate over all multipath components from wall and ceiling reflections [12, 85]. Therefore, the channel from an LED to the photodetector can be modeled as a flat fading channel with fixed propagation delay and DC gain

$$\Omega = \begin{cases} \frac{(m+1)A}{2\pi d^2} \cos^m(\phi) T_{\mathrm{s}}(\psi) g(\psi) \cos(\psi), & 0 \leq \psi_{\leq} \psi_{\mathrm{c}} \\ 0, & \psi > \psi_{\mathrm{c}} \end{cases} \tag{2.2.1}$$

where m is the Lambertian order, A is the area of the detector, d is the distance between the luminary and the photodetector, ψ is the angle of incidence, ϕ is the angle of irradiance, $T_s(\psi)$ is the gain of the optical filter, $g(\psi)$ is the gain of the optical concentrator, and ψ_{c} is the field-of-view (FOV) of the receiver.

In a typical luminary, LEDs will be separated on the order of centimetres while the distance between the receiver and luminary is typically 1-2 meters. In this case, the difference in path lengths from each LED to the receiver will be on the order of cm's, incurring propagation time differences on the order of 10's ps. Also, given the difference in path lengths (all other factors fixed) channel gains between LEDs will differ on the order of 1-2% between different LEDs. Thus, in the balance of this paper we assume that all LEDs in a given fixture are sufficiently close that they have identical gains and delays to the receiver. Our experimental experience confirms that the assumption is generally good and similar assumptions have been widely used by

many others in similar contexts (e.g., [77, 78, 79, 83, 84]).

It is important to emphasize that the assumption on equal gain and delays between LEDs and receiver is not essential to the operation of the SO-OFDM techniques described in Sec. 2.3. In particular, the compensation of different channel gains and delays between LEDs and receiver are briefly described in Sec. 2.3.1.

Under these assumptions, define the optical power received by the photodetector from the L LEDs of the luminary as

$$P_{\mathrm{R}} = L\Omega P_{\mathrm{T}}, \tag{2.2.2}$$

where P_{T} is the optical power output of an LED.

2.2.3 LED Nonlinearity

The luminous flux, ϕ_{v} [lm] versus forward current curve, I [mA] for a Luxeon Rebel LED is given in the datasheet [86] and has quadratic fit [74]

$$\phi_{\mathrm{v}}(I) = -0.0001I^2 + 0.3093I + 3.647. \tag{2.2.3}$$

Although there will be minor variations between LEDs, we consider the above fit for the purposes of design. For luminaries using phosphor-coated blue LEDs, the conversion from luminous flux to radiated optical power, P_{T}, has been shown to be [63]

$$P_{\mathrm{T}}(I)\ [\mathrm{mW}] = 2.1\phi_{\mathrm{v}}(I)\ [\mathrm{lm}].$$

To linearize the relation between I and P_{T}, predistortion of the driving current is

required. Using predistortion, the linearized relationship is given by

$$P_{\mathrm{T}}(I) = SI + P_0 \quad \text{for } I_{\mathrm{l}} \leq I \leq I_{\mathrm{u}}.$$

where the LED gain $S = (P_{\mathrm{T}}(I_{\mathrm{u}}) - P_{\mathrm{T}}(I_{\mathrm{l}}))/(I_{\mathrm{u}} - I_{\mathrm{l}})$ [W/A] and $P_0 = P_{\mathrm{T}}(I_{\mathrm{u}}) - SI_{\mathrm{u}}$. The constant P_0 does not affect the communication function of VLC, and thus will be ignored in the description and analysis of the various OFDM techniques introduced.

2.2.4 Impact of Modulation on Luminous Efficacy

The *luminous efficacy*, η [lm/W], of an LED is defined as the ratio of the luminous flux output, ϕ_{v} [lm], to the electrical power consumed by the LED, P_{LED} [W], i.e.,

$$\eta = \frac{\phi_{\mathrm{v}}}{P_{\mathrm{LED}}}. \tag{2.2.4}$$

The luminous efficacy is a key parameter in judging how well an LED converts electrical power into useful illumination.

Consider computing the value of η for a popular illumination LED [86] when it is driven with a DC supply. The power dissipated in the LED for a given forward current I is

$$P_{\mathrm{LED}} = V_{\mathrm{f}} I = \frac{I}{k} \ln\left(\frac{I}{I_0}\right) \tag{2.2.5}$$

where V_{f} is the forward voltage, $I_0 = 3.2\ \mu A$ is the reverse bias saturation current and $k = 3.64\ V^{-1}$ for the Luxeon Rebel LED. These parameters are obtained from a least-squares fit [74] to the current-voltage characteristics provided in the datasheet [86]. Notice that LED power dissipation P_{LED} increases more than linearly with the drive

I_{bias}	V_{f}	P_{LED}	ϕ_{v}	η_{DC}
350 mA	3.19 V	1.116 W	99.7 lm	89.3 lm/W
500 mA	3.29 V	1.643 W	133.3 lm	81.1 lm/W
700 mA	3.38 V	2.365 W	171.2 lm	72.4 lm/W

Table 2.1: Luminous efficacy under different DC bias currents.

current. Notice also that the luminous flux for the same device in (2.2.3), increases less than linearly with the current. Table 2.1 shows the DC luminous efficacy, η_{DC}, for three different values of DC current in the dynamic range of the LED: $I_{\text{bias}} = 350,\ 500,$ and 700 mA by substituting (2.2.5) and (2.2.3) into (2.2.4). Notice that the luminous efficacy decreases as the forward current increases. There is also a dependence between LED modulation bandwidth and I_{bias} [87] which is not considered here since it small for the values used in Table 2.1.

LEDs used for illumination are ideally driven by a DC current I_{bias} whose value is set to obtain the desired luminous flux output, ϕ_{v}, or illuminance E [lux], at a surface. However, when the driving current is modulated (e.g., by a power converter), there is typically a reduction in η [74]. To relate the loss in η to the VLC system parameters consider fixing $I_{\text{bias}} = 500$ mA. The driving signal for each LED group $x_g[n]$ is modeled as Gaussian distributed with zero mean and standard deviation σ_g [mA] which is accurate for large number of OFDM carriers [72, 88]. The efficacy penalty due to modulation is termed the *relative luminous efficacy* and is defined as

$$\eta_{\text{rel}} = \frac{\eta}{\eta_{\text{DC}}}. \tag{2.2.6}$$

where η_{DC} is tabulated in Table 2.1. Although the illumination performance is determined by the choice of I_{bias}, η_{rel} depends on the selection of σ_g as well as the dynamic

range $(I_{\mathrm{u}} - I_{\mathrm{l}})$.

Following Fig. 2.1, to estimate the mean η_{rel} for a given σ_g and dynamic range $(I_{\mathrm{u}} - I_{\mathrm{l}})$, a large number of $x_g[n]$ samples ($> 10^6$) are generated, clipped symmetrically (i.e., $I_{\mathrm{u}} = -I_{\mathrm{l}}$) and passed through the DPD block to give the LED modulating current. The bias current is set to $I_{\mathrm{bias}} = 500$ mA. The instantaneous luminous efficacy can then be computed using (2.2.5), (2.2.3), and (2.2.4). Averaging over a large number of samples and normalizing by η_{DC} gives an estimate of η_{rel}. A contour plot of the relative luminous efficacy as a function of σ_{g} and $(I_{\mathrm{u}} - I_{\mathrm{l}})$ (mA) is shown in Fig. 2.2. The results of Fig. 2.2 show that the luminous efficacy can be reduced by a factor of up to 10% due to modulation, depending on the current standard deviation and the clipping levels.

Figure 2.2 quantifies the tradeoff between VLC communication system parameters (σ_g and dynamic range) and the efficacy loss (η_{rel}). A system designer can select the amount of efficiency to be sacrificed to support VLC and then using Fig. 2.2 and the available dynamic range of the driver can find σ_g. In the simulations in this paper, we set $I_{\mathrm{u}} - I_{\mathrm{l}} = 500$ mA (i.e., $I_{\mathrm{u}} = -I_{\mathrm{l}} = 250$ mA) and $\sigma_g = 250$ [mA] in order to limit the reduction in the luminous efficacy to about 2%. Similar curves can be plotted for different I_{bias} (i.e. illumination) levels.

2.3 Spatial Optical OFDM

Spatial optical-OFDM (SO-OFDM) divides the incoming OFDM frame into a series of narrowband emissions which are transmitted using the spatial summing architecture. This section describes SO-OFDM and gives a design guide. Note that the description and analysis in this section are restricted to SO-OFDM based on the

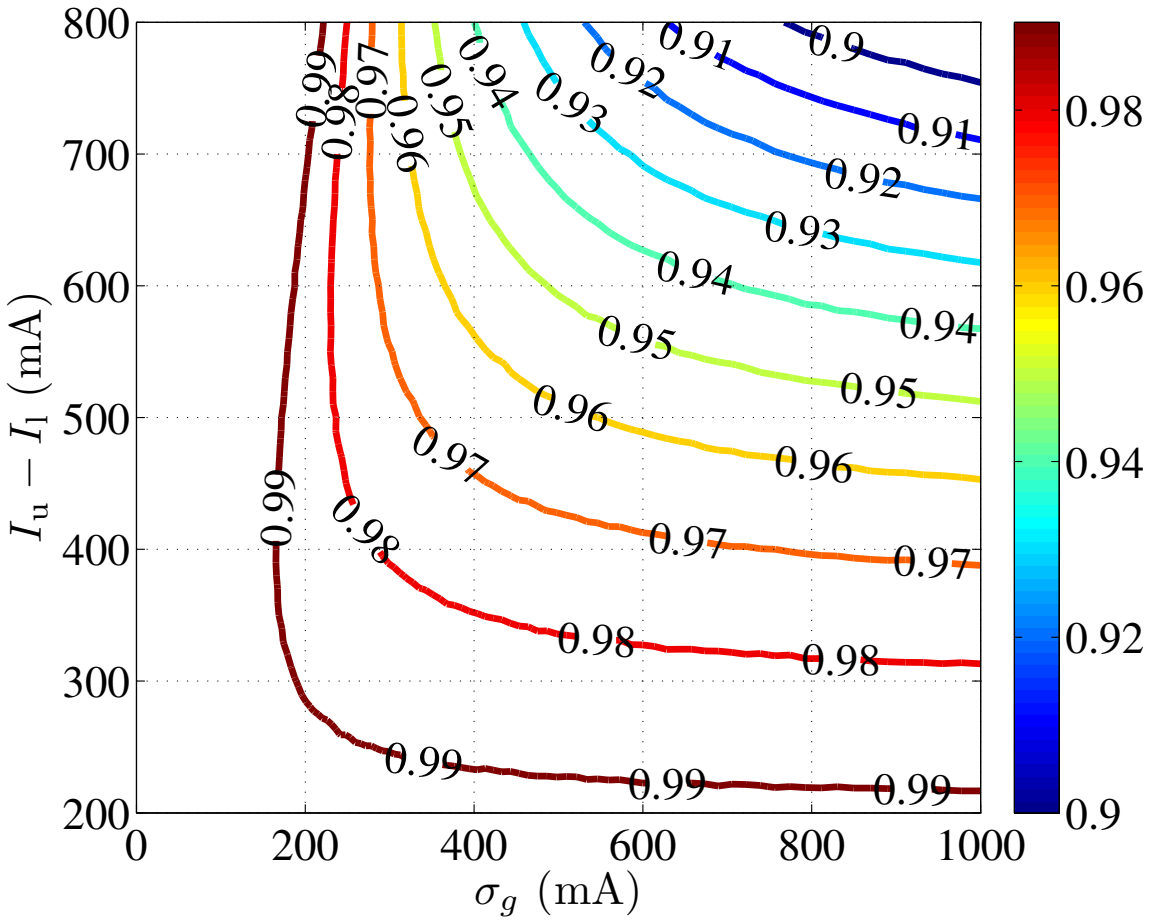

Figure 2.2: Effect of modulation on the luminous efficacy of the LED at a bias current of $I_{\text{bias}} = 500$ mA. The contour lines show the relative luminous efficacy as a function of the standard deviation of the modulating signal current before clipping (σ_g) [mA] and the dynamic range ($I_u - I_l$) [mA].

DCO-OFDM frame structure. Generalization to the asymmetrically clipped optical OFDM (ACO-OFDM) frame structure is straightforward [66].

2.3.1 SO-OFDM Definition

Figure 2.3 shows the details of the SP block for SO-OFDM systems. After serial-to-parallel (S/P) conversion, the QAM symbols, $X_{\mathrm{D}}[k]$ are mapped to the frequency domain OFDM frames so that $N_{\mathrm{D}} = N/2 - 1$ and

$$X[k] = \begin{cases} 0 & k = 0, N/2 \\ X_{\mathrm{D}}[k] & k = 1, \ldots, N_{\mathrm{D}} \\ X_{\mathrm{D}}^{*}[N-k] & k = N_{\mathrm{D}} + 2, \ldots, N-1 \end{cases}$$

Without loss of generality assume that the constellations are chosen so that

$$\mathrm{E}\big[|X[k]|^2\big] = 1,$$

for $k \neq 0, N/2$. It is straightforward to generalize this constraint to include power and bit loading for non-flat channels.

The OFDM frames for each group, $X_g[k]$ are formed by filtering the original OFDM frame $X[k]$ via

$$X_g[k] = H_g[k]X[k], \tag{2.3.1}$$

where $H_g[N-k] = H_g^{*}[k]$ for $k = 1, 2, \ldots, N/2 - 1$ and $g = 1, 2, \ldots, G$. To simplify discussion, all $H_g[k]$ will be defined for $k = 1, \ldots, N_{\mathrm{D}}$ and it is assumed extension to Hermitian symmetry is understood. The SO-OFDM time-domain group symbols are

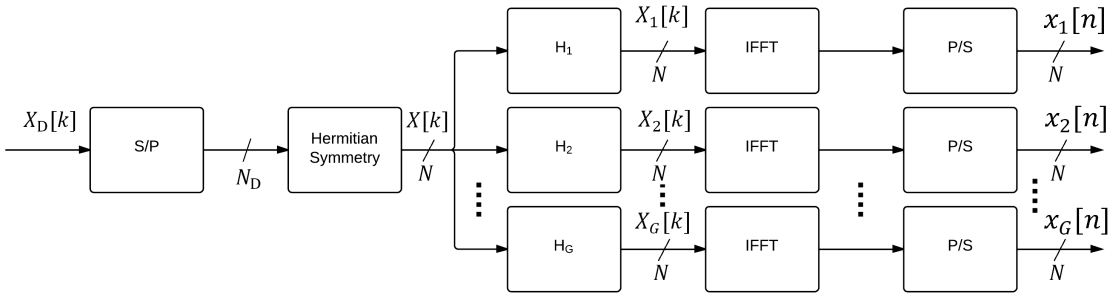

Figure 2.3: Details of the SO-OFDM spatial processing block.

then obtained by the IFFT operation.

In the channel modelling in Sec. 2.2.2, assumptions on identical gains and delays between individual LEDs and the receiver are made. Notice that small differences in the emission patterns and optical power output of individual LEDs as well as non-flat frequency response, channel gains or delays between individual LEDs and the receiver will result in a linear distortion in the resulting OFDM signal. A standard technique to deal with this distortion is to append a cyclic prefix (CP) to each symbol. The CP duration is designed to be longer than the VLC channel delay spread, effectively transforming the linear convolution of the signal with the channel impulse response into a circular convolution. From the frequency-domain perspective, the channel is converted into scalar parallel sub-channels which allows for simple frequency-domain equalization. The frequency-domain channel coefficients can be estimated using pilot subcarriers [19]. Here we assume that a CP of sufficient length is appended and used to compensate for any residual delay or linear channel distortion.

2.3.2 Analysis

Since the sample $x_g[n]$ is the sum of zero-mean independent random variables, by the central limit theorem (CLT), its distribution can be often be approximated as a zero-mean Gaussian distribution [72, 88] with variance

$$\sigma_g^2 = \mathrm{E}\big[|x_g[n]|^2\big] = \frac{2}{N}\sum_{k=1}^{N/2-1} |H_g[k]|^2. \tag{2.3.2}$$

Notice that this approximation is only reliable for sufficiently large N (i.e., $N \geq 64$ [72, 88]).

The SO-OFDM group signal, $x_g[n]$, is hard-clipped to fit into the dynamic range of the driver,

$$u_g[n] = \mathrm{F}(x_g[n]) = \begin{cases} I_{\mathrm{u}} & x_g[n] > I_{\mathrm{u}} \\ x_g[n] & I_{\mathrm{l}} \leq x_g[n] \leq I_{\mathrm{u}} \\ I_{\mathrm{l}} & x_g[n] < I_{\mathrm{l}} \end{cases}. \tag{2.3.3}$$

Define the *clipping factor*, γ_g, as the number of standard deviations per half the dynamic range

$$\gamma_g = \frac{(I_{\mathrm{u}} - I_{\mathrm{l}})/2}{\sigma_g}. \tag{2.3.4}$$

The clipping factor quantifies the severity of clipping suffered by a signal, and smaller γ_g means more severe clipping.

According to Bussgang's theorem [89], the output, $u_g[n]$, of the nonlinear clipping function, $F(\cdot)$, can be expressed as

$$u_g[n] = K_g x_g[n] + d_g[n], \tag{2.3.5}$$

where K_g is a scaling factor and $d_g[n]$ is an additive noise term that satisfies

$$\mathrm{E}[x_g[n]d_g[n]] = 0. \tag{2.3.6}$$

Using the CLT approximation for $x_g[n]$ and assuming symmetric clipping ($I_{\mathrm{u}} = -I_{\mathrm{l}} = C$) yields [28]

$$K_g = 1 - \mathrm{erfc}\left(\frac{\gamma_g}{\sqrt{2}}\right). \tag{2.3.7}$$

Notice that K_g is an increasing function in γ_g and that less severe clipping leads to larger K_g. Since all LEDs have the same σ_g^2, then the scaling factor K_g is the same for all groups and the subscript g can be dropped.

The total optical power received by the photodetector is the sum of the optical powers received from each LED. It is assumed that the LEDs are placed close to each other so that the optical channel gains and delays (2.2.1) corresponding to all LEDs are the same. The generated photocurrent, $y[n]$, is proportional to the received power with additive white Gaussian noise (AWGN), $w[n]$, with variance σ_w^2 i.e.,

$$\begin{aligned} y[n] =& G_{\mathrm{E}} \sum_{g=1}^{G} L_g(u_g[n] + I_{\mathrm{bias}}) + w[n] \\ =& G_{\mathrm{E}} \left[K \sum_{g=1}^{G} L_g x_g[n] + \sum_{g=1}^{G} L_g d_g[n] + L I_{\mathrm{bias}} \right] + w[n], \end{aligned} \tag{2.3.8}$$

where $G_{\mathrm{E}} = R\Omega S$ is the electrical gain of the system composed of the LED conversion factor S [W/A], the DC optical channel gain Ω in (2.2.1) and the photodetector responsivity R [A/W].

If the number of LEDs per group is the same for all groups, i.e. $L_g = L/G$, (2.3.8)

becomes

$$y[n] = G_{\mathrm{E}} \frac{L}{G} \left[K \sum_{g=1}^{G} x_g[n] + \sum_{g=1}^{G} d_g[n] + G I_{\mathrm{bias}} \right] + w[n]. \tag{2.3.9}$$

Noting that the I_{bias} term affects only the DC subcarrier that does not carry any data, the FFT of $y[n]$ for $k \neq 0$ is

$$Y[k] = \frac{G_{\mathrm{E}} L K}{G} \left(\sum_{g=1}^{G} H_g[k] \right) X[k] + \frac{G_{\mathrm{E}} L}{G} \sum_{g=1}^{G} D_g[k] + W[k], \tag{2.3.10}$$

where $D_g[k] = \mathrm{FFT}\{d_g[n]\}$ and $W[k] = \mathrm{FFT}\{w[n]\}$. The first term of (2.3.10) contains the transmitted signal. Define the *useful power* of subcarrier k as

$$\sigma^2[k] = \left(\frac{G_{\mathrm{E}} L K}{G} \left| \sum_{g=1}^{G} H_g[k] \right| \right)^2 = \left(G_{\mathrm{E}} L K \left| \bar{H}[k] \right| \right)^2, \tag{2.3.11}$$

where $\bar{H}[k] = \sum_{g=1}^{G} H_g[k]/G$. The second term in (2.3.10) is the frequency-domain clipping distortion noise term. Due to the CLT, the second term of (2.3.10) is approximately Gaussian-distributed with zero mean for large N. The CLT approximation is valid independent of the unknown distribution of $d_g[n]$. The variance of the clipping distortion noise term is generally a function of the subcarrier number k and is given by

$$\sigma_D^2[k] = \left(\frac{G_{\mathrm{E}} L}{G} \right)^2 \mathrm{E} \left[\left| \sum_{g=1}^{G} D_g[k] \right|^2 \right] \tag{2.3.12}$$

The performance of the VLC SO-OFDM system is affected by both the clipping distortion noise and the AWGN. The effect of the clipping distortion noise depends on γ_g as well as the $H_g[k]$. The signal-to-noise-and-distortion ratio (SNDR) for the

k-th subcarrier is given by

$$\mathrm{SNDR}[k] = \frac{\sigma^2[k]}{\sigma_D^2[k] + \sigma_W^2} = \frac{\left(G_{\mathrm{E}} LK \left|\bar{H}[k]\right|\right)^2}{\sigma_D^2[k] + \sigma_W^2}. \tag{2.3.13}$$

where $\sigma_W^2 = \mathrm{E}\left[|W[k]|^2\right] = \sigma_w^2$.

Using the SNDR, an approximation of BER can be derived for several modulation formats. In this paper, we specialize the derivation for square M-QAM constellations. In this case, assuming Gray labeling, the BER for the data modulated on the k-th subcarrier can be approximated as [90]

$$P_{\mathrm{e}}[k] \approx \frac{2\left(\sqrt{M}-1\right)}{\sqrt{M}\log_2 M}\mathrm{erfc}\left(\sqrt{\frac{3\cdot \mathrm{SNDR}[k]}{2\left(M-1\right)}}\right). \tag{2.3.14}$$

By averaging over the number of independent data-carrying subcarriers in the DCO-OFDM frame structure, $N_{\mathrm{D}} = N/2 - 1$, the overall BER is obtained as

$$P_{\mathrm{e}} = \frac{1}{N_{\mathrm{D}}} \sum_{k=1}^{N_{\mathrm{D}}} P_{\mathrm{e}}[k]. \tag{2.3.15}$$

Note, (2.3.14) relies on a Gaussian assumption for the distribution of clipping noise which is reasonable only when the number of carriers per group is sufficiently large. However, as shown in Sec. 2.5.2, (2.3.14) is often close to simulation results and is useful in predicting the general performance of different techniques.

2.3.3 Design of SO-OFDM Signals

Spatial Optical OFDM with Subcarrier Mapping

SO-OFDM with subcarrier mapping is a special case of SO-OFDM where each OFDM subcarrier is mapped to exactly one LED group. That is,

$$H_g[k] \neq 0 \rightarrow \forall g' \in \{1, \dots G\} \setminus \{g\} \;\; H_{g'}[k] = 0.$$

One possible method for mapping subcarriers to LED groups is contiguous subcarrier mapping where each LED group is assigned a number of adjacent subcarriers. In the case where subcarriers are divided equally among the LED groups, define $\epsilon = N_{\mathrm{D}}/G$ as the number of independent data-carrying subcarriers per LED group. The scaling factors for each group for $k = 1, \dots, N_{\mathrm{D}}$ are

$$H_g[k] = \begin{cases} H, & k = (g-1)\epsilon + 1, \dots, g\epsilon \\ 0, & \text{otherwise} \end{cases} \tag{2.3.16}$$

where H is a real-valued constant.

For SO-OFDM using contiguous subcarrier mapping with equal number of subcarriers per group, σ_g^2 in (2.3.2) is related to H and ϵ, as

$$\sigma_g^2 = \frac{2}{N}\epsilon H^2. \tag{2.3.17}$$

Substituting into (2.3.11) gives the useful subcarrier power

$$\sigma^2[k] = \frac{N}{2}\left(\frac{G_{\mathrm{E}}LK}{N_{\mathrm{D}}}\right)^2 \sigma_g^2\epsilon, \tag{2.3.18}$$

which is independent of k. Note that DCO-OFDM is a special case of SO-OFDM with subcarrier mapping and $G = 1$.

For the special case where $G = N_D$ (i.e., $\epsilon = 1$), a single independent subcarrier is assigned to each LED group and each group signal is sinusoidal with a PAPR of 3 dB, which is significantly smaller than the PAPR of conventional DCO-OFDM signals (see e.g. Fig. 3 in [69]). This special case enables a simple transmitter architecture where each transmit chain requires a simple oscillator to drive the LED. In another variation of this design, each LED can driven by a phase shift keying (PSK) modulated square wave carrier. In this case no DAC or DPD blocks per transmit chain are required.

Overlapped Spatial Optical OFDM

Overlapped SO-OFDM (OSO-OFDM) is a generalization of SO-OFDM which allows for subcarrier data to be repeated over more than one LED group. Given these added degrees of freedom, the $H_g[k]$ can be selected to optimize the PAPR or information rate of the resulting system. In this work, we adopt a simple design for $H_g[k]$ by constraining them to be the sampled Fourier transform of a Nyquist pulse. Recall that pulses satisfying the Nyquist criterion have the property that the sum of shifted replicas of the frequency responses is constant. In this way, the output OSO-OFDM signal is identical to that of a DCO-OFDM emitter. This scaling based on Nyquist pulses is chosen since the filters can be easily implemented, however, improved performance may be possible by optimizing $H_g[k]$.

In particular, in this work we consider the raised-cosine (RC) pulse and the double-jump (DJ) pulse [91]. The sampled frequency responses of the RC and DJ pulses,

used as the LED group filters for the first LED group $g = 1$, are given by

$$H_1^{\mathrm{RC}}[k] = \begin{cases} H, & |f[k]| \leq f_1 \\ \frac{H}{2}\left[1 + \cos\left(\frac{\pi}{\beta\epsilon}\left[|f[k]| - f_1\right]\right)\right], & f_1 < |f[k]| \leq f_2 \\ 0, & \text{otherwise} \end{cases} \tag{2.3.19}$$

and

$$H_1^{\mathrm{DJ}}[k] = \begin{cases} H, & |f[k]| \leq f_1 \\ \frac{H}{2} & f_1 < |f[k]| \leq f_2 \\ 0, & \text{otherwise} \end{cases} \tag{2.3.20}$$

respectively for $k = 1, 2, \ldots, N_{\mathrm{D}}$. The factor $\beta \in (0, 1]$ quantifies the degree of overlap with $f_1 = (1 - \beta)\epsilon/2$, and $f_2 = (1 + \beta)\epsilon/2$. The frequency sampling points, $f[k]$, are

$$f[k] = k - (\epsilon + 0.5).$$

For $g > 1$, $H_g[k]$ for $k = 1, \ldots, N_{\mathrm{D}}$ can be obtained by circularly shifting the elements of $[H_1[1]\ H_1[2]\ \ldots\ H_1[N_{\mathrm{D}}]]$ by $(g - 1)\epsilon$ samples. Note that $\beta \to 0$ corresponds to SO-OFDM with contiguous subcarrier mapping.

The DJ filter is the Nyquist pulse which, for a given energy and excess bandwidth β, maximizes H [92]. That is, for a given σ_g^2 (2.3.2), the DJ pulses have the largest useful power (2.3.11) reaching a maximum when $\beta = 1$ [92]. The RC filter was chosen due to its simple form and widespread use. In practice, $H_g[k]$ could be optimized for every σ_g to minimize BER.

For $\beta = 1$ and using the DJ pulse (2.3.20), the useful power of OSO-OFDM can

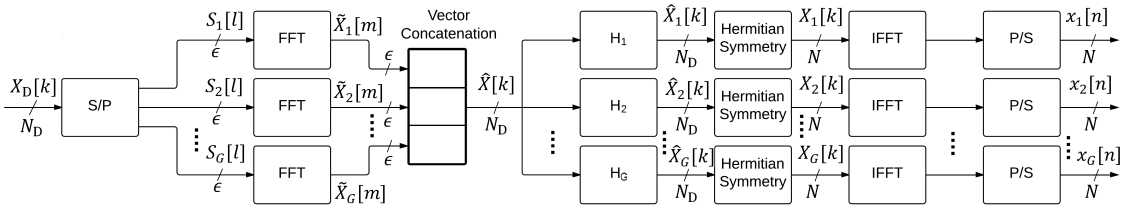

Figure 2.4: Details of the OSC-FDMA spatial processing block.

be found to be

$$\sigma^2[k] = N\left(\frac{G_{\mathrm{E}}LK}{N_{\mathrm{D}}}\right)^2 \sigma_g^2\epsilon, \tag{2.3.21}$$

which is 3 dB larger than (2.3.18) for the case of SO-OFDM with subcarrier mapping (i.e., OSO-OFDM with $\beta = 0$).

2.4 Optical Single-Carrier FDMA (SC-FDMA)

Single-Carrier FDMA (SC-FDMA) [73] precodes OFDMA with an FFT block, resulting in a single carrier output that has improved PAPR. SC-FDMA has been adopted for the uplink in 3GPP Long Term Evolution [93]. Previous work [79] directly applied SC-FDMA to VLC systems and applied clipping and biasing to be compatible with IM/DD channels. In this section, SC-FDMA is used in a novel fashion, termed *optical single-carrier FDMA* (OSC-FDMA) where spatial summing is applied to further improve PAPR performance.

Figure 2.4 presents the details of the spatial processing block of OSC-FDMA. The data vector $X_{\mathrm{D}}[k]$ is divided into G groups, each having $\epsilon = N_{\mathrm{D}}/G$ data symbols. The group symbols are denoted by $S_g[l]$ for $g = 1, 2, \ldots, G$ and $l = 0, 1, \ldots, \epsilon - 1$. The subcarrier data for group g, denoted by $\tilde{X}_g[m]$, are the FFT of the g-th group of data symbols, $S_g[l]$. The $\tilde{X}_g[m]$ are concatenated into a single vector $\hat{X}[k]$. Mapping

from $\hat{X}[k]$ to the groups is implemented by the bank of filters $H_g[k]$ as in SO-OFDM.

For OSC-FDMA, the $H_g[k]$ are defined to provide a disjoint set of carries in each of the $\hat{X}_g[k]$. This can be accomplished using conventional localized or interleaved mapping from SC-FDMA [73]. In this way, the LED groups data can be viewed as emitters for different virtual users in a multiple-access scheme where their emissions are not coordinated.

Overlapped OSC-FDMA (OOSC-FDMA) generalizes OSC-FDMA and permits for the power allocated to a given subcarrier to be distributed over multiple LED groups. This can be viewed as a coordinated emission amongst virtual users across different LED groups. Analogous to OSO-OFDM in Sec. 2.3.3, the $H_g[k]$ can chosen to optimize the PAPR or information rate. In this paper, we take the simple approach of selecting $H_g[k]$ from the sampled Fourier transforms of Nyquist pulses to ensure that the sum of the LED group outputs sum to produce an SC-FDMA signal.

2.5 Simulation Results

2.5.1 PAPR CCDF Results

In order to obtain an accurate estimate of the continuous-time PAPR, $x_g[n]$ is oversampled. Define $x_g^{\uparrow \ell}[n]$ as the ℓ-times oversampled version of $x_g[n]$. In practice this can be done by appending $(\ell - 1)N/2$ zeros to the end of $X_D[k]$ before applying Hermitian symmetry and taking the IFFT. The PAPR of the time-domain OFDM

symbol, before clipping, is defined as

$$\mathrm{PAPR}_g = \frac{\max\limits_{n=0,\ldots,\ell N-1} \left|x_g^{\uparrow\ell}[n]\right|^2}{\frac{1}{\ell N}\sum_{n=0}^{\ell N-1}\left|x_g^{\uparrow\ell}[n]\right|^2} = \frac{\left\|x_g^{\uparrow\ell}\right\|_\infty^2}{\frac{1}{\ell N}\left\|x_g^{\uparrow\ell}\right\|_2^2}. \tag{2.5.1}$$

In order to obtain an accurate approximation of the continuous-time PAPR, $\ell = 4$ was selected as demonstrated in [94].

A common way to assess the effectiveness of PAPR reduction techniques is the complementary cumulative distribution function (CCDF) of the PAPR at P dB is the probability that the PAPR is larger than P dB. The empirical CCDFs of PAPR for DCO-OFDM, SO-OFDM with contiguous subcarrier mapping (i.e., non-overlapped), and OSO-OFDM using RC and DJ pulse filtering with $\beta = 1$ are compared in Fig. 2.5(a). For all simulations $N = 194$ and $N_\mathrm{D} = N/2 - 1 = 96$. For all spatial summing techniques, $G = 12$ LED groups except for DCO-OFDM where $G = 1$ by construction. Similarly, the empirical CCDFs of PAPR of OSC-FDMA with $G = 1$ (proposed in [79]) and $G = 12$, and OOSC-FDMA using RC and DJ pulse filtering, both with $\beta = 1$ and $G = 12$ are compared in Fig. 2.5(b).

The PAPR CCDF results show that the proposed SO-OFDM techniques achieve a PAPR reduction gain with respect to DCO-OFDM. For instance, a PAPR reduction gain ranging from 0.87 dB for DJ filtered OSO-OFDM to 2.47 dB for SO-OFDM is achieved with respect to DCO-OFDM at a CCDF value of 10^{-3}. A general trend is that the PAPR increases with the number of modulated subcarriers in an LED group. Spatial optical OFDM achieves a PAPR reduction gain by distributing the OFDM subcarriers over G LED groups. DC-biased optical OFDM has N_D independent modulated subcarriers, while DJ filtered OSO-OFDM with $\beta = 1$ has $2\epsilon = 2N_\mathrm{D}/G$

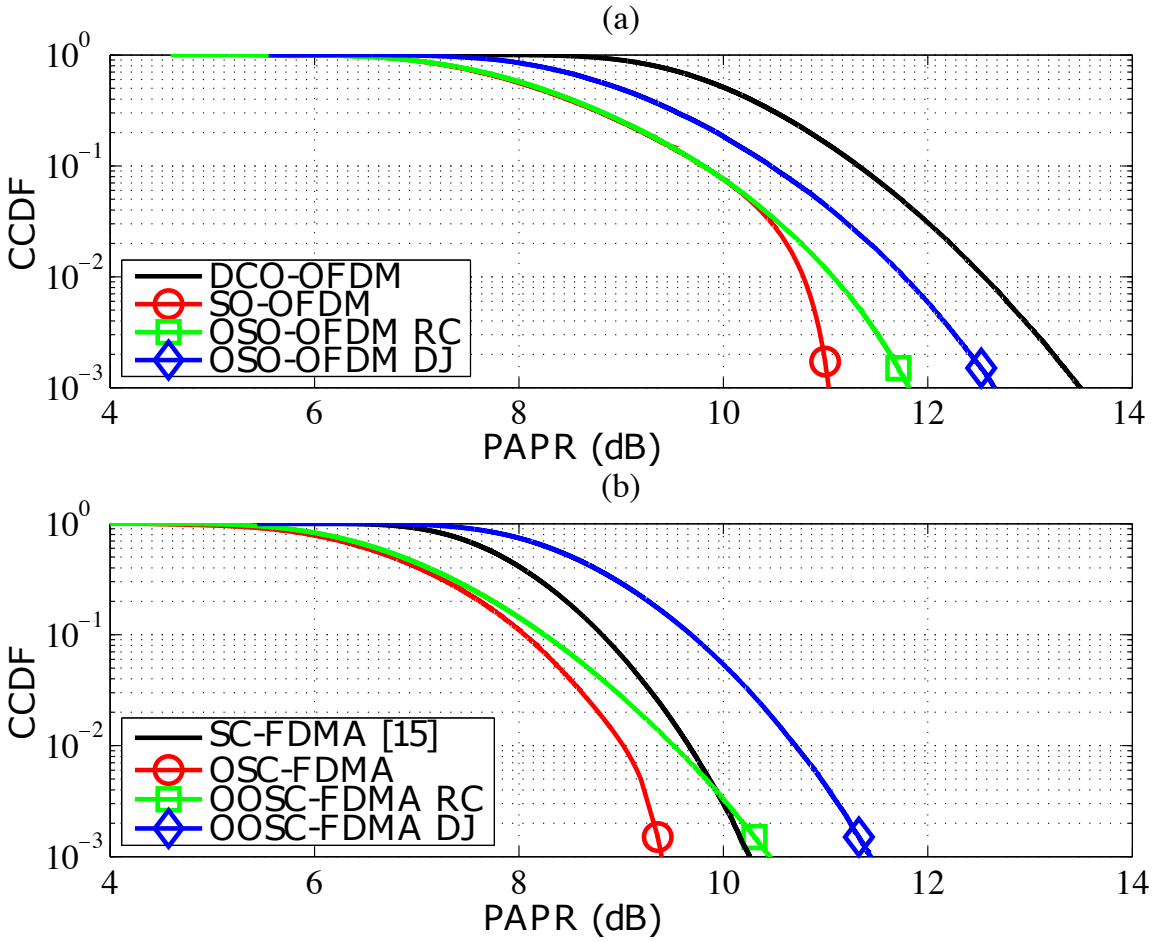

Figure 2.5: The CCDF of the PAPR for the different techniques based on (a) spatial optical OFDM and (b) optical SC-FDMA. In all cases, $N = 194$, $G = 12$ and $\beta = 1$ for overlapping techniques.

and SO-OFDM has $\epsilon = N_{\mathrm{D}}/G$ independent modulated subcarriers. Therefore, from Fig. 2.5(a), DCO-OFDM has the largest PAPR, followed by OSO-OFDM using DJ pulse filtering with $\beta = 1$, and SO-OFDM has the lowest PAPR. As for RC filtered OSO-OFDM with $\beta = 1$, the number of independent modulated subcarriers is the same as that of DJ filtered OSO-OFDM with $\beta = 1$, but the subcarriers are scaled by different scaling factor, leading to a PAPR close to that of SO-OFDM.

Comparing Figs. 2.5(a) and (b), it is clear that systems based on SC-FDMA have a lower PAPR than systems based on OFDM. Similar to SO-OFDM, overlapping involves modulating more carriers per LED group and increases PAPR. Also, OSC-FDMA and OOSC-FDMA using RC pulse filtering achieve lower PAPR than the SC-FDMA scheme proposed in [79]. The PAPR of OOSC-FDMA using DJ filter is higher that SC-FDMA due to the fact that the average mean squared value (denominator in (2.5.1)) is reduced to a greater extent than the peak amplitude. Note that the PAPR can also be reduced by using more LED groups, for a fixed FFT size N.

Using spatial optical OFDM, the PAPR can be reduced to 3 dB as $\epsilon \to 1$. It should be noted that although the PAPR indicates the likelihood of clipping distortion, it does not quantify the severity of the distortion induced.

2.5.2 BER Results

For all BER simulations, the Luxeon Rebel LED [86] is considered. The number of LEDs is $L = 12$ and $N < 200$. Simulations have verified that system performance depends on ϵ and analogous relative gains arise for larger N and G giving rise to the same ϵ values. The LEDs are oriented in the same direction and are placed close to each other, so that the channel gain to the receiver is assumed to be same for

each emitter. The levels in Fig. 2.1 are set to $I_{\mathrm{l}} = -250$ mA, $I_{\mathrm{u}} = 250$ mA and $I_{\mathrm{bias}} = 500$ mA. It is assumed that a DPD is used to linearize the relation between input current and the optical power output.

The receiver noise is assumed to be ambient induced shot noise and is modeled as AWGN. Using a worst case of the estimate of noise power spectral density is $N_0 \sim 10^{-16}$ mA^2/Hz and a receiver bandwidth of 20 MHz [63]. For all simulations, 4-QAM modulation with Gray labeling is used and the optical signal-to-noise ratio (OSNR) is defined as

$$\mathrm{OSNR} = \frac{RP_{\mathrm{R}}}{\sigma_W}.$$

The OSNR depends on the location and orientation of the receiver photodetector with respect to the LEDs, as well as the LED and photodetector parameters (Subsection 2.2.2).

For a given dynamic range, which is set by the LED driver, we assume that the communication designer is provided with a budget for the amount of luminous efficacy to be sacrificed for VLC. Using Figure 2.2, this fixes the value of σ_g, or equivalently γ_g, used in all simulations. This design approach differs significantly from previous work (e.g., [72]) where the value of σ_g is optimized at every OSNR to provide the best balance between clipping distortion and channel noise. While the approach in [72] optimizes communications performance for a single user, in practice it may be difficult to implement since it requires a complex luminary which tracks the OSNR at the receiver. In addition, it is not clear how this technique would be applied in the multi-user scenario. Spatial summing techniques and DCO-OFDM are compared for the same illumination performance with $\eta_{\mathrm{rel}} = 98\%$ in all simulations.

The BER is plotted against OSNR for $N = 26$ for an SO-OFDM system using

contiguous subcarrier in Fig. 2.6. For small values of OSNR, AWGN is the dominant source of noise. The simulation results show that using a smaller G, or equivalently, larger values of ϵ, results in lower BERs in this OSNR range. This can be explained from (2.3.18), which shows that the useful subcarrier power is proportional to ϵ. Therefore, in the low OSNR regime, where $\sigma_D^2[k]$ is negligible compared to σ_W^2, the SNDR (2.3.13) is also approximately proportional to ϵ. The best BER performance is achieved by using DCO-OFDM which has $G = 1$, and hence the maximum value of $\epsilon = N_{\mathrm{D}}$.

Clipping distortion dominates a high OSNR. Since $\sigma_D^2[k]$ is smaller for smaller ϵ, lower BER is achieved by using more LED groups. The high-OSNR BER advantage of spatial summing is more pronounced as ϵ is reduced (i.e., with a larger number of groups for a fixed N_D). In the special case of $\epsilon = 1$, the signals for each group are sinusoidal and PAPR = 3 dB, leading to less clipping distortion and a significantly smaller BER than DCO-OFDM. Similar gains can be had for larger numbers of carriers for the same value of ϵ. Notice that these gains in BER performance from reducing ϵ come at the expense of requiring additional transmit chains.

Figure 2.7 compares the BER of SO-OFDM, OSO-OFDM, SC-FDMA [79], OSC-FDMA with localized mapping, and OOSC-FDMA. The number of groups is 12, except for DCO-OFDM and SC-FDMA [79], where $G = 1$ by construction. The BER approximation (2.3.15) is also plotted for comparison for DCO-OFDM and all SO- and OSO-OFDM schemes.

There is a a small discrepancy between approximation and simulated BERs at high OSNR. This is due to the fact that (2.3.14) assumes that the clipping distortion is Gaussian distributed. This assumption becomes better for larger ϵ. For small

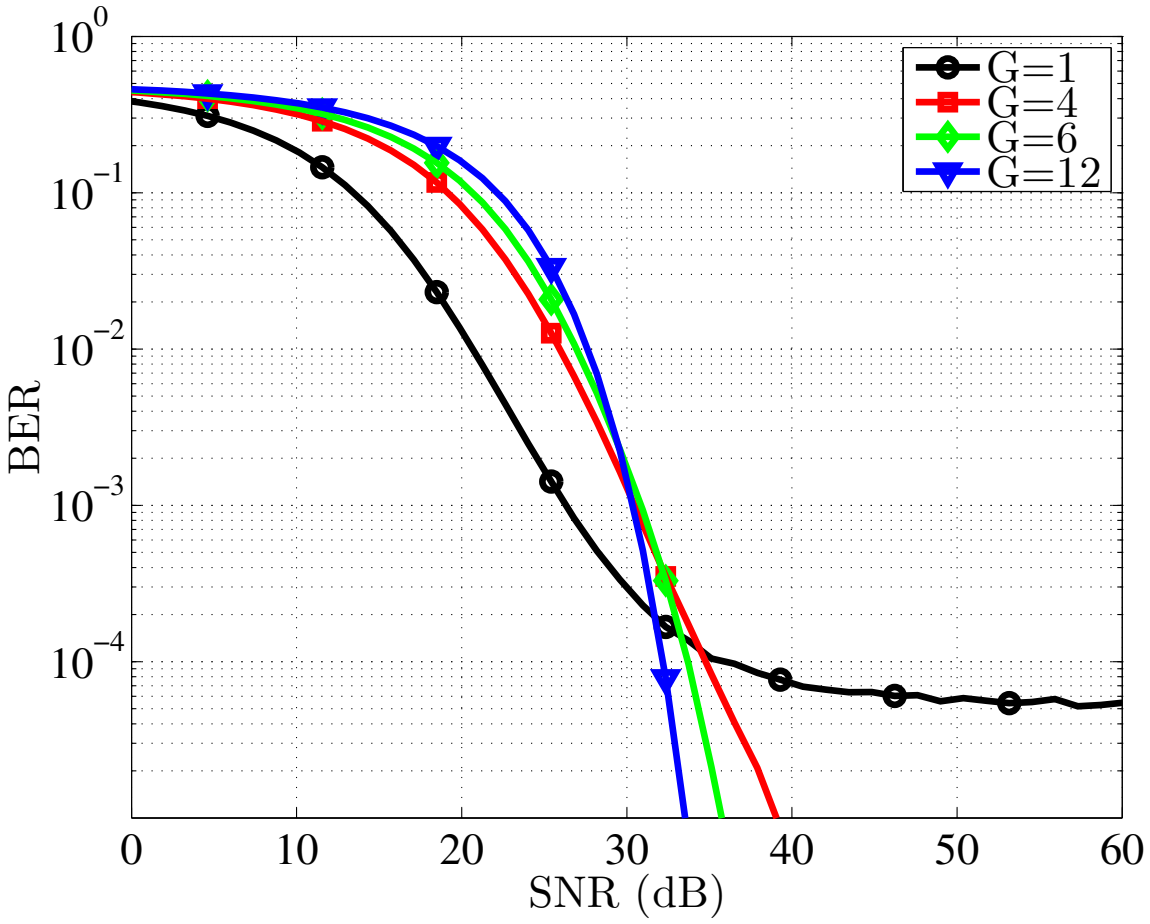

Figure 2.6: BER performance of SO-OFDM with contiguous subcarrier mapping, $G = 1, 4, 6, 12$, $N = 26$ and $\sigma_g = 250$ mA, corresponding to $\eta_{\text{rel}} = 98\%$.

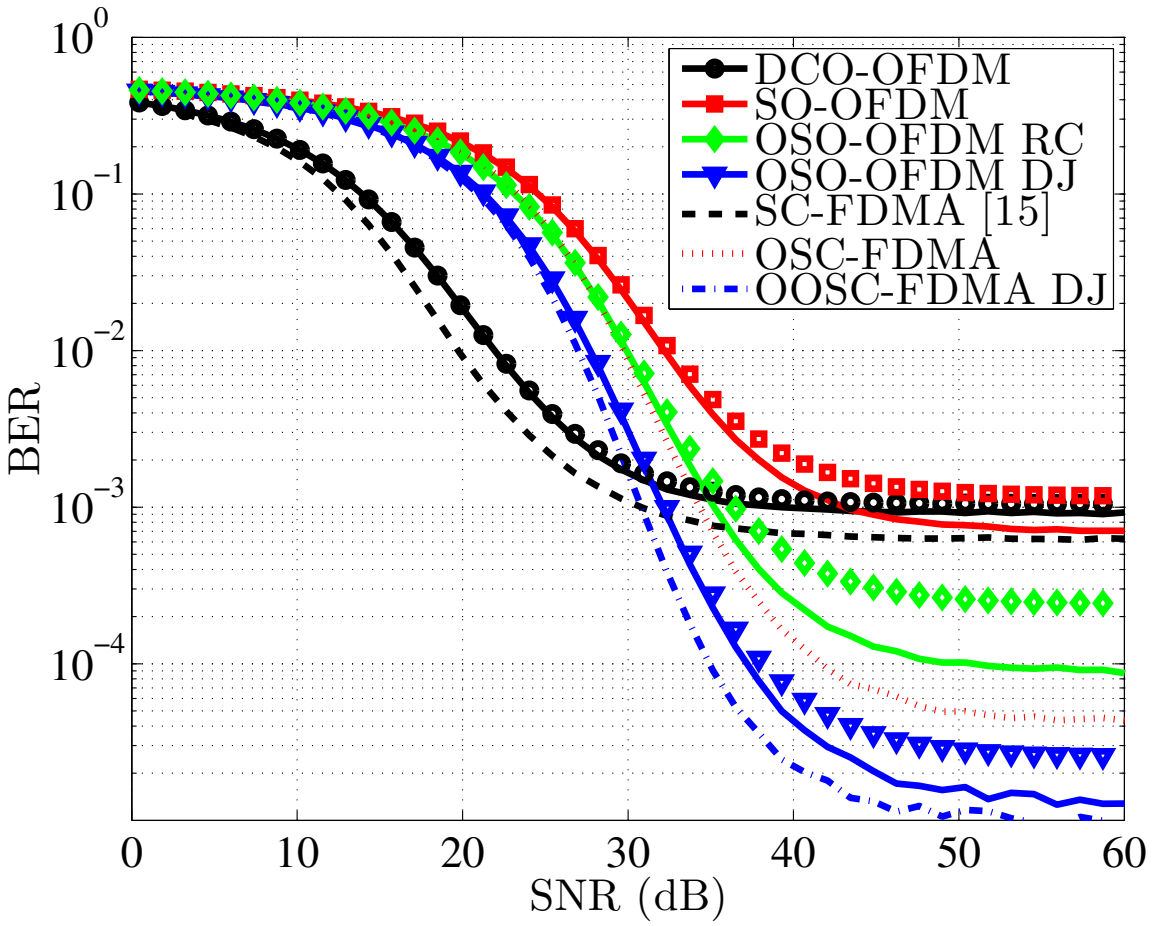

Figure 2.7: BER performance of different SO-OFDM and OSC-FDMA systems for $N = 194$, $G = 12$, $\beta = 1$, $\sigma_g = 250$ mA corresponding to $\eta_{\text{rel}} = 98\%$. Discrete points are the results of analytical approximation in (2.3.15).

OSNRs, the BER is determined by the AWGN channel noise, and the approximation and simulation BERs closely agree.

From Fig. 2.7, at high OSNRs, OSO-OFDM using DJ filtering outperforms OSO-OFDM using RC filtering. They both have a BER performance advantage over SO-OFDM with contiguous subcarrier mapping which does not offer a significant BER performance gain over DCO-OFDM for large N. This can be explained by considering Fig. 2.8(a) where the average useful subcarrier power σ^2 and σ_D^2 are plotted against G for SO-OFDM, OSO-OFDM using both RC and DJ filtering. The value for σ_D^2 is computed from (2.3.12) where the expectation is estimated by a Monte Carlo method. Figure 2.8(b) shows the signal-to-distortion ratio SDR $= \sigma^2/\sigma_D^2$ as a function of G for the same set of signaling techniques.

While DJ filtered OSO-OFDM has more clipping distortion than SO-OFDM and RC filtered OSO-OFDM (which have nearly equal σ_D^2), DJ filtered OSO-OFDM has higher σ^2 and higher σ^2/σ_D^2. This leads to lower BERs at high OSNRs (Fig. 2.7). Note also that SDR increases with G for all SO-OFDM techniques. Therefore, using more LED groups makes the group signals more resistant to clipping distortion, which is dominant at high OSNRs. The increase of SDR with G is modest for $N = 194$, as G is varied from 2 to 12 corresponding to a minimum $\epsilon = 8$. As noted in Fig. 2.6, the largest gains in SDR occur when $\epsilon \to 1$.

From Fig. 2.7, OOSC-FDMA using DJ filtering offers the best BER performance, followed by OSO-OFDM using DJ filtering. Overlapped optical SC-FDMA using DJ filtering with $\beta = 1$ combines the small PAPR of SC-FDMA techniques (e.g., see Fig. 2.5), with the high useful signal power of DJ pulses with $\beta = 1$.Notice that the error floors in the BER curves of Fig. 2.7 could be lowered by reducing σ_g^2 and thereby

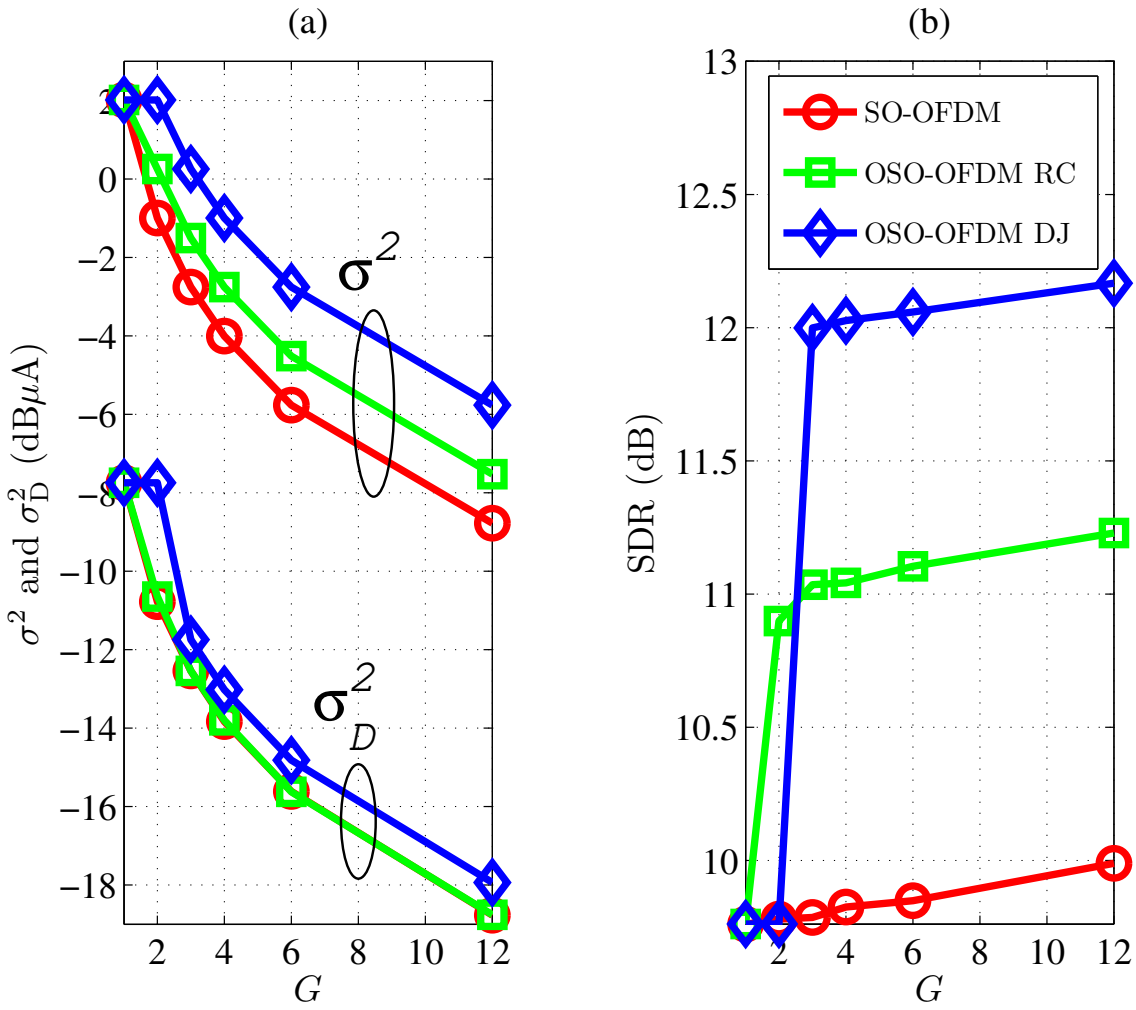

Figure 2.8: (a) The average useful subcarrier power, σ^2, and the average clipping distortion noise power, $\sigma_{\rm D}^2$, averaged over all $N_{\rm D}$ subcarriers, versus G for SO-OFDM and OSO-OFDM using both RC and DJ pulse filtering with $\beta = 1$. (b) The signal-to-distortion ratio SDR $= \sigma^2/\sigma_D^2$ versus G. In all cases, $N = 194$, $\sigma_g = 250$ mA, and OSNR $= 40$ dB.

incurring less clipping distortion and increasing η_{rel}.

2.6 Conclusions

This paper proposes spatial summing to alleviate many practical issues in the implementation of OFDM in VLC systems. The approach partitions wideband OFDM signals into a series of narrowband signals used to drive groups of LEDs and then to rely on spatial summing during propagation. Two main variations of optical OFDM based on spatial summing have been described based on their frequency-domain structure: SO-OFDM and OSC-FDMA. Both of these classes can use either one-to-one mapping of subcarriers to different LED groups, or allow for overlap of subcarriers between different LED groups using filtering. The BER results show that in the low OSNR regime, DCO-OFDM and SC-FDMA outperform spatial summing techniques. However, at high OSNRs typical of VLC systems, spatial summing techniques outperform DCO-OFDM and SC-FDMA due to their immunity to clipping distortion. Similar to the development of OSC-FDMA from SC-FDMA, spatial summing can extend other PAPR reduction techniques to improve their performance on VLC channels [71].

Since illumination is taken as the primary role of the luminary, a link between lighting design and communication system parameters was established by considering the impact of modulation on the luminous efficacy of the LEDs. All communication systems are compared on the basis of having identical illumination performance, as measured by η_{rel}.

Our ongoing research directions include optimizing group signals, applying spatial

summing to other PAPR reduction techniques, design of power and bit loading for SO-OFDM as well as prototypes. The goal is to realize OFDM based on spatial summing using a simple transmitter architecture. Of particular interest in this regard is the simple case of a single independent data-carrying subcarrier per LED group ($\epsilon = 1$), which allows the use of a digital signal to drive each LED, thereby eliminating the need for DACs and DPD blocks.

Chapter 3

Amplify-and-Forward Integration of Power Line and Visible Light Communications

In **Chapter 2**, SO-OFDM was shown to outperform conventional DCO-OFDM in PAPR reduction and BER performance at high optical SNRs typical of indoor VLC systems. In this chapter, the advantages of SO-OFDM are harnessed to improve the overall information capacity of integrated PLC/VLC systems discussed in Sec. 1.4. In particular, following the requirement for system simplicity and cost-effectiveness expressed in the thesis vision (Sec. 1.5), a simple all-analog amplify-and-forward module is used to frequency down-shift the PLC signal to match the bandwidth of the LEDs, and filter the wideband PLC signal into multiple narrowband signals. Each narrowband signal is assigned to a different LED group for SO-OFDM transmission. The PAPR and the overall capacity of the integrated PLC/VLC system using SO-OFDM in the VLC subsection are compared to those of conventional DCO-OFDM.

The work in this chapter appeared in the Proceedings of the *2015 IEEE Global Conference on Signal and Information Processing (GlobalSIP),* (Pages: 1322 – 1326, December 2015) [65].

Abstract This paper proposes a low-complexity scheme for the integration of power-line communication (PLC) and visible-light communication (VLC) systems. Rather than decoding the PLC signal prior to transmission from an LED luminary, a simple all-analog PLC/VLC amplify-and-forward (AF) module is described. The incoming PLC signals, which occupy a band of 2-28 MHz, are frequency down-shifted prior to transmission to increase the usable bandwidth of the LEDs. The required DC bias is then added to make the signals compatible with intensity modulation/direct detection (IM/DD). In addition to DC-biased optical OFDM (DCO-OFDM), spatial optical OFDM (SO-OFDM) is applied to PLC/VLC integration. In SO-OFDM, the LEDs are divided into groups, and each group of LEDs is modulated by a different filtered OFDM signal. The results show that frequency down-conversion of the PLC spectrum prior to forwarding provides an improvement in capacity, while SO-OFDM provides a peak-to-average power ratio (PAPR) reduction which translates into improved capacity when the VLC link is operating in the high signal-to-noise ratio (high-SNR) regime.

3.1 Introduction

The need for broadband distribution indoors, both wirelessly and wired, as well as the scarcity and congestion of radio bands has motivated research into complementary networks [95]. Two of such alternatives are power-line communication (PLC) [96] and visible light communication (VLC) [12]. Power-line communication exploits the existing AC electric power transmission infrastructure for data communication. However, stand-alone PLC networks do not support mobility or the ability to broadcast data over a wide area. In an analogous fashion, VLC systems use existing luminaries based

on energy-efficient light-emitting diodes (LEDs) to transmit data by imperceptibly modulating their brightness. Although VLC networks have the potential to provide wide-spread coverage indoors, they require a fast and cost-effective backbone.

There are many possible usage cases for the integration of PLC with VLC. An example of a narrowband application of the integration of VLC and PLC systems is in home automation, where one terminal is used to remotely control a variety of home appliances. While, a wideband application includes the use of an integrated PLC/VLC system as the downlink in a Wi-Fi assisted full-duplex system.

The integration of PLC and VLC networks seems natural as AC power infrastructure is already available at VLC luminaries. The promise of linking PLC and VLC to yield a simple and inexpensive solution which does not require extensive changes to infrastructure attracted interest since the early days of VLC research [97, 98]. More recently, the transmission between PLC and VLC has been cast as a *relaying* problem in [53] followed by an experimental demonstration in [52] and [99]. There are two fundamental ways in which the PLC-to-VLC relay can be categorized. In the decode-and-forward (DF) configuration, each luminary demodulates and decodes the incoming data on the PLC link and retransmits on the VLC link using appropriate modulation. In amplify-and-forward (AF), the luminary is able to filter and amplify the incoming analog signal from the PLC link before adding a DC bias and driving the LEDs. Although DF, may have better communication performance, it requires significant signal processing which will negatively impact energy efficiency and cost of the luminary. In contrast, AF can be implemented using simple analog circuits which can be power efficient and will result in a more compact luminary [52, 53]. Energy

efficiency is a key metric for any solid-state lighting fixture, not only for environmental reasons, but also to prolong premature device failure due to LED heating [74]. In addition, the orthogonal frequency division multiplexing (OFDM) modulation scheme used in many PLC links has also been proposed for high-speed VLC systems [100].

In this paper, due to the potential for simple, energy-efficient implementations, we consider the development of AF relaying systems to realize PLC-VLC integration. In contrast with earlier work on AF PLC/VLC relaying [52, 53, 99], here simple analog signal processing architectures are proposed in which the signals carried by PLC and VLC are *not identical*. We propose and investigate the use of an analog frequency shifter in the luminary to translate the PLC spectrum to make it compatible with the VLC channel. In addition, we study for the first time the use of spatial-optical-OFDM (SO-OFDM) in the integrated PLC/VLC system. In SO-OFDM, LEDs are divided into groups, and each group of LEDs is modulated by a different filtered OFDM signal in order to reduce peak-to-average power ratio (PAPR) and improve the high signal-to-noise ratio (high-SNR) performance of the overall system.

The remainder of the paper is organized as follows. In Section 3.2, the integrated AF PLC/VLC system is presented with SO-OFDM and frequency translation techniques. The performance of the analog AF relaying techniques are compared through numerical simulations in Section 3.3. Conclusions and future directions are provided in Section 3.4.

3.2 System Description

A functional block diagram of the proposed integrated AF PLC/VLC system is shown in Fig. 3.1. The first main block of the system is the PLC OFDM modulator

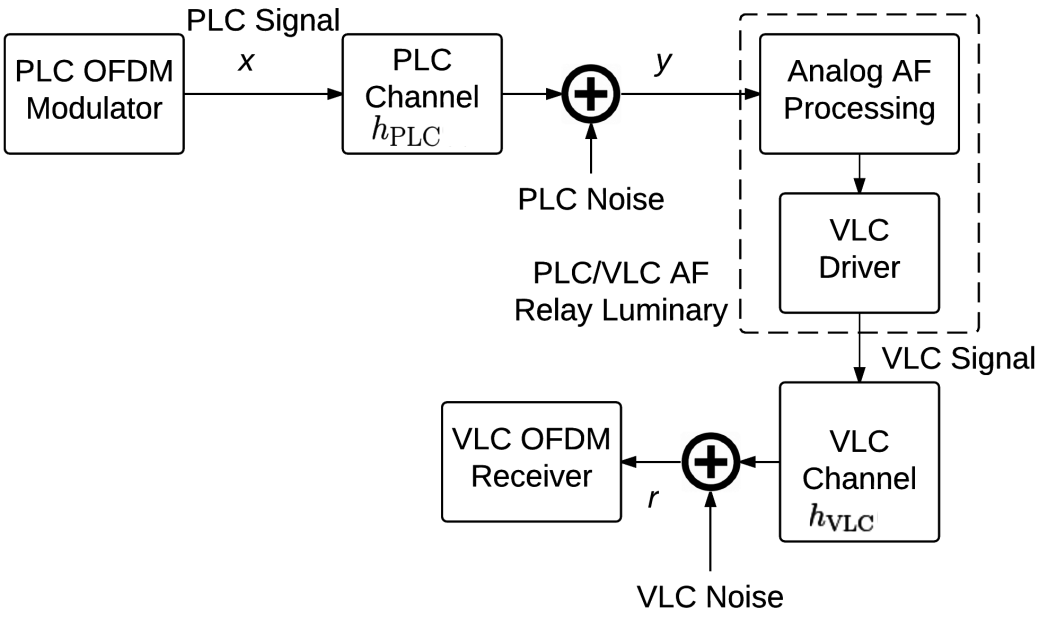

Figure 3.1: Functional block diagram of the proposed integrated PLC/VLC system. that modulates the OFDM subcarriers. The OFDM signal is transmitted through the power-line channel and is corrupted by PLC noise. A VLC-enabled luminary acts as an electrical-to-optical AF relay that uses the PLC OFDM signal to modulate the LED lights. After photodetection, an OFDM receiver recovers the data. Note, that an implicit assumption is that a control channel exists from VLC receiver to the PLC transmitter (e.g., WiFi or infrared uplink).

3.2.1 Power Line Communications

PLC channels suffer from a host of impairments: high attenuation, deep frequency notches, forbidden bands due to electromagnetic compatibility issues, narrowband interferers as well as impulsive noise and colored background noise [101, Ch. 2]. OFDM has been adopted for the physical layer of modern broadband PLC systems such as

those specified in the IEEE 1901[1] and ITU-T G.hn standards [102, 103, 104] due to its ability to mitigate and avoid many of these impairments [101, Ch. 5].

The PLC modem modulates the QAM constellation data, X onto the OFDM subcarriers, and performs the N-point inverse discrete Fourier transform (IDFT) and digital-to-analog conversion to obtain a time-domain signal x_{PLC} with variance $\sigma_x^2 = \mathrm{E}\{x_{\mathrm{PLC}}^2\}$. Due to Hermitian symmetry the number of independent data-carrying subcarriers is $N_{\mathrm{D}} = (N-2)/2$ [105]. The signal is transmitted through the power line, and is corrupted by the power-line channel with the impulse response h_{PLC} and PLC noise. Since mainly distortions due to h_{PLC} are relevant for the study of the proposed integrated AF PLC/VLC system, and for simplicity, we model the PLC noise as additive white Gaussian noise (AWGN)[2] with power spectral density (PSD) $N_{0,\mathrm{PLC}}$. Thus, the PLC signal received at the luminary is

$$y(t) = (h_{\mathrm{PLC}} * x_{\mathrm{PLC}})(t) + w_{\mathrm{PLC}}(t), \quad \forall t \in \mathbb{R}\,, \tag{3.2.1}$$

where w_{PLC} is the PLC noise. The PLC "transmitter SNR" is defined as

$$\mathrm{SNR}_{\mathrm{PLC}} = \frac{\sigma_x^2}{N_{0,\mathrm{PLC}} W}\,, \tag{3.2.2}$$

where W is the signal bandwidth. The time-domain OFDM signal, x_{PLC}, is well approximated as Gaussian random process and suffers from a high PAPR [71].

[1]The IEEE 1901 standard includes two physical layer formats, one referred to as windowed OFDM and the other as Wavelet-OFDM [102].

[2]The inclusion of narrowband and colored background noise is straightforward for the considered OFDM transmission. The addition of impulsive noise will cause outage events similar to the case of PLC-only transmission.

3.2.2 Visible Light Communications

OFDM has also been extensively studied for VLC [19, 61, 66, 106]. A number of techniques have been proposed to obtain a unipolar OFDM signal suitable for intensity modulation/direct detection VLC, however, adding a bias as in DCO-OFDM is most popular [67].

The received OFDM signal from the PLC channel is assumed to be zero mean and is scaled to have a power of σ^2. Then, the signal is hard-clipped to fit into the dynamic range of the LED driver. Denote the upper and lower LED current clipping levels by I_{u} and I_{l}, respectively. The clipping ratio, γ is defined as

$$\gamma = \frac{(I_{\mathrm{u}} - I_{\mathrm{l}})/2}{\sigma} \tag{3.2.3}$$

The clipping ratio γ quantifies the severity of the clipping and the nonlinear distortion (NLD) noise power. Lower values of γ correspond to more clipping distortion.

According to Bussgang's theorem [89], the output signal of the nonlinear clipping function can be modeled as

$$y_{\mathrm{clipped}}(t) = Ky(t) + d(t), \quad \forall t \in \mathbb{R}\,, \tag{3.2.4}$$

where K is a constant that depends on the variance of the input signal $\sigma_y^2 = \mathrm{E}\{y^2\}$ and the clipping levels I_{u} and I_{l}, as

$$K = \mathrm{erf}\left(\frac{I_{\mathrm{u}} - I_{\mathrm{l}}}{2\sqrt{2}\sigma}\right), \tag{3.2.5}$$

and d is the NLD noise.

In order to make the clipped DCO-OFDM signal compatible with intensity modulated/direct detection (IM/DD) system, a bias is added so that

$$y_B(t) = y_{\text{clipped}}(t) + B, \quad \forall t \in \mathbb{R} \, . \tag{3.2.6}$$

To ensure the non-negativity of all $y_B(t)$, $B \geq -I_{\text{l}}$.

For a system with L LEDs, the photodetector current is the sum of the contributions from all LEDs plus the receiver noise w_{VLC}, modeled as AWGN with (PSD) $N_{0,\text{VLC}}$:

$$r(t) = LG_{\text{E}}(h_{\text{VLC}} * y_B)(t) + w_{\text{VLC}}(t), \quad \forall t \in \mathbb{R} \, , \tag{3.2.7}$$

where h_{VLC} is the impulse response of the VLC channel normalized to have a DC gain of unity, and G_{E} is the overall electrical gain of the system including the gain of the AF block, LED conversion factor [W/A], the DC optical channel gain, and the photodetector responsivity [A/W]. The VLC channel response h_{VLC} is dominated by the slow response of the phosphor-coated LED. Note also that for DCO-OFDM, all LEDs in a luminary are modulated by the same signal.

The average photodetector current is given by

$$I_{\text{avg}} = \text{E}\{r\} = LG_{\text{E}}B \tag{3.2.8}$$

For later use, we define the SNR as

$$\text{SNR} = \frac{I_{\text{avg}}}{\sqrt{N_{0,\text{VLC}}W}} = \frac{RP_{\text{R}}}{\sqrt{N_{0,\text{VLC}}W}} \tag{3.2.9}$$

where R is the photodetector responsivity and P_{R} is the average received optical

power.

Finally, analog-to-digital conversion and a DFT are performed on the received signal r followed by perfect channel equalization and bit detection. Define the *useful signal* for the k-th subcarrier, $k \in \{1, 2, \ldots, N_{\mathrm{D}}\}$, as the received signal with no PLC or VLC noise,

$$S_{\mathrm{useful}}[k] = KLG_{\mathrm{E}}H_{\mathrm{PLC}}[k]H_{\mathrm{VLC}}[k]X[k] \,, \tag{3.2.10}$$

where $H_{\mathrm{PLC}}[k]$ and $H_{\mathrm{VLC}}[k]$ are samples of the Fourier transforms of h_{PLC} and h_{VLC}, respectively. The total noise (including PLC noise, VLC noise, and NLD) for the k-th subcarrier is then given by the difference:

$$W_{\mathrm{total}}[k] = R[k] - S_{\mathrm{useful}}[k], \quad k \in \{1, 2, \ldots, N_{\mathrm{D}}\} \,, \tag{3.2.11}$$

where $R[k]$ is the DFT of the sampled received signal.

The useful SNR for the k-th subcarrier is defined as the ratio of the useful signal power $\mathrm{E}\left\{|S_{\mathrm{useful}}[k]|^2\right\}$ to the total noise power $\mathrm{E}\left\{|W_{\mathrm{total}}[k]|^2\right\}$:

$$\mathrm{SNR}_{\mathrm{useful}}[k] = \frac{\mathrm{E}\left\{|S_{\mathrm{useful}}[k]|^2\right\}}{\mathrm{E}\left\{|W_{\mathrm{total}}[k]|^2\right\}}, \quad k \in \{1, 2, \ldots, N_{\mathrm{D}}\} \,. \tag{3.2.12}$$

The overall system capacity can then be computed as

$$C = \frac{1}{N} \sum_{k=1}^{N_{\mathrm{D}}} \log_2 \left(1 + \mathrm{SNR}_{\mathrm{useful}}[k]\right) \tag{3.2.13}$$

in units of bits/channel use.

3.2.3 Analog AF Relaying Techniques

This section outlines some details of the novel AF PLC/VLC techniques which do a limited amount of analog processing before transmission.

Spatial Optical OFDM

Spatial optical OFDM, introduced in [61, 66], divides the available LEDs into a number of LED groups. The incoming PLC signal is filtered (before clipping) at the luminary to obtain the LED group signals

$$y_g(t) = (h_g * y)(t), \quad \forall t \in \mathbb{R}, \tag{3.2.14}$$

for $g = 1, 2, \ldots, G$ where G is the number of LED groups. After filtering, each SO-OFDM group signal is scaled to have a specified variance σ^2, so that the desired value of the clipping ratio γ in (3.2.3) is obtained for all LED groups.

The filtered outputs emitted by each LED are allowed to overlap in time. In this paper, we consider overlapped SO-OFDM with raised-cosine (RC) pulse filtering (with an excess bandwidth factor $\beta = 1$) [61]. The sampled frequency response of the RC pulse with $\beta = 1$, used as the LED group filters for the first LED group $g = 1$, is given by [61]

$$H_1[k] = \begin{cases} \frac{1}{2}\left[1 + \cos\left(\frac{\pi}{\epsilon}\left[|f[k]|\right]\right)\right], & 0 < |f[k]| \leq \epsilon \\ 0, & \text{otherwise} \end{cases} \tag{3.2.15}$$

for $k = 1, 2, \ldots, N_{\mathrm{D}}$. The factor $\epsilon = N_{\mathrm{D}}/G$ is defined as the number of data carrying subcarriers per LED group. The other half of the filter is defined so that the

vector $H_1[k],\ k = 0, 1, \ldots, N-1$ satisfies Hermitian symmetry [66]. For $g > 1$, $H_g[k]$ for $k = 1, \ldots, N_{\mathrm{D}}$ can be obtained by circularly shifting the elements of $[H_1[1]\ H_1[2]\ \ldots\ H_1[N_{\mathrm{D}}]]$ by $(g-1)\epsilon$ samples.

The reason for this choice is that this filter has a smooth roll-off and thus an analog filter can be easily designed and implemented.

Spatial optical OFDM has a smaller PAPR than DCO-OFDM since only by a fraction of all PLC OFDM subcarriers are modulated in a given LED.

Frequency Translation

Broadband PLC systems typically operate in the frequency band from about 2 MHz to 28 MHz. If the PLC signal is used directly to modulate the LED lights, the portion from 0 to 2 MHz of the limited LED bandwidth is wasted. In this paper, we propose to frequency down-convert the PLC signal by 2 MHz in the PLC-to-VLC module. Since the VLC channel response is dominated by the frequency response of the LED [63], which has low-pass characteristics [74], this frequency-shifting leads to higher VLC channel gains for all OFDM subcarriers. This, in turn, leads to a superior bit-error rate (BER) performance and a higher overall channel capacity as compared to the conventional case where no frequency shifting is used. The frequency translation operation can be implemented in a number of ways, however, a simple technique amenable to analog implementation is the Weaver single-sideband modulator [107].

3.3 Simulation Results

In this section we compare our proposed SO-OFDM to the conventional DCO-OFDM in terms of PAPR and overall channel capacity. In addition, the gain due to

the frequency shifting of the PLC spectrum is assessed in terms of the improvement in the overall channel capacity as compared to the case where no frequency shifting is used.

3.3.1 Parameters

A software tool for channel generation, developed using the procedure described in [108], is available at [109] where three default channels (best, medium, worst) are provided. In all simulations, the medium PLC channel is used. The number of independent data-carrying subcarriers $N_{\mathrm{D}} = 256$. The smallest subcarrier frequency is 2.026 MHz and the subcarrier spacing is 24.4 kHz as specified in the IEEE 1901 PLC standard [102]. The PLC transmitter SNR is set to a typical value of $\mathrm{SNR}_{\mathrm{PLC}} = 55$ dB.

The VLC channel is modeled by a low-pass frequency response with a 3-dB bandwidth of 3 MHz [63]. This model takes into account the slow response of the phosphor coating used to obtain white light from a blue LED.

3.3.2 PAPR Results

An accurate estimate of the continuous-time PAPR can be obtained by sufficiently sampling y_g. Consider sampling y_g with ℓ-times the baud rate to yield $y_g^{\uparrow \ell}$. The PAPR of the time-domain OFDM symbol, before clipping, is

$$\mathrm{PAPR}_g = \frac{\max\limits_{n=0,\ldots,\ell N-1} \left| y_g^{\uparrow \ell}[n] \right|^2}{\frac{1}{\ell N} \sum_{n=0}^{\ell N-1} \left| y_g^{\uparrow \ell}[n] \right|^2} = \frac{\left\| y_g^{\uparrow \ell} \right\|_\infty^2}{\frac{1}{\ell N} \left\| y_g^{\uparrow \ell} \right\|_2^2}. \tag{3.3.1}$$

As demonstrated in [94], $\ell = 4$ is sufficient to obtain an accurate approximation of the continuous-time PAPR.

The empirical complementary cumulative distribution functions (CCDFs) of PAPR for DCO-OFDM and SO-OFDM using RC pulse filtering with $\beta = 1$ and 4-QAM data symbols are compared in Fig. 3.2. As noted in our earlier work [61, 66], as the number of groups grows G, SO-OFDM becomes less impacted by clipping noise. Notice this increase in groups, though useful to reduce clipping noise, comes at the expense of needing more drivers for the groups. However, since they have lower PAPR, energy efficient narrow band LED drivers are available.

3.3.3 Capacity Results

The overall capacity (3.2.13) of DCO-OFDM and SO-OFDM using RC pulse filtering with $\beta = 1$ and $G = 16$ are compared in Fig. 3.3 where the capacity is plotted against the electrical SNR (3.2.9) in dB. The solid curves correspond to the conventional case where no frequency shifting is used while the dashed curves correspond to Frequency-Shifted DCO-OFDM (FS-DCO-OFDM) and Frequency-Shifted SO-OFDM (FS-SO-OFDM) where frequency-shifting the PLC spectrum down by 2 MHz is used. The clipping levels are set to $I_{\mathrm{l}} = -250$ mA and $I_{\mathrm{u}} = 250$ mA. The clipping ratio for both DCO-OFDM and SO-OFDM is set to $\gamma = 2$ which gives a good balance between system noise effects (PLC noise and VLC noise) and NLD clipping noise.

Notice from Fig. 3.3 that, in the low-SNR regime, where VLC and PLC noise dominate over the NLD noise, DCO-OFDM has a higher capacity than SO-OFDM since DCO-OFDM has more useful subcarrier power. However, in the high-SNR

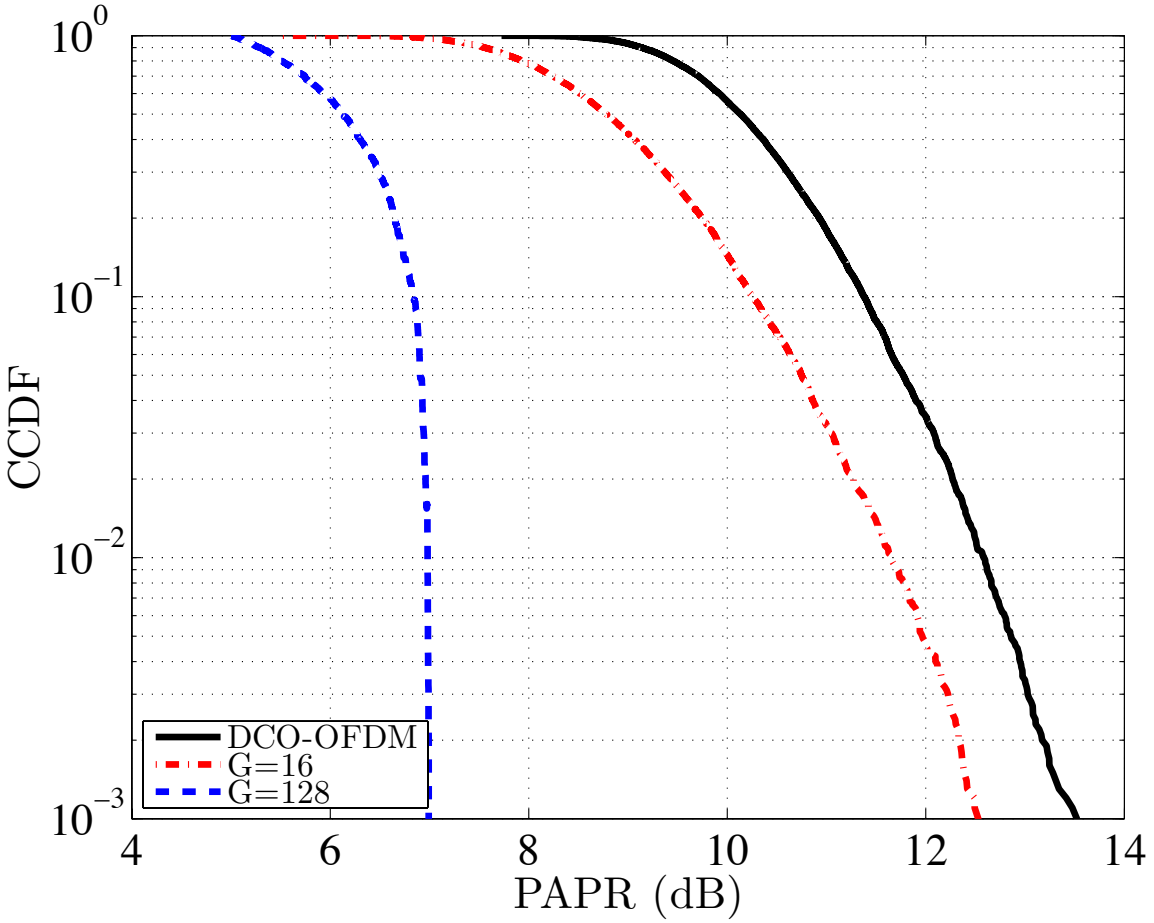

Figure 3.2: The CCDF of the PAPR for DCO-OFDM ($G = 1$) and SO-OFDM (with $G = 16, 128$). In all cases, $N_{\mathrm{D}} = 256$.

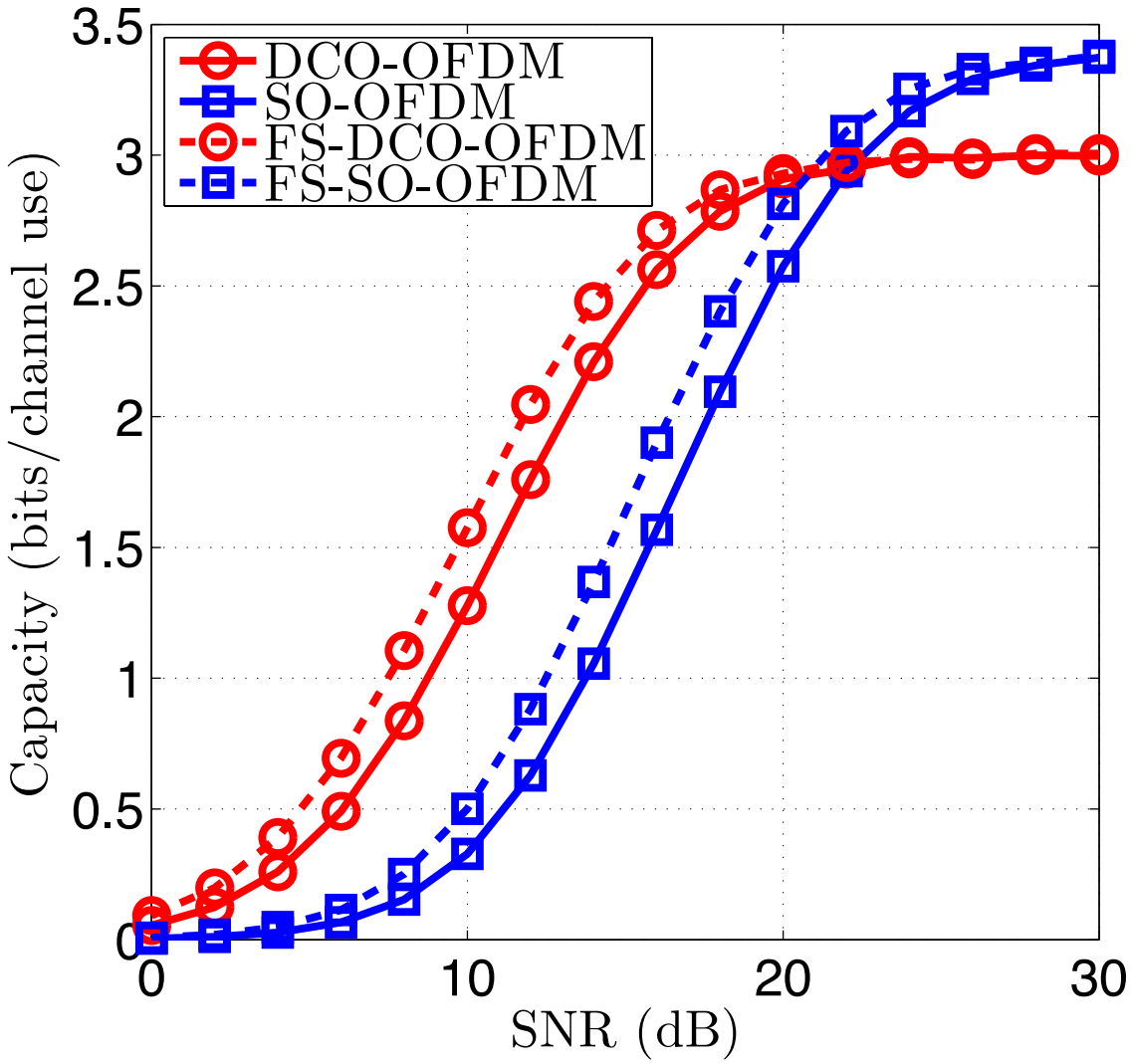

Figure 3.3: Capacity comparison between DCO-OFDM and SO-OFDM using RC pulse filtering with $G = 16$ and $\beta = 1$, both conventional (solid curve) and frequency-shifted (dotted curve).

regime, where NLD noise effects are dominant, the capacity of SO-OFDM becomes higher. Since SO-OFDM has a lower PAPR than DCO-OFDM, it is more robust to NLD effects, arising due to the limited dynamic range of the driver and the LED nonlinearities. We also note the effect of the proposed frequency-shifting in improving the capacity of both DCO-OFDM and SO-OFDM compared to the corresponding conventional cases where no frequency-shifting is used.

While these gains come at the expense of an increase in the overall system complexity, the increase in complexity is not significant since a simple AF relay is used in the VLC-enabled luminary where all the processing is done in analog domain.

3.4 Conclusions and Future Work

In this paper, we have proposed simple analog amplify-and forward PLC/VLC integration schemes where no demodulation of the PLC signal is performed at the luminary. The underlying approach was to not only echo the received PLC signal, but to do some simple pre-processing before driving the LED. Two novel ideas were introduced for PLC/VLC integration. The first is the use of spatial optical OFDM for PAPR reduction in PLC/VLC relays, leading to capacity gains in the high-SNR regime where NLD effects limit the performance of DCO-OFDM. Since SO-OFDM sends many narrowband signals, it has the benefit of being able to be implemented by energy efficient line drivers. The second key contribution in this paper is the recognition that frequency translating the PLC signal down by 2 MHz to make better use of the limited LED bandwidth can produce gains in the capacity of the overall system. This frequency translation technique can be applied to both DCO- or SO-OFDM modulation methods.

Future work includes extending the analysis to a more complete PLC model which includes the effect of impulsive noise. In addition, a prototype implementation of this simple analog AF techniques coupled to a standard PLC modem is also planned.

Chapter 4

Square-Wave Spatial Optical Orthogonal Frequency-Division Multiplexing

One of the primary findings of the work presented in **Chapter 2** is that in order to increase the effectiveness of the SO-OFDM technique in reducing the PAPR and NLD noise, a large number of SO-OFDM LED groups is required. Each LED group requires a complex transmit chain containing an IFFT block, a DPD block, and a multi-level DAC. This increases the complexity and cost of the VLC transmitter. This is the motivation behind the work in this chapter, where the need for simpler transmitter designs is addressed. In particular, this chapter introduces SW-SO-OFDM, a novel signaling design technique that uses a binary-level signal to modulate the LED current. Binary-level signals can be generated by simple clock division and do not require IFFT, DPD, or DAC, which considerably reduces VLC transmitter complexity. The use of square-wave carriers also comes with an SNR advantage over the

use of sinusoidal carriers since, in this chapter, it is proven through an optimization problem that, under symmetrical clipping constraints, a 50% duty cycle square wave has the largest fundamental-frequency component of all periodic carriers. The use of square-wave carriers is motivated by the insight of VLC channels and the fact that they are not spectrally confined, i.e., out-of-band emissions (in this case higher order frequency harmonics of square-wave carriers) can be transmitted and the low-pass VLC channel filters out these components. In addition, in order to extend the modulation capability of SW-SO-OFDM to multi-level QAM constellations, C-SW-SO-OFDM coordinates the transmission of pairs of LEDs modulated by a binary-level signal. Finally, relative luminous efficacy, introduced in **Chapter 2**, is revisited in this chapter, where a time-domain approach is used in the computation of the relative luminous efficacy since the statistical approach used in **Chapter 2** is not accurate for low numbers of modulated subcarriers per LED group.

The work in this chapter is being finalized for submission to a journal.

Abstract Visible light communication (VLC) systems use solid-state illumination devices, such as light-emitting diodes (LEDs), to serve a dual role as high-speed communication links. Indoor VLC channels are bandwidth-limited and have high signal-to-noise ratios (SNRs) and low-complexity and energy efficient approaches are necessary to leverage the capacity of these bandwidth constrained IM/DD channels.

In this paper, *square-wave spatial optical OFDM* (SW-SO-OFDM) is proposed which transmits an OFDM signal by transmitting G square-wave subcarriers from G LED groups and allowing them to sum in space. A 2-level square-wave signal is used as the carrier signal, eliminating the need for digital-to-analog conversion, non-linear pre-distortion hardware and the transmitter IFFT, thereby greatly reducing system complexity. Through the coordination of the transmission of binary-level waveforms in pairs of LED groups, SW-SO-OFDM is generalized to form multi-level QAM constellations which improve the bandwidth efficiency. This coordinated SW-SO-OFDM system is analyzed both in simulations and experiment. Simulations show that the proposed SW-SO-OFDM retains the advantages of SO-OFDM and significantly outperforms conventional DCO-OFDM in terms of BER performance at high SNRs, while considerably reducing the overall transmitter complexity.

4.1 Introduction

Visible light communication (VLC) systems utilize existing lighting devices (i.e., LEDs), to enable high-speed communication in the range from 100s of Mbps and beyond [110]. The migration of illumination to LEDs due to their higher power efficiency has resulted in the growing interest into complementary VLC applications [111].

Simple and cost-effective VLC systems use intensity modulation/direct detection (IM/DD) [85, 112, 113], by modulating the light source intensity with the information signal and using a simple photodetector at the receiver to directly convert the received optical signal into an electrical current. While various modulation techniques, such as on-off keying (OOK) and pulse-position modulation (PPM), have been proposed for IM/DD-based VLC systems, OFDM offers a high spectral efficiency, robustness against multipath dispersion and ease of channel estimation and equalization in time-varying environments [19]. Various techniques have been proposed to adapt OFDM to IM/DD, including DC-biased Optical OFDM (DCO-OFDM) and Asymmetrically-Clipped Optical OFDM (ACO-OFDM) [105]. The most common approach, DCO-OFDM imposes Hermitian symmetry on the OFDM frame and adds a DC bias. The resulting signal is then clipped at zero to ensure that it is non-negative and real and hence suitable for IM/DD channels.

High peak-to-average power ratio (PAPR) is an inherent problem in optical OFDM systems [114]. Since the dynamic range of the LED is limited, parts of the signal are clipped, causing non-linear clipping distortion and a bit-error rate (BER) penalty [115]. In particular for illumination systems, the high PAPR DCO-OFDM signal has been shown to reduce the luminous efficacy of the luminaire [61] and reduce the driver energy efficiency [116].

Spatial Optical OFDM (SO-OFDM) was proposed in [66] to combat the high PAPR of OFDM signals. The key concept behind SO-OFDM is a frequency-to-space mapping achieved by the allocation of a subset of OFDM subcarriers to separate LEDs in the luminaire and the summing in space of the signals from different LEDs.

Wideband, high PAPR OFDM signals are thus partitioned into many low-PAPR narrowband signals that are transmitted from multiple LEDs. The signals from different LEDs are allowed to sum in space before being detected by a conventional OFDM receiver.

In the simplest form of SO-OFDM, explored in [61, 83, 117], each LED group is assigned a different OFDM subcarrier. In this case, the time-domain OFDM signal of each group is a sinusoidal signal with a PAPR of 3 dB at the expense of a large number of LED groups, G. In general, SO-OFDM requires a large number of LED groups, G, in order to achieve a low PAPR and BER at high SNR. Note that each group requires a transmit chain consisting of an IFFT, a digital-to-analog converter (DAC), and digital predistortion device (DPD) and an analog driver, which add considerably to overall complexity of the SO-OFDM system. One approach to reducing the hardware complexity of SO-OFDM is to combine it with other PAPR reduction techniques (e.g., pilot-assisted PAPR reduction) [118]. However, this comes at the expense of increased computational complexity.

To reduce complexity by eliminating the need for DACs, DPDs, and IFFT blocks, several recent approaches have considered using spatial summing to modulate multiple LEDs with binary-level signals to produce complex modulation. Du *et al.* [119] use spatial summing architecture to construct a multilevel Pulse-Amplitude Modulation (PAM) signal at the receiver from the spatial superposition of multiple On-Off Keying (OOK) signals from multiple transmitters. A similar approach was employed by Kong *et al.* to generate a 4-PAM signal from OOK signals in an underwater wireless optical communication setting [120]. In [121], a bipolar optical OFDM signal was converted into a binary pulse time modulation (PTM) signal for switching the LEDs on and off,

thereby reducing the PAPR of the original OFDM signal and combatting the LED nonlinearity. DAC-less transmission has also been explored for other communication systems, such as optical fiber communication. For example, [122] employed two binary signals to drive a Mach-Zehnder modulator to produce a 4-PAM signal. Recently, a digital-to-light converter (DLC) has been proposed by Yang *et al.* [123], enabling the transmission of an OFDM signal constructed by the superposition of 255 binary signal from 255 distinct LEDs.

In this paper, we propose *square-wave spatial optical OFDM* (SW-SO-OFDM) which transmits a single subcarrier per LED group by modulating an on/off square wave carrier rather than a sinusoid. That is, each LED group is assigned a specific subcarrier frequency and the signal emitted from each LED group is a binary square-wave carrier where data are transmitted by phase-shift keying (PSK). Unlike [123], where a traditional OFDM frame is transmitted using an optical DAC consisting of many LEDs, our approach directly modulates LEDs and is lower in complexity. Our approach also differs from [121], where the OFDM signal does not modulate the LEDs directly, but is converted to a binary PTM signal to eliminate the need for DACs. While the idea of DAC-less transmission and the concept of spatial summation for indoor VLC systems have been studied before in literature [61, 119, 120, 122], and applied to OFDM [121, 123], to our knowledge, this is the first paper to propose using square-wave carriers for OFDM-based VLC systems to enable DAC-less transmission and simplify the transmitter design. Furthermore, we extend SW-SO-OFDM and present a new multi-level signaling approach by coordinating the transmission of two (or more) LEDs to generate complex QAM constellations using only binary-level carriers. This *coordinated* SW-SO-OFDM (C-SW-SO-OFDM) approach is shown both

in simulation and experiment to enable the transmission of large QAM constellations without the need for a D-to-A and using only binary level waveforms.

The remainder of this paper is organized as follows. In Section 4.2, the indoor VLC channel model and considerations such as LED nonlinearity and its impact on the luminous efficacy of signaling LEDs are described. Section 4.3 details the basic SW-SO-OFDM transmitter architecture and provides a bit-error probability analysis. In Section 4.3.4, C-SW-SO-OFDM is introduced that allows for multi-level signaling by coordinating the binary level transmissions of pairs of LED groups to produce a complex QAM constellation point. In Section 4.4, SW-SO-OFDM is compared to other techniques such as the conventional DCO-OFDM and SO-OFDM in terms of BER, obtained both analytically and through Monte-Carlo simulations. Section 4.5 provides a detailed description of an experimental validation of C-SW-SO-OFDM technique. Finally, conclusions and future directions are discussed in Section 4.6.

4.2 System Modelling

4.2.1 Indoor VLC Channel Model

The LEDs in the luminaire are modeled as having a Lambertian emission pattern. Since in a typical indoor VLC setting, the distance d between the luminaire and the receiver photodetector (e.g., meters) is at least two orders-of-magnitude larger than the distance between individual LEDs in the luminaire (on the order of a few centimeters), a reasonable assumption to make is that the optical propagation channels between all LEDs and the receiver photodetector are nearly identical (following [61]). Moreover, it is reasonable to assume that the line-of-sight component dominates over

all multipath reflections from the ceiling and walls [12, 85]. Therefore, the indoor VLC channel is modeled as a flat fading channel with a propagation delay $\tau = d/c$, where c is the speed of light, and a DC gain

$$\Omega = \begin{cases} \frac{(m+1)A_{\mathrm{d}}}{2\pi d^2} \cos^m(\phi) T_{\mathrm{s}}(\psi) g(\psi) \cos(\psi), & 0 \leq \psi_{\leq} \psi_{\mathrm{c}} \\ 0, & \psi > \psi_{\mathrm{c}} \end{cases} \tag{4.2.1}$$

where m is the Lambertian order, A_{d} is the area of the detector, ψ is the angle of incidence, ϕ is the angle of irradiance, $T_s(\psi)$ is the gain of the optical filter, $g(\psi)$ is the gain of the optical concentrator, and ψ_{c} is the field-of-view (FOV) of the receiver.

The optical power received by the photodetector is the sum of the optical power from the L LEDs of the luminaire:

$$P_{\mathrm{R}} = L\Omega P_{\mathrm{T}}, \tag{4.2.2}$$

where P_{T} is the optical power output of an LED.

4.2.2 LED Nonlinearity

The relation between the luminous flux output ϕ_{v} [lm] and the LED current I [mA] is nonlinear, and typically provided in datasheets. For a popular illumination LED, a quadratic fit [74] to the characteristics specified in the datasheet [86] is given by

$$\phi_{\mathrm{v}}\ (\mathrm{lm}) = -0.0001I^2 + 0.3093I + 3.647 \tag{4.2.3}$$

where I is the LED current in mA. The conversion factor between the luminous flux and the radiated optical power for this setup has been evaluated at 2.1 mW/lm [63].

Since the OFDM signal has large peaks, hard-clipping is necessary for the driving LED current I to fit within the limited dynamic range of the LED. The upper and lower LED current clipping levels are denoted by I_{u} and I_{l}, respectively. In case of symmetric clipping, used throughout this paper, $I_{\mathrm{u}} = -I_{\mathrm{l}} = C$, where C is half the dynamic range.

For conventional DCO-OFDM and Spatial Optical OFDM (SO-OFDM) [61], digital pre-distortion (DPD) is required for each LED group to linearize the relation between I and P_{T} [61]. Accordingly, a linear relation between the instantaneous optical power output, P_{T}, and the OFDM signal current, I, is achieved, where the LED conversion factor in (W/A) is denoted by S. In addition, an IFFT block and a DAC are needed for each LED group. As described in Sec. 4.3, SW-SO-OFDM does not require at DPD or D-to-A converter given it emits only binary waveforms.

4.2.3 Impact of Modulation on Luminous Efficacy

The DC current driving the LEDs in a luminaire determines the luminous flux output ϕ_{v} (lm) or illuminance E (lx) at a surface. Throughout this paper, a DC current level of 500 mA is considered, unless otherwise indicated. In a VLC system, a modulating current is imposed onto the DC driving current. The *luminous efficacy* is defined as the ratio of the luminous flux of the LED to the electrical power consumed by the LED. For a given average current, modulating the LED with a time varying signal reduces the luminous efficacy of an LED [61, 74, 86]. The luminous efficacy is an important parameter in lighting as it quantifies how well the LED converts

electrical power into useful illumination [61]. The relative luminous efficacy, η_{rel} is defined as the ratio of the luminous efficacy of communication LEDs to that of LEDs driven by a DC current [61].

In [61], the impact of modulation on luminous efficacy was assessed by computing the relative luminous efficacy (RLE) under the assumption of a Gaussian modulating signal. While this Gaussian approximation is reasonable when the number of sub-carriers is large, it is not accurate in the case of a few (or single) carrier per LED group.

In this work, the relative luminous efficacy is defined as the ratio of the time average of the luminous flux output to the electrical power consumed by the LED, i.e.,

$$\eta_{\text{rel}} = \frac{\int_{\langle T_{\text{sym}} \rangle} \phi_{\text{v}}(t)\, dt / \int_{\langle T_{\text{sym}} \rangle} P_{\text{LED}}(t)\, dt}{\eta_{\text{DC}}} \tag{4.2.4}$$

where T_{sym} is the OFDM symbol duration and η_{DC} is the DC luminous efficacy.

Analogous to [61], Figure 4.1 presents a contour plot or relative luminous efficacy (η_{rel}) computed using (4.2.4) for SO-OFDM using a single sinusoidal subcarrier per LED group. The root mean square (RMS) value (σ_g) of the time-domain signal before clipping, $x_g(t)$, is defined as,

$$\sigma_g = \sqrt{\frac{1}{T_{\text{sym}}} \int_{\langle T_{\text{sym}} \rangle} x_g^2(t) dt}, \tag{4.2.5}$$

is represented on the horizontal axis. The dynamic range ($I_{\text{u}} - I_{\text{l}}$) is represented on the vertical axis. The results show that η_{rel} decreases as either σ_g and ($I_{\text{u}} - I_{\text{l}}$) increases. This is expected since operating at the extremes of the dynamic range incurs more NLD and causes the luminous efficacy to drop [61]. In Sec. 4.4, the

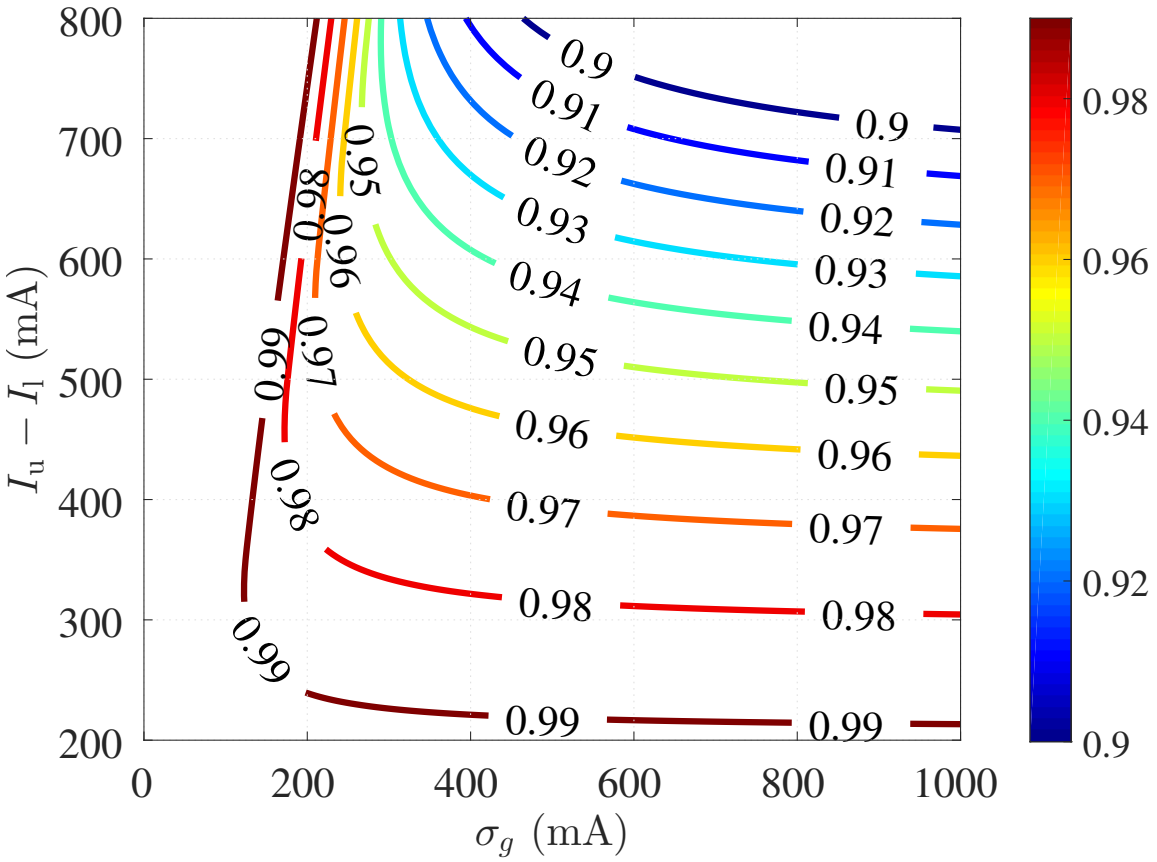

Figure 4.1: Contour plot of the relative luminous efficacy η_{rel} as a function of the signal RMS value (σ_g) [mA] and dynamic range ($I_u - I_l$) [mA].

definition of relative efficacy in (4.2.4) will be employed to provide a fair comparison of SW-SO-OFDM versus SO-OFDM considering illumination constraints..

4.3 Square-Wave Spatial Optical OFDM

4.3.1 Background and Motivation

Conventional OFDM communication systems, which dominate wireless applications such as Wi-Fi and mobile communications, are based on the modulation of multiple orthogonal sinusoidal carriers [124]. Sinusoidal signals are chosen to control the emission spectrum and comply with wireless spectrum management regulations. In contrast, for indoor VLC communication systems, the spectrum is unregulated and unlicensed. This motivates the search for alternative periodic carrier waveforms that balance communication performance, illumination and system complexity.

With the aim of retaining the use of commercially available OFDM receivers (as in the upcoming VLC standard 802.11bb [125]), the receiver in this work is considered to be a conventional OFDM receiver matched to sinusoidal carriers. The focus in this work is on transforming the transmitter design in order to reduce system complexity in the luminaire transmitter by considering alternative carrier signals. Since typical VLC channels have a low-pass frequency response dominated by the slow yellow light component of phosphor-coated white LEDs [63], the higher-frequency harmonics of a periodic carrier signal are likely to be more highly attenuated by the VLC channel than the fundamental. Moreover, the higher-frequency components are further attenuated or filtered out by the low-pass anti-aliasing and/or noise rejection filter at the receiver front-end. Therefore, in this work, only the fundamental frequency

component is used for detection at the receiver, and its power is defined as the useful signal power, while higher-order harmonic components are considered inter-carrier interference (ICI), and signaling at these harmonic frequencies is avoided. A complete discussion along with methods to avoid the harmonics is described in Sec. 4.3.2. Hence, one parameter of particular interest in assessing periodic carrier waveforms is the fundamental frequency term of the Fourier Series (FS) expansion of the periodic signal. In particular, let $p(t)$ denote a periodic signal with fundamental frequency f_0 and restricted to amplitude range $[-C, C]$ in order to avoid nonlinear clipping. Since only the fundamental frequency component is used for detection, of particular interest is the fundamental frequency coefficient of the Fourier Series expansion of $p(t)$, denoted by $K_{[p]}$, which can be written as

$$K_{[p]} = \frac{2}{T} \int_{-T/2}^{T/2} p(t) \cos(2\pi f_0 t) dt \tag{4.3.1}$$

for an even signal $p(t)$ for simplicity and without loss of generality, and where $T = 1/f_0$ is the fundamental period of $p(t)$. It is shown in the Appendix that of all possible signals $p(t)$ satisfying the constraints, square waves with a 50% duty cycle have the largest $K_{[p]}$. For 50% duty-cycle square waves, the fundamental coefficient of the Fourier Series expansion in (4.3.1) is $K_{[\text{sq}]} = 4C/\pi$, while for a sinusoidal wave having an amplitude of C, $K_{[\text{sin}]} = C$. This gives square-wave carriers an SNR advantage of $20 \log_{10}(4/\pi) = 2.10$ dB over sinusoidal carriers.

In addition, square-wave carriers are simpler to generate using digital electronic circuits and do not require a complex D-to-A as is the case with sinusoidal carriers [126, 127]. Moreover, since a square wave is a binary-level signal with only two intensity levels, there is no need for a DAC or DPD to linearize the output optical

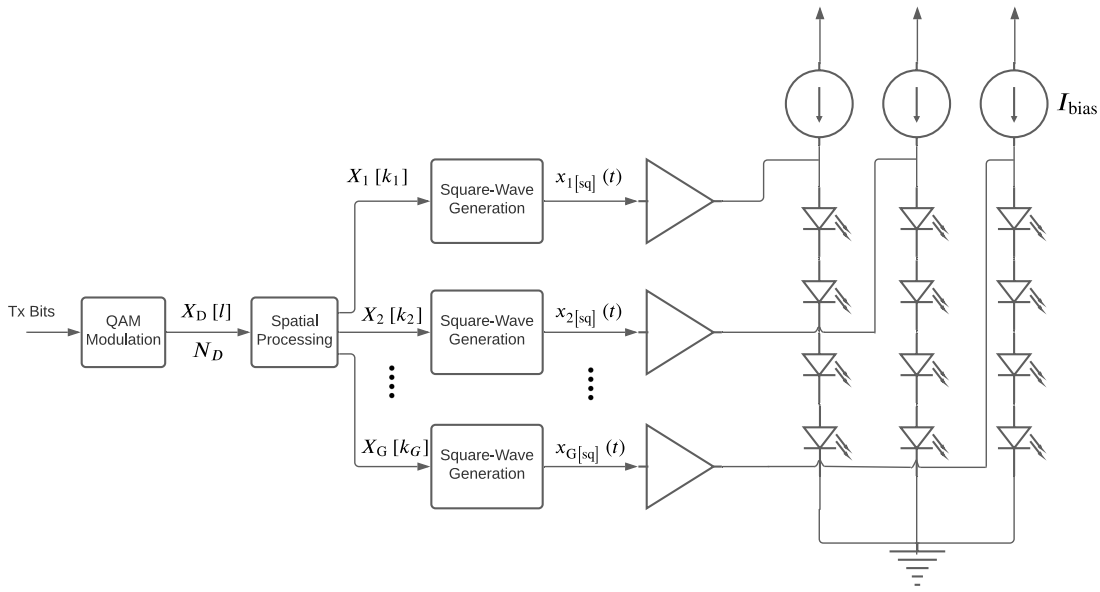

Figure 4.2: Architecture of SW-SO-OFDM with G LED groups and $L_g = 4$ LEDs per group.

power versus input drive current relationship for each LED group in SO-OFDM.

4.3.2 Square-Wave Spatial Optical OFDM Definition

The functional block diagram of the SW-SO-OFDM architecture is shown in Fig. 4.2. The transmitter design is based on the spatial summing architecture, introduced in [61], where the L available LEDs are divided into G LED groups, and the signaling of LEDs in the same group is identical, and allowed to sum in space to produce the desired signal at the receiver. In case of SW-SO-OFDM, however, each LED group is modulated by a binary-level signal.

Let G denote the number of groups and L_g denote the number of LEDs in the

g-th group, where

$$\sum_{g=1}^{G} L_g = L. \tag{4.3.2}$$

As shown in Fig. 4.2, the data bits are modulated to produce the QAM constellation data symbols, $X_{\mathrm{D}}[l]$, for $l = 1, 2, \ldots, N_{\mathrm{D}}$.

The spatial processing block maps the N_{D} data symbols, $X_{\mathrm{D}}[l]$, into G LED group SW-SO-OFDM symbols

$$X_g[k_g] = |X_g[k_g]| \exp(j\phi_g[k_g]) \tag{4.3.3}$$

for $g = 1, 2, \ldots, G$, where k_g is the subcarrier index associated with LED group g and $\phi_g[k_g]$ denotes the angle of $X_g[k_g]$. Note that the subcarrier indexing does not necessarily start from 1, not all available subcarriers in the set $\{1, 2, \ldots, N_{\mathrm{D}}\}$ are modulated, and the data-carrying subcarriers indexed by $k_1, k_2, \ldots, k_G$ need not be contiguous. Since only a binary-level square-wave signals are transmitted, $|X_g[k_g]| = 1$ without loss of generality.

Note that this mapping from $X_{\mathrm{D}}[l]$ to $X_g[k_g]$ is not necessarily one-to-one. Generally, a single data symbol $X_{\mathrm{D}}[l]$ can be mapped to either one or two or more LED group SW-SO-OFDM symbols $X_g[k_g]$ depending on the SW-SO-OFDM structure used. Hence, in general $G \geq N_{\mathrm{D}}$. The mapping can take various forms. In this paper, two mapping techniques are described: the simplest approach, termed *uncoordinated* transmission in Section 4.3.3, performs a one-to-one mapping between X_D and X_g, implying $G = N_{\mathrm{D}}$, while a *coordinated* technique, presented in Section 4.3.4 coordinates the transmission of two LED groups to represent a complex QAM symbol, implying $G = 2N_{\mathrm{D}}$.

For simplicity, only the m-th SW-SO-OFDM symbol is considered in the following analysis, however, the analysis applies to all transmitted SW-SO-OFDM symbols. The phase of the binary-level SW-SO-OFDM time-domain signal of the g-th LED group g, $x_{g[\mathrm{sq}]}[t]$, is determined by the data symbol $X_g[k_g]$,

$$x_{g[\mathrm{sq}]}[t] = C\mathrm{sq}(2\pi k_g f_o t + \phi_g[k_g]) \tag{4.3.4}$$

for $(m-1)T_{\mathrm{sym}} \leq t < mT_{\mathrm{sym}}$, where T_{sym}, the SW-SO-OFDM symbol duration, is the inverse of the subcarrier spacing, f_o, which ensures the orthogonality of the continuous-time SW-SO-OFDM signal. The square wave function $\mathrm{sq}(\cdot)$ is defined as:

$$\mathrm{sq}(\chi) = \mathrm{sgn}(\cos(\chi)). \tag{4.3.5}$$

A DC bias current I_{bias} is added to the group signal $x_{g[\mathrm{sq}]}[n]$ to ensure nonnegativity, and the LEDs in each group are driven by the resulting signal.

The optical signals from all LEDs are attenuated by the VLC channel response with a DC optical gain Ω, as described in Sec. 4.2.1, and are summed spatially at the receiver.

The receiver block diagram is shown in Fig. 4.3. The photodetector, with responsivity R (A/W), converts the received optical sum signal into an electrical signal. The signal is then filtered with an anti-aliasing/noise rejection lowpass filter (LPF). The signal is then sampled with a sampling interval T_{s} and input to the FFT block with an FFT size N. The OFDM symbol duration is the product of to the sampling interval and the FFT size ($T_{\mathrm{sym}} = NT_{\mathrm{s}}$). Finally, the received frequency-domain OFDM symbols produced by the FFT are demodulated and converted to bits.

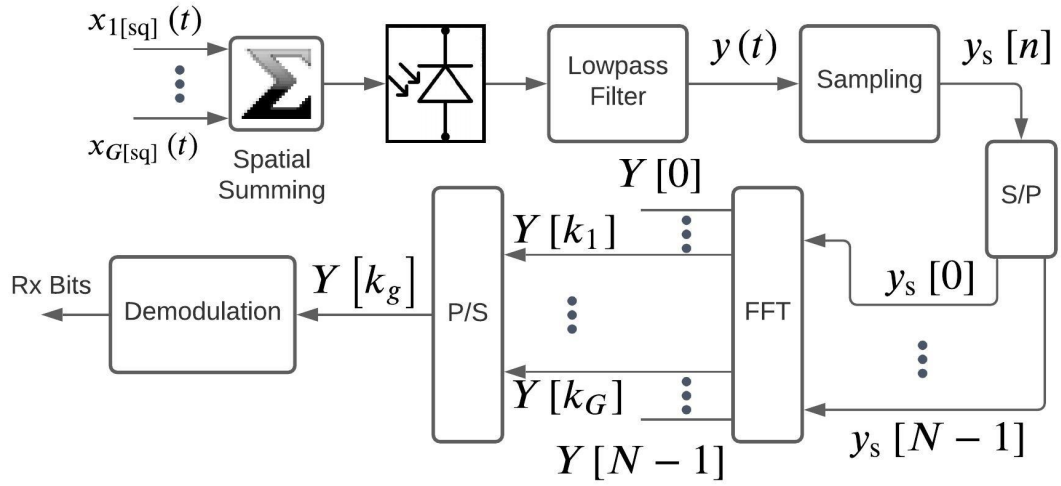

Figure 4.3: Architecture of SW-SO-OFDM receiver. Note that only the subset $\{Y[k_1], \ldots, Y[k_G]\}$ of the set of received OFDM frequency-domain symbols $\{Y[0], Y[1], \ldots, Y[N-1]\}$ is used for demodulation and bit detection.

Although for the purpose of this analysis, the indoor VLC channel is considered flat, as described in Sec. 4.2.1, which is a valid assumption for narrowband signals, the indoor VLC channel can alternatively be modeled as a lowpass channel, as explained in Sec. 4.3.1. By designing the subcarrier assignment so that the fundamental frequencies of the modulated subcarriers are in the passband of the channel, the flat channel model can be used to accurately analyze the communication performance. In contrast, higher-order frequency harmonics of the square-wave carriers are either significantly attenuated or filtered out completely by the indoor VLC channel frequency response. Moreover, a lowpass anti-aliasing/noise rejection filter is used at the receiver front end and can be modeled as an ideal LPF with a cut-off frequency $f_c = Nf_o = N/T_{sym}$, and all harmonic frequency components beyond f_c are filtered out. Therefore, the higher-order frequency harmonics of the square-wave carriers are

not used for detection, do not contribute to the useful signal power, and are considered ICI. Whereas it is possible to use successive interference cancellation techniques to eliminate ICI, in this paper, these subcarrier frequencies occupied by the harmonics are left unmodulated to avoid ICI.

Therefore, the output of the receiver LPF can be written as

$$y(t) = \frac{G_{\mathrm{E}} L}{G} \sum_{g=1}^{G} \widetilde{x}_{g[\mathrm{sq}]}(t) + G_{\mathrm{E}} L I_{\mathrm{bias}} + w(t), \tag{4.3.6}$$

where $G_{\mathrm{E}} = R\Omega S$ is the overall electrical gain of the system, $\widetilde{x}_{g[\mathrm{sq}]}(t)$ is the received SW-SOFDM signal, and $w(t)$ is the receiver noise waveform. For simplicity, the case of equal numbers of LEDs per group, i.e. $L_g = L/G$ for $g = 1, 2, \ldots, G$, is considered. Notice that $\widetilde{x}_{g[\mathrm{sq}]}(t)$ differs from $x_{g[\mathrm{sq}]}(t)$ (4.3.4) in that $\widetilde{x}_{g[\mathrm{sq}]}(t)$ has higher frequency harmonics attenuated by the VLC channel or filtered out by the receiver LPF. The fundamental-frequency components are equal for both $x_{g[\mathrm{sq}]}(t)$ and $\widetilde{x}_{g[\mathrm{sq}]}(t)$ since the DC channel gain Ω already takes into account the VLC channel attenuation suffered by the fundamental-frequency data-carrying subcarriers. The DC bias term is ignored in the following, since it does not carry any information.

The filtered received signal, $y(t)$, is then sampled to yield

$$\begin{aligned} y_{\mathrm{s}}[m, n] &= y\left((m-1)T_{\mathrm{sym}} + nT_{\mathrm{s}} + \delta\right) \\ &= \frac{G_{\mathrm{E}} L}{G} \sum_{g=1}^{G} \widetilde{x}_{g[\mathrm{sq}]}[n] + w[n], \end{aligned} \tag{4.3.7}$$

for $n = 0, 1, \ldots, N-1$, where $\delta = d/c$ is the propagation delay from transmitter to receiver, $\widetilde{x}_{g[\mathrm{sq}]}[n]$ and $w[n]$ are the sampled received SW-SO-OFDM signal and

the sampled receiver noise, respectively. The variance of the zero-mean Gaussian-distributed samples $w[n]$ is denoted by σ_w^2. The index m is dropped from $y_{\mathrm{s}}[m,n]$ in the following for convenience.

4.3.3 Uncoordinated Transmission

Uncoordinated SW-SO-OFDM (U-SW-SO-OFDM) transmission maps QAM data symbols $X_{\mathrm{D}}[l]$ to the frequency-domain OFDM subcarrier symbols in a one-to-one fashion, i.e., $X_g[k_g] = X_{\mathrm{D}}[g]$ for $g = 1, 2, \ldots, N_{\mathrm{D}}$. In this case the number of LED groups $G = N_{\mathrm{D}}$. Given that $X_g[k_g]$ is restricted to a constant magnitude, the QAM data symbols $X_{\mathrm{D}}[l]$ are also limited to be constant modulus (i.e., PSK constellations).

The received SW-SO-OFDM frequency-domain frame, $Y[k]$ for $0, 1, \ldots, N-1$, is obtained by using the N-point FFT operation. However, only the receiver subcarrier symbols $Y[k_g]$ for $k_g = k_1, k_2, \ldots, k_G$ carry useful QAM data and are demodulated after the FFT operation. Given that the subcarrier assignment is designed so that the subcarriers located at odd harmonics of the data subcarriers are unused to avoid interference, for the purpose of analysis, only fundamental components located at $k_1, k_2, \ldots$ are considered in the subsequent analysis.

Hence, $Y[k_g]$, the output of the FFT operation for $k_g = k_1, \ldots, k_G$, can be written as

$$Y[k_g] = \mathrm{FFT}\left[y_{\mathrm{s}}[n]\right] = \underbrace{\frac{\sqrt{N} G_{\mathrm{E}} K_{[\mathrm{sq}]} L}{2G} X_g[k_g]}_{\text{Useful Signal Term}} + \underbrace{W[k_g]}_{\text{Noise Term}}, \tag{4.3.8}$$

where $X_g[k_g] = |X_g[k_g]| \exp\left(X_g[k_g]\right) = X_{\mathrm{D}}[g]$, and $W[k_g]$ is the FFT of the receiver noise.

The useful signal power is the variance of the signal term in (4.3.8).

$$\sigma^2_{[\mathrm{sq}]}[k_g] = \frac{N}{4}\left(\frac{G_{\mathrm{E}} K_{[\mathrm{sq}]} L}{G}\right)^2 = 4N\left(\frac{G_{\mathrm{E}} LC}{\pi G}\right)^2, \tag{4.3.9}$$

where the second equation follows by substituting $K_{\mathrm{sq}} = 4C/\pi$. Hence, the signal-to-noise ratio (SNR) per subcarrier channel is

$$\begin{aligned}\mathrm{SNR}_{[\mathrm{sq}]}[k_g] = \frac{\sigma^2_{[\mathrm{sq}]}[k_g]}{\sigma^2_W} &= \frac{N\left(G_{\mathrm{E}} K_{[\mathrm{sq}]} L/G\right)^2}{4\sigma^2_W} \\ &= 4N\left(\frac{G_{\mathrm{E}} LC}{\pi G \sigma_W}\right)^2,\end{aligned} \tag{4.3.10}$$

where $\sigma^2_W = \mathrm{E}\left(|W[k_g]|^2\right) = \sigma^2_w$.

For M-PSK modulation, to which SW-SO-OFDM is restricted given the use of fixed-intensity LED signals, the probability of error, P_{e}, for the data modulated on the k_g-th subcarrier, can be approximated as [128]:

$$P_{\mathrm{e}[\mathrm{sq}]}[k_g] \approx \frac{1}{\log_2 M}\mathrm{erfc}\left(\sin\left(\frac{\pi}{M}\right)\sqrt{\mathrm{SNR}_{[\mathrm{sq}]}[k_g]}\right). \tag{4.3.11}$$

Under the assumption that all subcarriers have the same SNR, the overall BER is given by the same expression (4.3.11). Therefore, for $M = 4$, the BER for 4-PSK can be written as,

$$P_{\mathrm{e}[\mathrm{sq}]} \approx \frac{1}{2}\mathrm{erfc}\left(\frac{\sqrt{2N} G_{\mathrm{E}} LC}{\pi G \sigma_W}\right). \tag{4.3.12}$$

Notice that SW-SO-OFDM does not suffer from any NLD clipping noise, which is a major advantage over conventional DCO-OFDM, since VLC systems operate at high SNRs where the effect of NLD clipping noise is dominant over that of receiver AWGN.

Modulation technique	Hardware complexity	Computational complexity
DCO-OFDM	1 IFFT, 1 DPD, and 1 DAC.	$\mathcal{O}\left(N\log_2\left(2N_{\mathrm{D}}\right)\right)+\mathcal{DPD}(N)$ $+\mathcal{DAC}(N)$
SO-OFDM	G Spatial Filters, G IFFTs, G DPDs, and G DACs.	$G\left(\mathcal{O}\left(N\log_2\left(2\epsilon\right)\right)+\mathcal{DPD}(N)\right.$ $\left.+\mathcal{DAC}(N)+\mathcal{S}(N)\right)$
SW-SO-OFDM	Generation of G square waves from QAM data.	No IFFT required.

Table 4.1: Comparison of hardware complexity and computational complexity of DCO-OFDM, SO-OFDM, and SW-SO-OFDM.

Moreover, SW-SO-OFDM offers the advantage of a simpler transmitter architecture compared to SO-OFDM and DCO-OFDM. Table 4.1 compares the hardware complexity of DCO-OFDM, SO-OFDM, and SW-SO-OFDM. The computational complexities of DPDs, DACs, and spatial filters are denoted by $\mathcal{DPD}(\cdot)$, $\mathcal{DAC}(\cdot)$, and $\mathcal{S}(\cdot)$, respectively. Table 4.1 shows that SW-SO-OFDM has lower hardware and computational complexity than both DCO-OFDM and SO-OFDM since it eliminates the need for DACs, DPDs, IFFTs, and spatial filters. Section 4.4 presents a BER comparison of DCO-, SO- and SW-SO-OFDM.

4.3.4 Coordinated Transmission

A clear disadvantage of the simple U-SW-SO-OFDM described in Sec. 4.3 is that using square-wave carriers with fixed intensity level for each LED restricts the QAM constellations to be constant modulus (i.e., PSK). In this section, Coordinated SW-SO-OFDM (C-SW-SO-OFDM) is introduced which preserves the simple transmitter

architecture introduced in Sec. 4.3, but allows for multi-level QAM signaling by coordinating the binary-level transmissions of pairs of LEDs. In contrast to U-SW-SO-OFDM where the mapping between the QAM constellation data symbols $X_{\mathrm{D}}[l]$ and the LED group SW-SO-OFDM subcarrier symbols $X_g[k_g]$ is one-to-one, for C-SW-SO-OFDM, each data symbol is mapped to two group subcarrier symbols signaling at the same frequency. Hence, for C-SW-SO-OFDM, double the number of LED groups is required for C-SW-SO-OFDM compared to U-SW-SO-OFDM, i.e., $G = 2N_{\mathrm{D}}$.

The phasor diagram in Fig. 4.4 demonstrates how a multi-level constellation can be constructed from two fixed-intensity signals. Consider two constant-modulus LED group signals $X_g[k] = \exp(\phi_g[k])$ and $X_h[k] = \exp(\phi_h[k])$ (represented by black arrows in the figure) from groups g and h respectively, where the fixed magnitude of $X_g[k]$ and $X_h[k]$ (represented by the red dotted circle) is normalized to 1, without loss of generality (since the square-wave group signals $x_g(t)$ and $x_h(t)$ are scaled to have a fixed amplitude C). The phases of $X_g[k]$ and $X_h[k]$ are denoted by $\phi_g[k]$ and $\phi_h[k]$, respectively. The fixed magnitude emitted by LEDs in both groups ensures a simple design that avoids the need for DACs and DPDs. By coordinating the emissions from $X_g[k]$ and $X_h[k]$ (i.e., $\phi_g[k]$ and $\phi_h[k]$), the resultant QAM data symbol, $X'[k] = |X'[k]| \exp(j\phi'[k])$ (represented by a blue arrow in the figure) is generated. In particular, assuming group g and h are adjacent and their intensities sum in space, $X'[k]$ is obtained by the sum of $X_g[k]$ and $X_h[k]$,

$$X'[k] = X_g[k] + X_h[k] = \exp(j\phi_g[k]) + \exp(j\phi_h[k]). \tag{4.3.13}$$

Considering the spatial summing property of VLC channels, $X'[k]$ is obtained at the receiver as the sum of the two LED group symbols, $X_g[k]$ and $X_h[k]$.

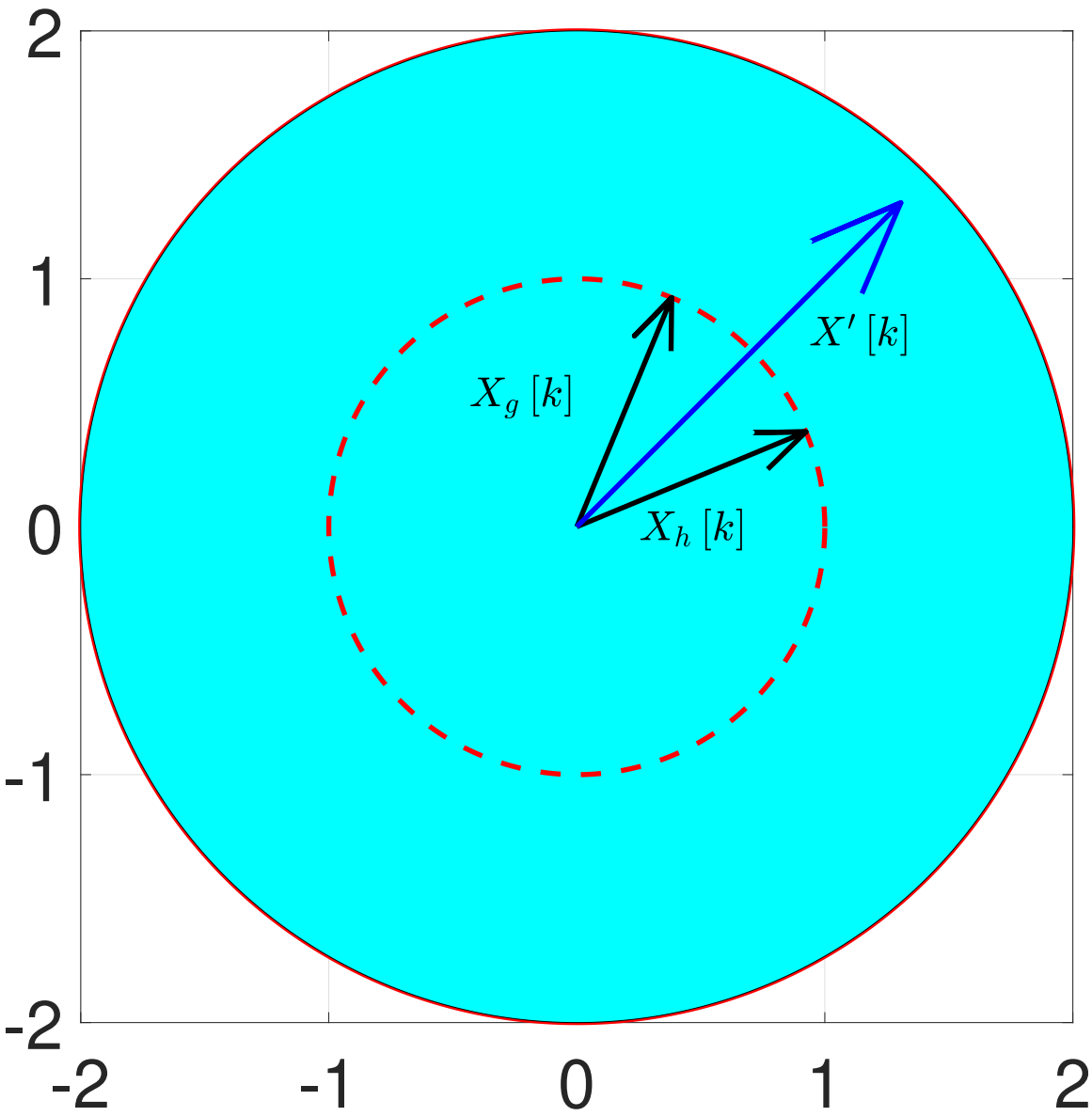

Figure 4.4: Phasor diagram showing how two signals with the same fixed intensity level can be added the same way as vector addition, to give a resultant signal in the intensity range from 0 to double the original intensity.

It is straightforward to prove that the magnitude of the sum can be expressed in terms of the difference $\Delta\phi[k] = \phi_g[k] - \phi_h[k]$:

$$|X'[k]| = 2\left|\cos\left(\frac{\Delta\phi[k]}{2}\right)\right|. \tag{4.3.14}$$

Since $0 \leq \left|\cos\left(\frac{\Delta\phi[k]}{2}\right)\right| \leq 1$, then the possible normalized range for $|X'[k]|$ is from 0 to 2, and the QAM constellation are not limited to a single magnitude level, as it is the case for U-SW-SO-OFDM introduced in 4.3. The phase $\phi'[k]$, can be shown in a straightforward manner, to be equal to the average of $\phi_g[k]$ and $\phi_h[k]$. Thus,

$$\phi'[k] = \frac{\phi_g[k] + \phi_h[k]}{2}. \tag{4.3.15}$$

Hence, with the proper selection of $\phi_g[k]$ and $\phi_h[k]$, any QAM constellation point $X_{\mathrm{D}}[l]$ in the normalized magnitude range from 0 to 2 can be obtained as the resultant QAM data symbol $X'[k]$.

Starting from any target QAM data symbol $X_{\mathrm{D}}[l]$, such that $0 \leq |X_{\mathrm{D}}[l]| \leq 2$, the LED group symbols $X_g[k]$ and $X_h[k]$ used to construct $X'[k]$ so as to ensure that $X'[k] = X_{\mathrm{D}}[l]$, can be obtained as follows. From (4.3.14), it can be seen that the phase difference, $\Delta\phi[k]$, can be written in terms of $X'[k]$ as,

$$\Delta\phi[k] = 2\cos^{-1}\left(\frac{|X'[k]|}{2}\right). \tag{4.3.16}$$

From (4.3.15), $\phi_g[k]$ and $\phi_h[k]$ can be written in terms of $\phi'[k]$ and $\Delta\phi[k]$,

$$\phi_g[k] = \phi'[k] + \Delta\phi[k]/2 = \phi'[k] + \cos^{-1}\left(\frac{|X'[k]|}{2}\right), \tag{4.3.17}$$

$$\phi_h[k] = \phi'[k] - \Delta\phi[k]/2 = \phi'[k] - \cos^{-1}\left(\frac{|X'[k]|}{2}\right), \tag{4.3.18}$$

where the second equation in each line follows by substituting for $\Delta\phi[k]$ from (4.3.16). Thus, the phases $\phi_g[k]$ and $\phi_h[k]$ of the LED group signals $X_g[k]$ and $X_h[k]$ can be computed in terms of the resultant QAM data symbol $X'[k]$, or equivalently, in terms of the target QAM data symbol $X_{\mathrm{D}}[l]$.

Following the same analysis procedure outlined in Sec. 4.3, for C-SW-SO-OFDM, $Y[k]$,the output of the FFT operation for subcarrier k is obtained by replacing $X_g[k]$ in (4.3.8) by $X'[k]$. Thus,

$$Y[k] = \underbrace{\frac{\sqrt{N}G_{\mathrm{E}}K_{[\mathrm{sq}]}L}{2G}X'[k]}_{\text{Useful Signal Term}} + \underbrace{W[k]}_{\text{Noise Term}} . \tag{4.3.19}$$

The useful signal power for C-SW-SO-OFDM is defined as the variance of the useful signal term in (4.3.19), and thus can be written as,

$$\sigma^2_{\mathrm{CSW}}[k] = \frac{N}{4}\left(\frac{G_{\mathrm{E}}K_{[\mathrm{sq}]}L}{G}\right)^2 \mathrm{E}\left[|X'[k]|^2\right]. \tag{4.3.20}$$

To maximize the M-QAM constellation energy and the minimum Euclidean distance, the maximum possible value of 2 for $|X_{\mathrm{D}}[l]|$ is assigned to the highest-energy QAM symbols (located at the vertices of the QAM constellation). In this case, for square

M-QAM constellations, the mean square value of $X'[k]$ can be computed as,

$$\mathrm{E}\left[|X'[k]|^2\right] = \frac{4}{3}\frac{\sqrt{M}+1}{\sqrt{M}-1}. \tag{4.3.21}$$

Hence, by substituting for $\mathrm{E}\left[|X'[k]|^2\right]$ from (4.3.21) into (4.3.20) and substituting $K_{[\mathrm{sq}]} = 4C/\pi$, the following expression can be obtained for the useful signal power,

$$\sigma^2_{\mathrm{CSW}}[k] = \frac{16N}{3}\frac{\sqrt{M}+1}{\sqrt{M}-1}\left(\frac{G_{\mathrm{E}}LC}{\pi G}\right)^2. \tag{4.3.22}$$

Under the assumptions of a flat channel and white noise, the useful signal power is independent of the subcarrier index k, the index k can be dropped, and the useful signal power can be denoted simply as σ^2_{CSW}. Thus, the SNR of the C-SW-SO-OFDM is given by,

$$\mathrm{SNR}_{\mathrm{CSW}} = \frac{\sigma^2_{\mathrm{CSW}}}{\sigma^2_W} = \frac{16N}{3}\frac{\sqrt{M}+1}{\sqrt{M}-1}\left(\frac{G_{\mathrm{E}}LC}{\pi G\sigma_W}\right)^2. \tag{4.3.23}$$

And hence, for square M-QAM constellations, the overall BER for C-SW-SO-OFDM can be written as [90],

$$P_{\mathrm{e}[CSW]} = \frac{2\left(\sqrt{M}-1\right)}{\sqrt{M}\log_2 M}\mathrm{erfc}\left(\sqrt{\frac{3\cdot\mathrm{SNR}_{\mathrm{CSW}}}{2\left(M-1\right)}}\right). \tag{4.3.24}$$

4.3.5 BER of single-carrier SO-OFDM

Single-carrier SO-OFDM introduced in [61] as a special case of SO-OFDM, where a single OFDM data subcarrier is modulated per LED group (i.e., $\epsilon = 1$ in [61]). This special case of SO-OFDM bears many similarities to SW-SO-OFDM. Both techniques have the same OFDM subcarrier structure, while SW-SO-OFDM uses square-wave

carriers instead of sinusoidal carriers and has a less complex transmitter architecture. For that reason, it is of particular interest to compare the proposed SW-SO-OFDM technique to single carrier SO-OFDM with in terms of the BER performance.

An analytical BER formula for SO-OFDM was obtained in [61] using a Gaussian model for the time-domain OFDM signal and Bussgang's model [89] for clipping. However, these models are not accurate when each LED group modulates a single carrier. In this paper, a different approach is followed considering that detection is performed on the fundamental component only.

Using PSK modulation on subcarriers, the group OFDM time-domain signal for single-carrier SO-OFDM before clipping is

$$x_{g[\text{sin}]}[t] = A\cos\left(2\pi k_g f_0 t + \phi_g[k_g]\right) \tag{4.3.25}$$

Following the same analysis procedure outlined in this section, a BER formula can be obtained for single-carrier SO-OFDM, where each OFDM time-domain symbol, before clipping, is a sinusoidal wave. In this case the SNR is given as

$$\text{SNR}_{[\text{sin}]}[k] = \frac{\sigma^2[k]}{\sigma_W^2} = \frac{N\left(G_{\text{E}} K_{[\text{sin}]} L/G\right)^2}{4\sigma_W^2} \tag{4.3.26}$$

where $K_{[\text{sin}]}$ is the fundamental coefficient of the Fourier series expansion of the time-domain OFDM signal. In case of no clipping (i.e., $A \leq C$), $K_{[\text{sin}]} = A$, whereas if $A > C$,

$$K_{[\text{sin}]} = A - \frac{2A}{\pi}\cos^{-1}(C/A) + \frac{2C}{\pi A}\sqrt{A^2 - C^2} \tag{4.3.27}$$

Notice that, as $A \to \infty$, the signal approximates a 50% duty-cycle square wave with amplitude C, and hence $\lim_{A\to\infty} K_{[\text{sin}]} = 4C/\pi$. The analytical BER formula can be

obtained by replacing $\mathrm{SNR}_{[\mathrm{sq}]}[k]$ in (4.3.11) with $\mathrm{SNR}_{[\mathrm{sin}]}[k]$, and is used to plot the analytical BER curves for single-carrier SO-OFDM in Section 4.4.

4.3.6 Luminous Efficacy Consiederations for SW-SO-OFDM

Since square waves are well approximated by clipped sinusoids with amplitudes that are very large compared to the clipping level, the rightmost side of the contour plots in Fig. 4.1 represent the relative luminous efficacy (η_{rel}) for SW-SO-OFDM (i.e., large σ_g) permitting comparison with SO-OFDM. Notice that for a given dynamic range $I_{\mathrm{u}} - I_{\mathrm{l}}$, η_{rel} increases as σ_g is decreased, since the clipping distortion becomes less severe and the signal appears more sinusoidal (SO-OFDM). Sec. 4.4 presents a comparison of SO- and SW-SO-OFDM when operating at the same η_{rel}.

For SW-SO-OFDM, the relative luminous efficacy, η_{rel}, can be computed for different values of the dynamic range ($I_{\mathrm{u}} - I_{\mathrm{l}}$). Therefore, in Fig. 4.5, η_{rel} is plotted vs. the dynamic range ($I_{\mathrm{u}} - I_{\mathrm{l}}$). From Fig. 4.5, it can be observed that increasing the upper and lower levels of the square-wave signal leads to a reduction in the luminous efficacy. The plot in Fig. 4.5 serves as a design tool for indoor VLC systems. Given a recommended maximum value for the luminous efficacy loss due to modulation, the dynamic range for SW-SO-OFDM can be directly determined from the plot.

4.4 Simulation Results

In this section, the BER performance of SW-SO-OFDM, including both the uncoordinated and coordinated variants, is compared against the main OFDM techniques used for VLC: DCO-OFDM and SO-OFDM with $\epsilon = 1$.

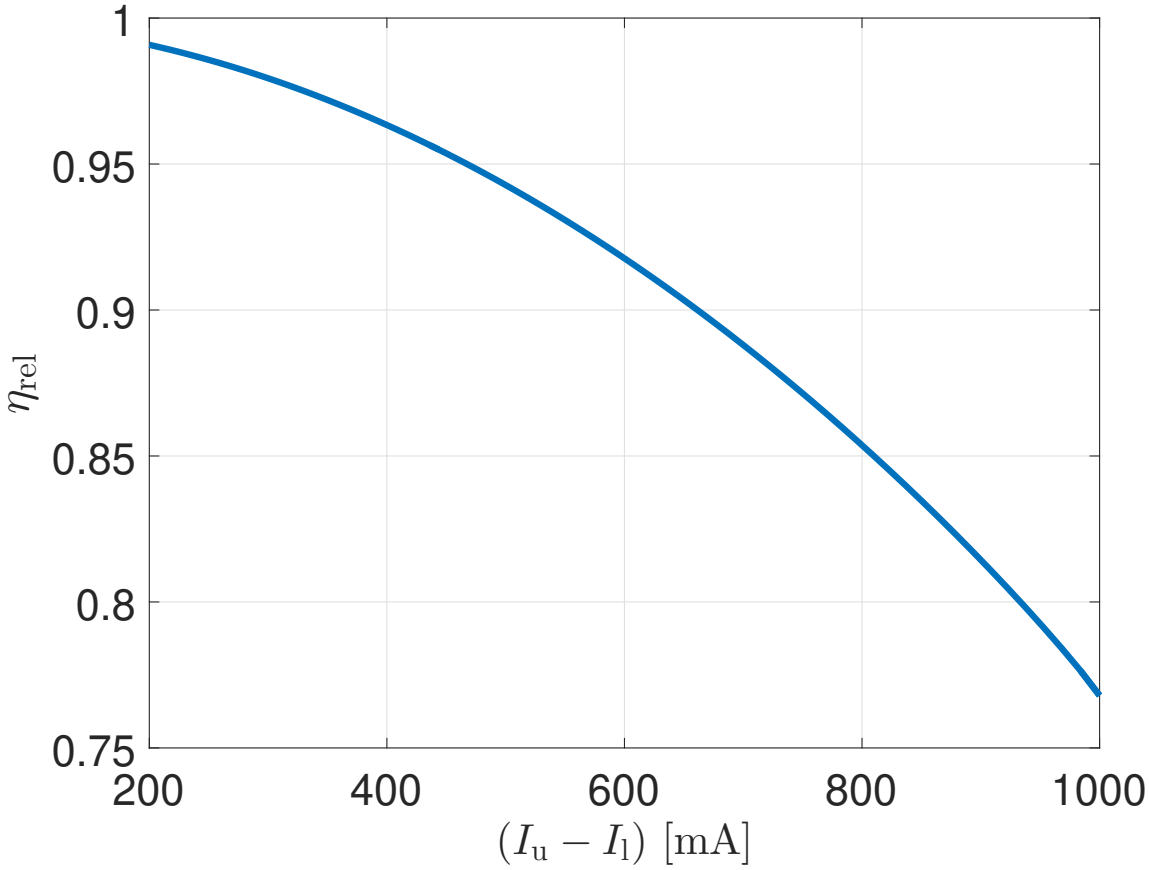

Figure 4.5: Relative luminous efficacy vs. dynamic range for SW-SO-OFDM.

Table 4.2: Simulation Parameters

Lambertian order m	1
Area of the detector A	1 cm^2
Gain of the Optical Concentrator g	3
Gain of the Optical Filter T_{S}	1
Responsivity R	0.28 A/W
Noise power spectral density N_0	10^{-16} mA^2/Hz
Receiver bandwidth B	20 MHz

The transmitter and receiver specifications and the channel parameters are the same as in [61] and are listed in Table 4.2. The receiver is assumed to be oriented so that the optical axis coincides with the luminaire and the distance between the individual LEDs is considered negligibly smaller than the distance between the luminaire and the receiver photodetector, so that the channel between each LED and the photodetector is the same and the angle of incidence $\psi = 0$.

For all simulations, the total number of LEDs is $L = 24$ and the number of independent data-carrying subcarriers is $N_{\mathrm{D}} = 12$. For DCO-OFDM, all LEDs are modulated by the same signal which includes the data from all 12 subcarriers. For U-SW-SO-OFDM and SO-OFDM with $\epsilon = 1$, the number of LED groups G is equal to the number of independent data-carrying subcarriers ($G = N_{\mathrm{D}} = 12$), and hence the number of LEDs per group is $L_g = L/G = 2$ for $g = 1, 2, \ldots, 12$. As for C-SW-SO-OFDM, the 24 LEDs are divided into 24 groups, each containing one LED. The transmission of pairs of LEDs is coordinated and the signals from both LEDs combine to produce the target signal (constellation point) to provide the multi-level functionality, as detailed in Sec. 4.3.4. The minimum FFT size required for a DCO-OFDM-based frame with $N_{\mathrm{D}} = 12$ is $2N_{\mathrm{D}} + 1 = 26$. In simulations, the FFT size

N is set to 2600, which means an oversampling factor of 100 is used to accurately represent the transmitted waveforms.

The dynamic range of the LED is set to 500 mA, and the full dynamic range is used in all simulations unless stated otherwise. Symmetric clipping is also used, so that the clipping levels are $I_{\mathrm{u}} = -I_{\mathrm{l}} = 250$ mA.

In the first simulation, the group signal standard deviation, σ_g, is set to $250/\sqrt{2}$ mA, for DCO-OFDM and SO-OFDM with $\epsilon = 1$. This sets the peak-to-peak value of the SO-OFDM sinusoidal signal to 500 mA, which is the full dynamic range of the LED. Similarly, for SW-SO-OFDM, the high and low levels of the square wave are I_{u} and I_{l}, respectively. The BER is obtained via Monte-Carlo simulations and plotted vs. SNR in Fig. 4.6 for DCO-OFDM, SO-OFDM with $\epsilon = 1$, the proposed U-SW-SO-OFDM and C-SW-SO-OFDM. The modulation used on subcarriers for all signaling techniques is 4-QAM, except for C-SW-SO-OFDM which uses 16-, 64-, 256-, and 1024-QAM.

The results show that DCO-OFDM performs better than all other approaches based on group modulation at low SNRs. As shown and discussed in [61], this due to DCO-OFDM having a higher useful signal power and that the dominant source of noise at low SNR is the channel AWGN, not the NLD noise. However, as the channel SNR increases, the NLD becomes the dominant source of noise and since DCO-OFDM has a high PAPR, and hence less immunity to NLD noise, the BER saturates and stops decreasing significantly with increasing SNR. For SO-OFDM with $\epsilon = 1$ and SW-SO-OFDM, clipping causes only attenuation of the signal as the fundamental term of the Fourier Series expansion is affected by clipping. The signal obtained by clipping a periodic waveform is a periodic waveform with an attenuated

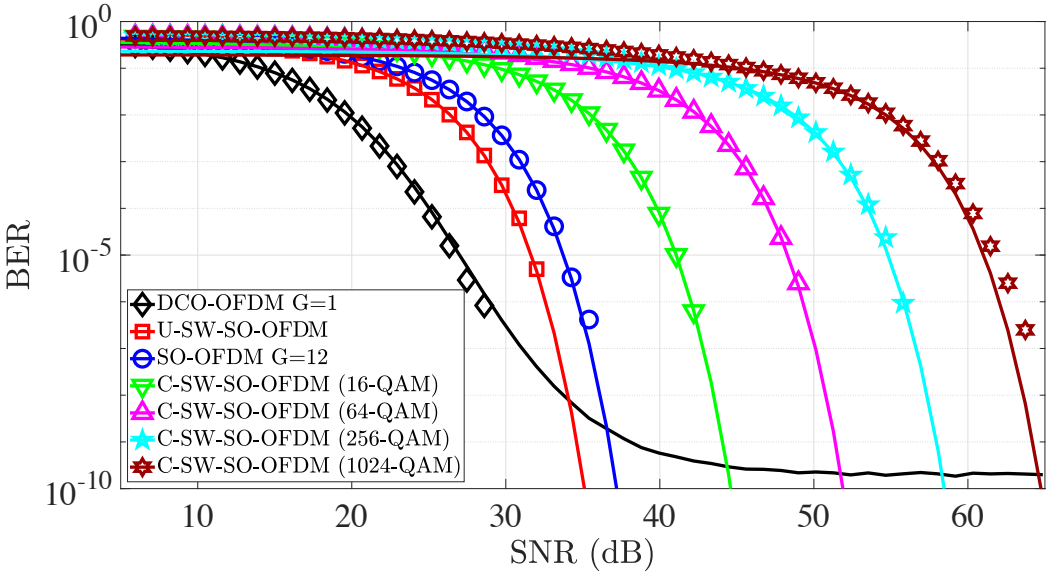

Figure 4.6: Probability of error comparison between the proposed SW-SO-OFDM technique, including both the uncoordinated and coordinated transmitted cases, the conventional DCO-OFDM, and Spatial Optical OFDM with $\epsilon = 1$. Continuous-line plots are the result of the analytical approximations in (4.3.12), (4.3.24), and [61] for DCO-OFDM.

fundamental frequency component. It can be seen from Fig. 4.6 that the proposed U-SW-SO-OFDM outperforms SO-OFDM in terms of probability of error. This is due to the fact that the fundamental coefficient of the Fourier Series expansion (4.3.1), is $K_{[\text{sq}]} = 4C/\pi$, while for SO-OFDM with $\epsilon = 1$ using the full dynamic range without clipping, it is $K_{[\text{sin}]} = C$, as discussed in Sec. 4.3.1. This corresponds to an SNR advantage of 2.10 dB as discussed in Sec. 4.3, and as evident from the BER results in Fig. 4.6.

In the second simulation, the SW-SO-OFDM system is compared to SO-OFDM with $\epsilon = 1$ at the same relative efficacy loss. With a dynamic range of 500 mA, and a target relative luminous efficacy of 95%, a signal standard deviation of 745 mA is required for SO-OFDM, as computed from Fig. 4.1, and is also used for DCO-OFDM. For SW-SO-OFDM, from Fig. 4.5, the value of $I_{\text{u}} - I_{\text{l}}$ that corresponds to a relative luminous efficacy of 95% is 467 mA. This means that the full dynamic range of the LED (500 mA) is not used. The BER vs. SNR is plotted in Fig. 4.7.

The BER results in Fig. 4.7, show that, SO-OFDM with $\epsilon = 1$ slightly outperforms the proposed U-SW-SO-OFDM at the same luminous efficacy. Specifically, SO-OFDM has a small SNR advantage of 0.53 dB over U-SW-SO-OFDM at a BER of 10^{-6}. This is due to the fact U-SW-SO-OFDM does not use the full dynamic range of 500 mA in order to obtain a relative luminous efficacy of $\eta_{\text{rel}} = 95\%$. Though the performance of U-SW-SO-OFDM and SO-OFDM is comparable, the complexity of U-SW-SO-OFDM is much lower. In particular, for both simulations in this section, with the number of LED groups $G = 12$, the U-SW-SO-OFDM transmitter has 12 less DACs, DPDs, and IFFT blocks than SO-OFDM transmitters.

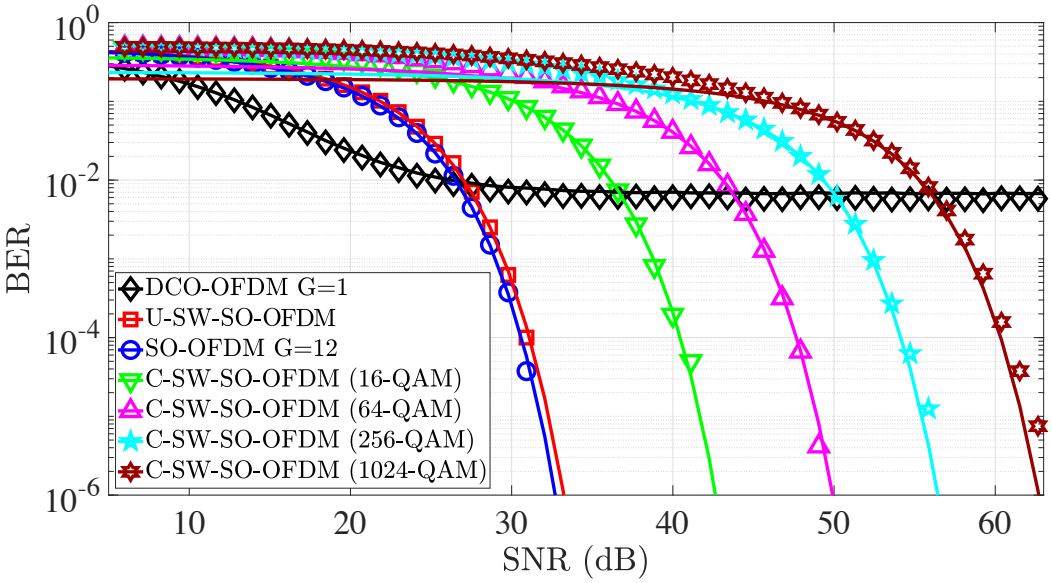

Figure 4.7: Probability of error comparison between the proposed SW-SO-OFDM technique, including both the coordinated and uncoordinated scenarios, the conventional DCO-OFM, and SO-OFDM with $\epsilon = 1$, at the same relative luminous efficacy $\eta_{\text{REL}} = 95\%$. Continuous-line plots are the result of the analytical approximations in (4.3.12), (4.3.24), and [61] for DCO-OFDM.

4.5 Experimental Validation

In this section, an experimental demonstration of the C-SW-SO-OFDM VLC transmitter is described. As a proof-of-concept of C-SW-OFDM based on the spatial summing architecture, binary-level signals from two LEDs are combined in space to transmit a single complex QAM symbol. The subcarrier is modulated using 64-QAM modulation, which shows experimentally that the proposed SW-SO-OFDM can be extended to higher-order/multi-level constellations, by coordinating the transmission of 2 LEDs, as described for C-SW-SO-OFDM in 4.3.4. Figure 4.8 depicts the functional block diagram of the transmitter and receiver used to demonstrate C-SW-SO-OFDM.

The transmitter modulation circuit is implemented with the Altera Cyclone IV FPGA DE2-115 development board produced by Terasic. Data is generated using a 20-bit linear finite shift register (LFSR). The taps of the register is set to 1st, 3rd, 4th, and 6th bit of the registers. The LFSR is capable of generating 2^{20} or approximately 1 million unique values before repeating. A subset of the LFSR is then used as the data to the LED controller. A data file is generated on a computer and loaded into the on-board memory of the FPGA. For simplicity, each data stream is modulated onto a single square-wave carrier, implemented as a set of counters. The main clock of the controller is based upon the on-board oscillator set to 50 MHz, and is used as the reference clock. The controller symbol period is set to 130.2 kilosymbols per second, resulting in a data rate of 781.25 kbps. This is achieved by clock division of the 50 MHz clock by 384 clock cycles. The controller operates the coordinated LED pair. The wave address is controlled by a 400 MHz clock generated through a phase lock loop. This clock is then used in clock division to generate the required carrier frequency.

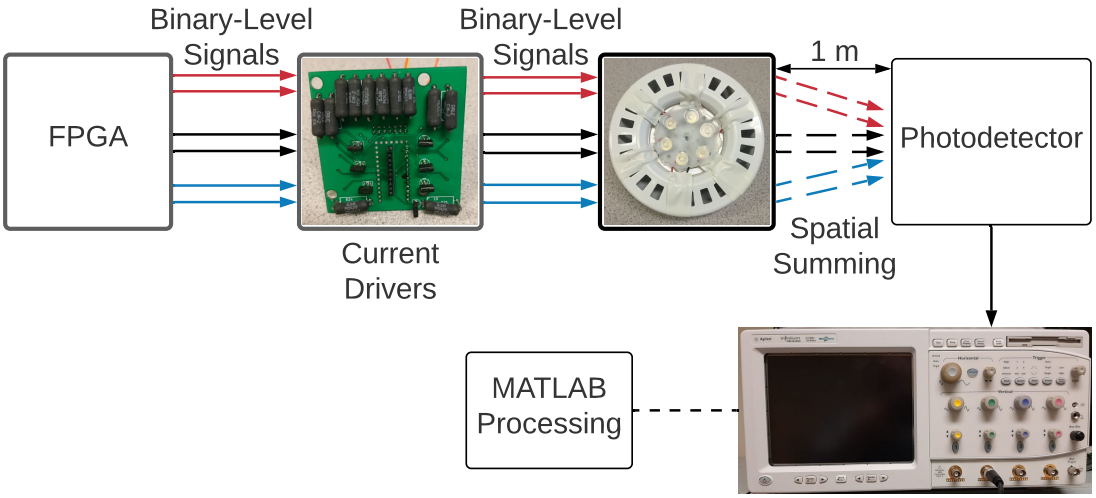

Figure 4.8: Block diagram showing the coordinated SW-SO-OFDM experimental setup. Although 3 pairs of LEDs are shown in the figure as the luminaire used has 6 LEDs, only one pair is modulated in the experiment as a proof-of-concept.

The carrier frequency is set to 781.25 kHz. The frequency is calculated based upon three factors. The first is that the carrier frequencies must be an even harmonic of the symbol frequency which is 130.2 kilosymbols per second. The value of 781.25 kHz corresponds to the 6th harmonic of symbol frequency. Secondly, in a typical setting where many subcarriers are modulated, the harmonics of the carrier frequency can not overlap each other to reduce error. The harmonics of the used carrier frequency (781.25 kHz) are located at 2343.75 kHz and 3906.25 kHz for the 3rd and 5th harmonic, respectively. As discussed in Sec. 4.3, these carrier frequencies should be unused for data transmission to avoid ICI. Alternatively, successive interference cancellation [129] can be used to eliminate the interference, allowing the use of more OFDM subcarriers for data transmission, and thereby increasing the overall bandwidth efficiency. Lastly the frequency must be achievable using discrete clock division. The used carrier frequency is achieved through a clock divisor using 400

MHz clock. The value used is set to 4 clock ticks.

The binary/square-wave carrier signal then modulates the intensity of a high power Philips Lumilieds Luxeon Rebel LXML-PWN1-0100 LED using two independent current drivers. The white light component of the LXML-PWN1-0100 has an optical 3 dB bandwidth of approximately 2 MHz, a maximum continuous current of 1 A, a typical forward voltage of 3.2 V and a luminous efficacy of 80 lm/W at 700 mA. Each LED is driven with an average current of 400 mA and 100% modulation depth.

As shown in Fig. 4.8, the signals from both LEDs sum in space and are detected at the receiver placed at 1 m from the transmitter. The receivers analog front end is implemented using the Thorlabs PDA 36A variable gain amplified photo diode directly coupled to an Agilent Infiniium 54855 DSO oscilloscope. The PDA 36A is configured to operate with a 10 dB gain and bandwidth of 5 MHz. The oscilloscope then samples the waveform at 10 Msps and is capable of producing binary data files of 16 Mpts. To guarantee synchronization, the oscilloscope also probes a synchronization signal generated on the FPGA directly through an auxiliary wire.

Demodulation of the received signal is performed by post processing using MATLAB [130]. First, the start and the end of each OFDM time-domain symbol are identified with the help of the synchronization signal. Each OFDM symbol is then separated and processed individually. The frequency-domain OFDM symbols are obtained by using FFT demodulation. Since the modulation bandwidth of the LED is smaller than the inverse of the maximum excess delay of the non-line-of-sight (NLoS) signal component, the multipath effect is negligible, resulting in no ISI, and the VLC channel is considered flat for the narrowband fundamental-frequency signal [63, 131].

Therefore, the use of a cyclic prefix (CP) is unnecessary and single-tap channel equalization is used to obtain the received QAM constellation data symbols. Finally, bit detection and BER computation are performed.

Figure 4.9 shows sample waveforms for a single OFDM symbol. The first and second subplots show the binary/square-wave transmitted signals of the first ($x_1(t)$) and second ($x_2(t)$) LEDs. The third subplot compares the sum $x_1(t) + x_2(t)$ (shown in blue) to the experimental received signal $y(t)$ (shown in red). It can be noticed that, due to the the lowpass frequency response of the LED [63], the higher order harmonics of the transmitted square-wave signals are attenuated, and the received signal resembles a sinusoidal wave. For multiple subcarriers, the received signal resembles the sum of sinusoidal signals, each corresponding to a particular OFDM subcarrier, i.e. a full OFDM signal is received by the photodetector. This allows for the use of a conventional OFDM receiver.

Figure 4.10 depicts the measured constellation. It is clear from Figure 4.10 that the SNR (27.5 dB) in this experiment is large enough to cause a near zero symbol error rate over the $13,617$ measured symbols. While it remains clear that the carriers sum optically in space, these results successfully demonstrate the concept of C-SW-SO-OFDM based on spatial summing in an experimental framework.

This experimental demonstration shows that we were able, for the first time in literature to our knowledge, to produce an OFDM symbol by summing two binary signals in space, which was detected using a conventional OFDM receiver.

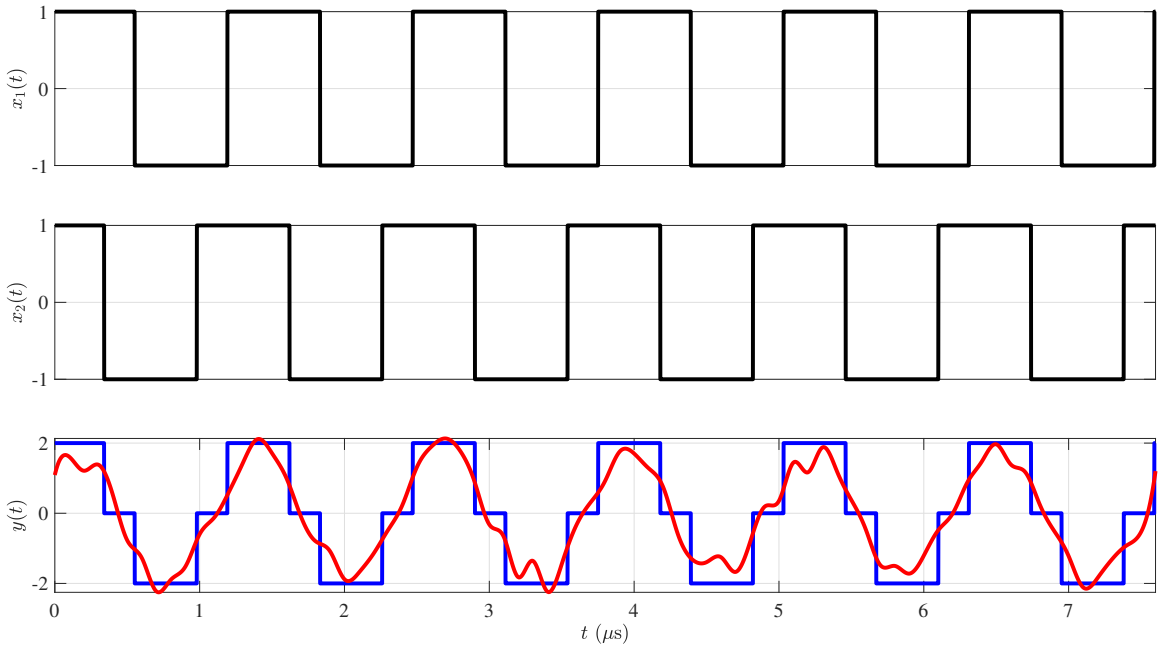

Figure 4.9: Time-Domain waveforms of C-SW-SO-OFDM. The binary-level signals of both LEDs are shown in the first two subplots, while their sum (blue) is compared to the experimental received signal (red) in the bottom subplot.

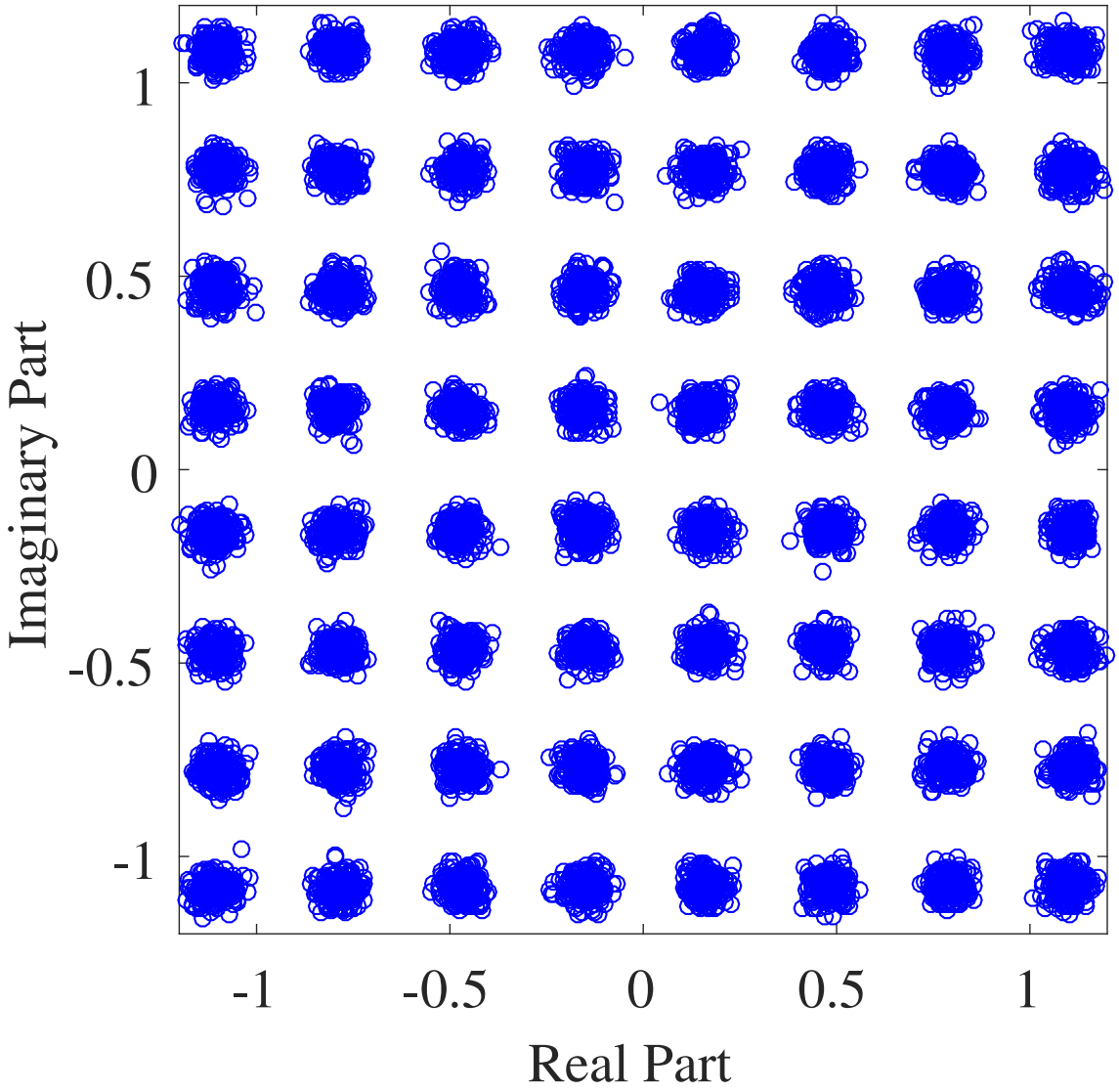

Figure 4.10: Experimental received 64-QAM constellation. A total of $13,617$ QAM symbols are shown. The high calculated SNR of 27.5 dB results in a zero symbol-error rate over this number of QAM symbols.

4.6 Conclusions

This chapter presents Square-Wave Spatial Optical OFDM (SW-SO-OFDM) which combines spatial summing with a simple transmitter architecture. The new technique combines the high spectral efficiency, robustness against multipath effects, and simple equalization of OFDM systems, with the low PAPR and immunity to nonlinear effects of SO-OFDM, while avoiding the complex transmitter architecture of SO-OFDM. This is achieved by modulating the LEDs with binary-level signals, thereby eliminating the need for DPDs and DACs. This also allows for the use of energy-efficient power drivers. In addition, coordinated SW-SO-OFDM (C-SW-SO-OFDM) was proposed to allow for multi-level QAM signaling.

A BER analysis of SW-SO-OFDM techniques, as well as BER simulations, shows their superior performance compared to SO-OFDM with one subcarrier per LED group when the full dynamic range of the LED is used. Moreover, the proposed techniques are more resilient to NLD given they have only two amplitude levels.

To validate our work, the multi-level technique was implemented experimentally by transmitting a 64-QAM signal by coordinating the transmission of 2 LEDs driven by binary-level signals, over a distance of 1 m and were able to successfully demodulate the signal at a receiver SNR of 27.5 dBs.

Future work includes extending the concept of SW-SO-OFDM to further increase the bandwidth efficiency by considering the modulation of multiple subcarriers per LED, and/or by modulating the odd-harmonic subcarriers and using successive interference cancellation techniques to eliminate the resulting inter-carrier interference. Also, the optimization of the subset of subcarriers of each LED to be modulated to minimize the PAPR should be considered.

4.A Appendix: Optimality of Square-Wave Signals

In the appendix, we prove the optimality of square-wave signals in the sense that they achieve the highest fundamental frequency component among all periodic signals restricted to a dynamic range between $-C$ and C. For simplicity, and without loss of generality, the proof is given in Theorem 1 for even functions, but the result is also valid when an arbitrary time shift is applied, since the magnitude of the fundamental frequency term of the Fourier Series expansion is not impacted by time shifting.

Theorem 1. *Let $p(t)$ be a zero-mean, even, and periodic carrier signal with fundamental period T, such that $-C \leq p(t) \leq C$. Then $p^*(t)$ that maximizes the fundamental coefficient of the Fourier Series expansion of $p(t)$, $a_1 = \frac{2}{T}\int_{-T/2}^{T/2} p(t)\cos(2\pi f_0 t)dt$, is a 50% duty-cycle square wave alternating between $-C$ and C, that is:*

$$p^*(t) = \begin{cases} C & |t| \leq T/4 \\ -C & |t| > T/4 \end{cases} \tag{4.A.1}$$

for $-T/2 \leq t < T/2$.

Proof. The optimization problem is formulated as follows:

$$\begin{aligned} \underset{p}{\text{maximize}} \quad & a_1 = \frac{2}{T}\int_{-T/2}^{T/2} p(t)\cos(2\pi f_0 t)dt \\ \text{subject to} \quad & -C \leq p(t) \leq C \end{aligned}$$

This problem can be written as a continuous-time nonlinear programming problem

of the form [132, 133, 134, 135, 136, 137]:

$$\begin{aligned} \underset{p}{\text{minimize}} \quad & \varphi(t) = \int_{-T/2}^{T/2} f(t, p(t))\, dt \\ \text{subject to} \quad & g_1(t, p(t)) \leq 0 \quad \text{a.e. in } [-T/2, T/2] \\ & g_2(t, p(t)) \leq 0 \quad \text{a.e. in } [-T/2, T/2] \\ & i \in I = \{1, 2, \ldots, m\} \end{aligned}$$

where for this problem $f(t, p(t)) = -p(t)\cos(2\pi f_0 t)$, $g_1(t, p(t)) = p(t) - C$, and $g_2(t, p(t)) = -p(t) - C$.

Since $f(t, p(t))$ and $g_i(t, p(t))$ are invex functions, then the Karush–Kuhn–Tucker (KKT) conditions are sufficient for a global minimum [132].

The KKT optimality conditions are listed:

$$-\cos(2\pi f_0 t) + v_1(t) - v_2(t) = 0 \tag{4.A.2}$$

$$v_1(t) \geq 0 \tag{4.A.3}$$

$$v_2(t) \geq 0 \tag{4.A.4}$$

$$v_1(t)\,(p(t) - C) = 0 \tag{4.A.5}$$

$$v_2(t)\,(-p(t) - C) = 0 \tag{4.A.6}$$

For $\cos(2\pi f_0 t) \neq 0$, we have from (4.A.2): $v_1(t)$ and $v_2(t)$ cannot both be zeros. From (4.A.5) and (4.A.6), $v_1(t)$ and $v_2(t)$ cannot both be nonzero, implying $p(t) = C$ and $p(t) = -C$, which cannot both be simultaneously true. Therefore, either $v_1(t) = 0$ and $v_2(t) \neq 0$ or $v_1(t) \neq 0$ and $v_2(t) = 0$ depending on the sign of $\cos(2\pi f_0 t)$. Therefore, for $\cos(2\pi f_0 t) > 0$, the upper bound constraint is active and $p(t) = C$, and for $\cos(2\pi f_0 t) < 0$, the lower bound constraint is active and $p(t) = -C$. This solution is the 50% duty-cycle square wave (4.A.1).

□

Chapter 5

Conclusions

5.1 Summary

This thesis presents a novel modulation approach, spatial optical OFDM (SO-OFDM), which for the first time, exploited the availability of multiple LEDs in typical indoor VLC systems and the spatial summing property of VLC channels to reduce PAPR and nonlinear clipping distortion, leading to BER performance improvement. Unlike previous work on PAPR reduction techniques where all LEDs are driven by the same signal, the work in this thesis divides the LEDs into groups where each group is driven by a different signal. The thesis also applies SO-OFDM to the practical scenario of PLC/VLC integration. It proposes a novel design for the all-analog amplify-and-forward (AF) PLC/VLC module, which down-converts the frequency of the incoming PLC signal in frequency to fit the limited bandwidth of LEDs. Furthermore, in a quest to further reduce the transmitter complexity, a novel signaling technique, square-wave SO-OFDM (SW-SO-OFDM), based on the SO-OFDM structure

but using square-wave carriers instead of sinusoidal carriers, is developed. Square-wave SO-OFDM transmitters do not require digital-to-analog converters (DACs), digital pre-distortion (DPD), or IFFT blocks. Not only does the use of square-wave carriers reduce the transmitter complexity, in this thesis, it is shown that square waves also have the largest useful signal power among all periodic signals confined within symmetric clipping levels. Moreover, an experimental validation for SW-SO-OFDM was conducted to demonstrate, for the first time, the use of the concept of spatial summing of signals from multiple LEDs for PAPR and transmitter complexity reduction while also preserving the conventional structure of the OFDM receiver. Finally, relative luminous efficacy was introduced in this thesis to quantify the impact of VLC-enabled LEDs on lighting efficiency and quality. In what follows, a detailed description of the work is presented.

In **Chapter 2**, motivated by the need for PAPR reduction techniques designed specifically for OFDM-based VLC systems, SO-OFDM was proposed. The basic idea of SO-OFDM is to divide OFDM subcarriers into filtered subsets and assign each subset of subcarriers to a different LED group. The spatial summing property of VLC channels means that the signals from all LED groups sum constructively at the receiver. The group filters were designed with two goals in mind:

1. To effectively reduce the PAPR. This was achieved designing the group filters to assign a smaller number of subcarriers to LED groups and/or scale subcarrier data symbols by a factor less than 1.

2. To obtain the original OFDM signal from the sum of all group signals. This allows for the use of conventional OFDM processing at the receiver.

In accordance with these goals, two general design variations for SO-OFDM were

proposed:

1. Spatial optical OFDM with subcarrier mapping maps each OFDM subcarrier to exactly one LED group. In this thesis, the focus is on contiguous subcarrier mapping, where a number of adjacent subcarriers are assigned to each LED group, i.e., the group filers are non-overlapping rectangular filters. The special case where only one subcarrier is modulated per LED group and the group signal is a sinusoidal signal can achieve a PAPR of 3 dB. However, it requires a large number of LED groups and transmit chains.

2. Overlapped spatial optical OFDM (OSO-OFDM) allows the assignment of subcarrier data to more than one LED group. In this thesis, a simple design for OSO-OFDM was adopted by constraining the frequency response of the group filters to Nyquist pulses. Since these pulses satisfy the Nyquist criterion, the sum of shifted replicas of the frequency responses is constant, and the sum of the group OSO-OFDM signals is identical to that of a DCO-OFDM transmitter. Two OSO-OFDM variations based on Nyquist filters were described: raised-cosine (RC) OSO-OFDM and double-jump (DJ) SO-OFDM.

In addition, the same grouping and filtering concept was applied to SC-FDMA to produce optical SC-FDMA (OSC-FDMA) using rectangular non-overlapping group filters and overlapped optical SC-FDMA (OOSC-FDMA) using either RC or DJ pulse filtering.

All of the aforementioned signaling design techniques based on the SO-OFDM structure were analyzed mathematically to give analytical expressions for the useful signal power and BER, and compared to DCO-OFDM and SC-FDMA in terms of

the CCDF of the PAPR, the BER, the useful signal power, the NLD noise, and the signal-to-distortion ratio (SDR) using Monte Carlo simulations.

Relative luminous efficacy was introduced in **Chapter 2** as a parameter to evaluate the impact of modulating the current of VLC-enabled LEDs on the lumen output of LEDs per Watt of of electrical power consumed. Using a statistical approach, the SO-OFDM signal was modeled as a Gaussian signal and the relative luminous efficacy was computed and plotted as a contour plot with the horizontal axis representing the signal standard deviation and the vertical axis representing the dynamic range of the LED.

In **Chapter 3**, an amplify-and-forward (AF) scheme was proposed for PLC/VLC integration using a simple all-analog AF module and SO-OFDM modulation for the VLC link was proposed. Unlike previous work on PLC/VLC integration, the design presented in **Chapter 3** achieves PAPR reduction using a simple analog signal processing architecture in which the PLC and VLC signals are not identical: the incoming PLC OFDM signal is filtered using analog group filters to produce the SO-OFDM group signals for VLC transmission. In addition, the AF module down-converts the spectrum of the PLC signal to produce a baseband signal that takes full advantage of the limited bandwidth of the LED leading to gains in the overall system capacity.

A detailed mathematical analysis of the integrated PLC/VLC system was conducted to derive an analytical expression for the overall system capacity. A numerical simulation of an integrated PLC/VLC system using RC OSO-OFDM was used to compare it to DCO-OFDM in terms of the CCDF of the PAPR and the overall system capacity.

The work in **Chapter 4** was motivated by the need to further reduce the complexity of SO-OFDM, as a large number of LED groups is required to effectively reduce the PAPR. Therefore, square-wave SO-OFDM (SW-SO-OFDM), introduced in **Chapter 4**, modulates only one subcarrier per LED group and uses square-wave carriers instead of sinusoidal carriers. This implies that a binary-level signal modulates each LED, and thus, no DAC, DPD, or IFFT block is required for each group. Square-wave SO-OFDM was extended to allow for the multi-level QAM constellations by coordinating the transmission of pairs of LEDs modulated by binary-level signals, thereby increasing the spectral efficiency. Coordinated SW-SO-OFDM (C-SW-SO-OFDM) was experimentally demonstrated by coordinating the binary-level signals of 2 LEDs to transmit 64-QAM data on the OFDM subcarrier frequency of 781.25 kHz over a distance of 1 m. Both uncoordinated SW-SO-OFDM and C-SW-SO-OFDM were analyzed mathematically to produce BER formulas and their BER performance was compared to that DCO-OFDM and SO-OFDM using Monte-Carlo simulations.

Relative luminous efficacy, introduced in **Chapter 2**, was revisited in **Chapter 4**, and computed using time-domain averages instead of statistical averages based on a Gaussian model, which is not accurate for a low number of modulated subcarriers.

5.2 Conclusions

The work in this thesis is centered around spatial optical OFDM, the novel signaling design method for indoor VLC systems, which is the unifying theme of the thesis. Throughout the development of this thesis, where several variations of SO-OFDM were introduced, and it was applied to PLC/VLC integration, several conclusions can be drawn. They are summarized in the following.

Luminous efficacy was identified as a lighting design parameter affected by using the LED for VLC. In particular, due to LED nonlinearity, the luminous efficacy decreases as either the standard deviation of the modulating signal or the set dynamic range of the LED increases. Contour plots of the relative luminous efficacy as a function of standard deviation and dynamic range for the popular Luxeon Rebel LED were computed and serve as a design tool for lighting and VLC system design. Given the operating dynamic range of the LED and a target relative luminous efficacy, the range of allowable values for the standard deviation of the modulating signal can be directly inferred from the contour plots.

The two main factors that determine the PAPR reduction capability of OFDM-based VLC modulation schemes are the spatial filter used and the number of independent data-carrying subcarriers per LED group, denoted by ϵ. While all proposed SO-OFDM techniques achieve a lower PAPR than conventional DCO-OFDM for the same ϵ, SO-OFDM with contiguous subcarrier mapping achieves more PAPR reduction than overlapped optical OFDM techniques. Single-carrier FDMA techniques also achieve a lower PAPR than techniques based on the simple OFDM structure using the same spatial filters. Decreasing ϵ can also achieve lower PAPR. However, for a fixed total number of subcarriers, decreasing ϵ requires more LED groups and therefore comes at the expense of an increased system cost and complexity. Setting $\epsilon = 1$ means that the SO-OFDM group signal degenerates to a sinusoidal signal with a low PAPR of 3 dB.

The lower PAPR of SO-OFDM variations compared to DCO-OFDM leads to lower NLD noise. This leads to a better BER performance for SO-OFDM variations than DCO-OFDM at high optical SNRs where NLD noise is the dominant source of noise.

However, the spatial filtering operation results in lower useful signal power for SO-OFDM variations, and hence higher BER at low optical SNRs, where receiver noise is dominant. However, since indoor VLC systems typically provide high SNRs (in excess of 60 dB), SO-OFDM variants are more advantageous in practice.

The result that the SO-OFDM variants offer better performance at high optical SNRs also extends to overall system capacity results in an integrated PLC/VLC system based on amplify-and-forward relaying. Combining SO-OFDM with analog frequency translation further improves the overall system capacity.

Square-wave SO-OFDM takes full advantage of the grouped SO-OFDM structure by setting $\epsilon = 1$, while also reducing the transmitter complexity and achieving an optical SNR gain of 2.10 dB over SO-OFDM with $\epsilon = 1$ using sinusoidal carriers having the same amplitude.

5.3 Future Work

This thesis proposed SO-OFDM as a new modulation technique and PAPR reduction method for indoor VLC systems. Several SO-OFDM variants were introduced and SO-OFDM was applied to PLC/VLC integration. Several future research directions and extensions can be motivated by the work in this thesis and the vision behind it and are suggested in the following.

5.3.1 SO-OFDM Optimization

Since using a larger number of LED groups for SO-OFDM provides better performance at high optical SNRs while using a smaller number of groups provides better

performance at low SNRs, this result calls for optimization of the number of LED groups or equivalently the parameter ϵ based on the knowledge of the optical SNR. The SNR measured by the receiver can be relayed back to the VLC transmitter using a low rate RF or infrared uplink. The optimization process can be extended to include spatial filter design (i.e., to optimize spatial filter coefficients for each subcarrier in each LED group) and can be executed in real-time to create an adaptive SO-OFDM modulation scheme capable of adjusting the spatial filter design to respond to SNR changes.

5.3.2 Lighting Design Constraints: Dimming Control

While the work in this thesis considered the effect of VLC modulation on the luminous efficacy of the LED, further research is in order to consider other lighting design requirements, such as dimming and flicker mitigation. For example, SO-OFDM could be applied, tested, and compared to DCO-OFDM under different dimming requirements, while operating within permissible flickering and luminous efficacy limits. More design flexibility can be provided by SO-OFDM than DCO-OFDM for dimming control since each LED group can be controlled independently for non-overlapped SO-OFDM.

5.3.3 Channel Modeling

The work in this thesis modeled the indoor VLC channel as a frequency-flat channel, considering only the line-of-sight (LoS) component of the transmitted optical

signal. This is a reasonable assumption for typical modulation bandwidths of off-the-shelf LED. However, for broadband transmission, non-line-of-sight (NLoS) components causing multipath effects should also be taken into account, and the VLC channel should be modeled as a frequency-selective channel. Future research on SO-OFDM signaling design could consider different frequency-selective indoor VLC channel models. For example, it is possible to use power and bit loading on subcarriers and control the optical power and signal standard deviation for each LED group. In a similar manner, channel modeling for the PLC subsystem in integrated PLC/VLC scenarios could be improved by modeling the PLC channel response as a linear and periodically time-varying (LPTV) filter with additive cyclostationary noise consisting of background noise, impulsive noise, and narrowband interference.

5.3.4 Receiver Design

The work in this thesis focuses on VLC transmitter design. A possible future research direction is to consider different receiver configurations and architectures. In particular, the use of imaging versus non-imaging receivers, spatial arrays of receivers, and spatial filtering receivers to reduce optical interference, should be considered. The system bandwidth can also be increased by using optical filters to recover the blue light component.

5.3.5 Experimental Testing

Finally, the work in this thesis provided an experimental demonstration as a proof-of-concept for C-SW-SO-OFDM in a lab setting using a simple LoS link where the optical signal is transmitted and received at a distance of 1 m. Possible future work

could test different variations of SO-OFDM in more practical indoor VLC scenarios with multiple luminaires fixed in the ceiling and a fixed desk-level receiver or a mobile hand-held receiver.

Bibliography

[1] J. Zhu, C. Gong, S. Zhang, M. Zhao, and W. Zhou, "Foundation study on wireless big data: Concept, mining, learning and practices," *China Communications*, vol. 15, no. 12, pp. 1–15, 2018.

[2] J. Lian, Z. Vatansever, M. Noshad, and M. Brandt-Pearce, "Indoor visible light communications, networking, and applications," *Journal of Physics: Photonics*, vol. 1, no. 1, p. 012001, jan 2019. [Online]. Available: https://doi.org/10.1088/2515-7647/aaf74a

[3] C. Branas, F. J. Azcondo, and J. M. Alonso, "Solid-state lighting: A system review," *IEEE Industrial Electronics Magazine*, vol. 7, no. 4, pp. 6–14, 2013.

[4] L. E. M. Matheus, A. B. Vieira, L. F. M. Vieira, M. A. M. Vieira, and O. Gnawali, "Visible light communication: Concepts, applications and challenges," *IEEE Communications Surveys & Tutorials*, vol. 21, no. 4, pp. 3204–3237, 2019.

[5] R. Ji, S. Wang, Q. Liu, and W. Lu, "High-speed visible light communications: Enabling technologies and state of the art," *Applied Sciences*, vol. 8, no. 4, 2018.

[6] H. Parikh, J. Chokshi, N. Gala, and T. Biradar, "Wirelessly transmitting a

grayscale image using visible light," in *Proceedings of the 2013 International Conference on Advances in Technology and Engineering (ICATE)*, 2013, pp. 1–6.

[7] H. Marshoud, P. C. Sofotasios, S. Muhaidat, and G. K. Karagiannidis, "Multi-user techniques in visible light communications: A survey," in *Proceedings of the 2016 International Conference on Advanced Communication Systems and Information Security (ACOSIS)*, 2016, pp. 1–6.

[8] H. Chun, A. G. Wang, C. Quintana, W. Zhang, G. Faulkner, and D. O'Brien, "A wide-area coverage 35 Gb/s visible light communications link for indoor wireless applications," *Scientific Reports*, vol. 9, no. 4592, 2019.

[9] S. U. Rehman, S. Ullah, P. H. J. Chong, S. Yongchareon, and D. Komosny, "Visible light communication: A system perspective—overview and challenges," *Sensors*, vol. 19, no. 5, 2019. [Online]. Available: https://www.mdpi.com/1424-8220/19/5/1153

[10] R. A. Pinto, M. R. Cosetin, M. Cervi, A. Campos, and R. N. do Prado, "Emergency lighting system integrated into a compact high-brightness LED lamp," in *Proceedings of the 2009 Brazilian Power Electronics Conference*, 2009, pp. 593–597.

[11] H. Abuella, M. Elamassie, M. Uysal, Z. Xu, E. Serpedin, K. A. Qaraqe, and S. Ekin, "Hybrid RF/VLC systems: A comprehensive survey on network topologies, performance analyses, applications, and future directions," 2020, arXiv preprint, https://arxiv.org/pdf/2007.02466.pdf.

[12] T. Komine and M. Nakagawa, "Fundamental analysis for visible-light communication system using LED lights," *IEEE Transactions on Consumer Electronics*, vol. 50, no. 1, pp. 100–107, Feb. 2004.

[13] "International electrotechnical commission." [Online]. Available: www.iec.ch

[14] S. Rajagopal, R. D. Roberts, and S. Lim, "IEEE 802.15.7 visible light communication: Modulation schemes and dimming support," *IEEE Communications Magazine*, vol. 50, no. 3, pp. 72–82, 2012.

[15] N. Marchetti, M. Rahman, S. Kumar, and R. Prasad, *OFDM: Principles and challenges*, 08 2009, pp. 29–62. [Online]. Available: https://doi.org/10.1007/978-1-4419-0673-1_

[16] "IEEE standard for local and metropolitan area networks–part 15.7: Short-range wireless optical communication using visible light," *IEEE Std 802.15.7-2011*, pp. 1–309, Sept 2011.

[17] F. M. Wu, C. T. Lin, C. C. Wei, C. W. Chen, Z. Y. Chen, H. T. Huang, and S. Chi, "Performance comparison of OFDM signal and CAP signal over high capacity RGB-LED-based WDM visible light communication," *IEEE Photonics Journal*, vol. 5, no. 4, 2013.

[18] N. Chi, *The Modulation Technologies of Visible Light Communication.* Berlin, Heidelberg: Springer Berlin Heidelberg, 2018, pp. 91–110. [Online]. Available: https://doi.org/10.1007/978-3-662-56660-2_5

[19] M. Afgani, H. Haas, H. Elgala, and D. Knipp, "Visible light communication using OFDM," in *Proceedings of the 2nd International Conference on Testbeds*

and Research Infrastructures for the Development of Networks and Communities (TRIDENTCOM), 2006, pp. 129–134.

[20] Z. Wang, T. Mao, and Q. Wang, "Optical OFDM for visible light communications," in *Proceedings of the 13th International Wireless Communications and Mobile Computing Conference (IWCMC)*, 2017, pp. 1190–1194.

[21] Q. Wang, Z. Wang, and L. Dai, "Asymmetrical hybrid optical OFDM for visible light communications with dimming control," *IEEE Photonics Technology Letters*, vol. 27, no. 9, pp. 974–977, 2015.

[22] Y. Hong, T. Wu, and L. Chen, "On the performance of adaptive MIMO-OFDM indoor visible light communications," *IEEE Photonics Technology Letters*, vol. 28, no. 8, pp. 907–910, 2016.

[23] D. Tsonev, H. Chun, S. Rajbhandari, J. J. D. McKendry, S. Videv, E. Gu, M. Haji, S. Watson, A. E. Kelly, G. Faulkner, M. D. Dawson, H. Haas, and D. O'Brien, "A 3-Gb/s single-LED OFDM-based wireless VLC link using a Gallium Nitride μLED," *IEEE Photonics Technology Letters*, vol. 26, no. 7, pp. 637–640, 2014.

[24] A. H. Azhar, T. Tran, and D. O'Brien, "A gigabit/s indoor wireless transmission using MIMO-OFDM visible-light communications," *IEEE Photonics Technology Letters*, vol. 25, no. 2, pp. 171–174, 2013.

[25] H. Haas, L. Yin, Y. Wang, and C. Chen, "What is LiFi?" *Journal of Lightwave Technology*, vol. 34, no. 6, pp. 1533–1544, 2016.

[26] Z. Zeng, M. Dehghani Soltani, Y. Wang, X. Wu, and H. Haas, "Realistic indoor hybrid WiFi and OFDMA-based LiFi networks," *IEEE Transactions on Communications*, vol. 68, no. 5, pp. 2978–2991, 2020.

[27] J. Armstrong and A. Lowery, "Power efficient optical OFDM," *Electronics Letters*, vol. 42, no. 6, pp. 370–372, 2006.

[28] S. Dimitrov, S. Sinanovic, and H. Haas, "Clipping noise in OFDM-based optical wireless communication systems," *IEEE Transactions on Communications*, vol. 60, no. 4, pp. 1072–1081, Apr. 2012.

[29] Seung Hee Han and Jae Hong Lee, "An overview of peak-to-average power ratio reduction techniques for multicarrier transmission," *IEEE Wireless Communications*, vol. 12, no. 2, pp. 56–65, 2005.

[30] Y. Wang and Z. Luo, "Optimized iterative clipping and filtering for PAPR reduction of OFDM signals," *IEEE Transactions on Communications*, vol. 59, no. 1, pp. 33–37, Jan. 2011.

[31] S. Müller and J. Huber, "OFDM with reduced peak-to-average power ratio by optimum combination of partial transmit sequences," *Electronics Letters*, vol. 33, pp. 368–369, February 1997. [Online]. Available: https://digital-library.theiet.org/content/journals/10.1049/el_19970266

[32] R. Bäuml, R. Fischer, and J. Huber, "Reducing the peak-to-average power ratio of multicarrier modulation by selected mapping," *Electronics Letters*, vol. 32, pp. 2056–2057, October 1996. [Online]. Available: https://digital-library.theiet.org/content/journals/10.1049/el_19961384

[33] A. Jayalath and C. Tellambura, "Reducing the peak-to-average power ratio of orthogonal frequency division multiplexing signal through bit or symbol interleaving," *Electronics Letters*, vol. 36, pp. 1161–1163, June 2000. [Online]. Available: https://digital-library.theiet.org/content/journals/10.1049/el_20000822

[34] S. Lu, D. Qu, and Y. He, "Sliding window tone reservation technique for the peak-to-average power ratio reduction of FBMC-OQAM signals," *IEEE Wireless Communications Letters*, vol. 1, no. 4, pp. 268–271, 2012.

[35] S. H. Han, J. M. Cioffi, and J. H. Lee, "Tone injection with hexagonal constellation for peak-to-average power ratio reduction in OFDM," *IEEE Communications Letters*, vol. 10, no. 9, pp. 646–648, 2006.

[36] B. S. Krongold and D. L. Jones, "PAR reduction in OFDM via active constellation extension," in *Proceedings of the 2003 IEEE International Conference on Acoustics, Speech, and Signal Processing (ICASSP '03)*, vol. 4, 2003, pp. 525–528.

[37] J. Sebastián, D. G. Lamar, D. G. Aller, J. Rodríguez, and P. F. Miaja, "On the role of power electronics in visible light communication," *IEEE Journal of Emerging and Selected Topics in Power Electronics*, vol. 6, no. 3, pp. 1210–1223, 2018.

[38] H. Qian, S. J. Yao, S. Z. Cai, and T. Zhou, "Adaptive postdistortion for nonlinear LEDs in visible light communications," *IEEE Photonics Journal*, vol. 6, no. 4, pp. 1–8, 2014.

[39] H. Elgala, R. Mesleh, and H. Haas, "A study of LED nonlinearity effects on optical wireless transmission using OFDM," in *Proceedings of the 2009 IFIP International Conference on Wireless and Optical Communications Networks*, 2009, pp. 1–5.

[40] Y. Yang, Z. Zeng, S. Feng, and C. Guo, "A simple OFDM scheme for VLC systems based on μ-law mapping," *IEEE Photonics Technology Letters*, vol. 28, no. 6, pp. 641–644, 2016.

[41] K. Bandara, P. Niroopan, and Y. Chung, "PAPR reduced OFDM visible light communication using exponential nonlinear companding," in *Proceedings of the 2013 IEEE International Conference on Microwaves, Communications, Antennas and Electronic Systems*, 2013, pp. 1–5.

[42] C. Wu, H. Zhang, and W. Xu, "On visible light communication using LED array with DFT-spread OFDM," in *Proceedings of the 2014 IEEE International Conference on Communications (ICC)*, 2014, pp. 3325–3330.

[43] J. G. Doblado, A. C. O. Oria, V. Baena-Lecuyer, P. Lopez, and D. Perez-Calderon, "Cubic metric reduction for DCO-OFDM visible light communication systems," *Journal of Lightwave Technology*, vol. 33, no. 10, pp. 1971–1978, 2015.

[44] W. O. Popoola, Z. Ghassemlooy, and B. G. Stewart, "Pilot-assisted PAPR reduction technique for optical OFDM communication systems," *Journal of Lightwave Technology*, vol. 32, no. 7, pp. 1374–1382, 2014.

[45] W. Hu and D. Lee, "PAPR reduction for visible light communication systems

without side information," *IEEE Photonics Journal*, vol. 9, no. 3, pp. 1–11, 2017.

[46] T. Jiang, M. Tang, R. Lin, Z. Feng, X. Chen, L. Deng, S. Fu, X. Li, W. Liu, and D. Liu, "Investigation of DC-biased optical OFDM with precoding matrix for visible light communications: Theory, simulations, and experiments," *IEEE Photonics Journal*, vol. 10, no. 5, pp. 1–16, 2018.

[47] K. Ying, Z. Yu, R. J. Baxley, and G. T. Zhou, "Constrained clipping for PAPR reduction in VLC systems with dimming control," in *Proceedings of the 2015 IEEE Global Conference on Signal and Information Processing*, 2015, pp. 1327–1331.

[48] A. A. Abdulkafi, M. Y. Alias, Y. S. Hussein, N. Omar, and M. K. B. Salleh, "PAPR reduction of DC biased optical OFDM using combined clipping and PTS techniques," in *Proceedings of the 2017 IEEE 13th Malaysia International Conference on Communications (MICC)*, 2017, pp. 207–212.

[49] N. Sharan, S. K. Ghorai, and A. Kumar, "Peak-to-average power ratio (PAPR) reduction using combination of precoding and companding techniques for VLC OFDM systems," in *Proceedings of the 2019 TEQIP III Sponsored International Conference on Microwave Integrated Circuits, Photonics and Wireless Networks (IMICPW)*, 2019, pp. 149–153.

[50] S. Galli, A. Scaglione, and Z. Wang, "For the grid and through the grid: The role of power line communications in the smart grid," *Proceedings of the IEEE*, vol. 99, no. 6, pp. 998–1027, 2011.

[51] "IEEE standard for broadband over power line networks: Medium access control and physical layer specifications," *IEEE Std 1901-2010*, pp. 1–1586, 2010.

[52] J. Song, W. Ding, F. Yang, H. Yang, B. Yu, and H. Zhang, "An indoor broadband broadcasting system based on PLC and VLC," *IEEE Transactions on Broadcasting*, vol. 61, no. 2, pp. 299–308, 2015.

[53] H. Ma, L. Lampe, and S. Hranilovic, "Integration of indoor visible light and power line communication systems," in *Proceedings of the 2013 IEEE 17th International Symposium on Power Line Communications and Its Applications*, 2013, pp. 291–296.

[54] X. Liu, X. Wei, L. Guo, Y. Liu, Q. Song, and A. Jamalipour, "Turning the signal interference into benefits: Towards indoor self-powered visible light communication for IoT devices in industrial radio-hostile environments," *IEEE Access*, vol. 7, pp. 24 978–24 989, 2019.

[55] A. Kumar, S. K. Ghorai, and A. Chaudhury, "BER performance of OFDM based hybrid PLC-VLC system," in *Proceedings of the 2020 International Conference on Computer, Electrical Communication Engineering (ICCECE)*, 2020, pp. 1–6.

[56] M. Jani, P. Garg, and A. Gupta, "Performance analysis of a mixed cooperative PLC–VLC system for indoor communication systems," *IEEE Systems Journal*, vol. 14, no. 1, pp. 469–476, 2020.

[57] Y. Yan, W. Ding, H. Yang, and J. Song, "The video transmission platform for the PLC and VLC integrated system," in *Proceedings of the 2015 IEEE*

International Symposium on Broadband Multimedia Systems and Broadcasting, 2015, pp. 1–5.

[58] S. M. Nlom, K. Ouahada, A. R. Ndjiongue, and H. C. Ferreira, "Evaluation of the SFSK-OOK integrated PLC-VLC system under the influence of sunlight," in *Proceedings of the 2017 International Symposium on Networks, Computers and Communications (ISNCC)*, 2017, pp. 1–5.

[59] J. Gao, F. Yang, and W. Ding, "Novel integrated power line and visible light communication system with bit division multiplexing," in *Proceedings of the 2015 International Wireless Communications and Mobile Computing Conference (IWCMC)*, 2015, pp. 680–684.

[60] Wei Yu, W. Rhee, S. Boyd, and J. M. Ciofli, "Iterative water-filling for Gaussian vector multiple access channels," in *Proceedings of the 2001 IEEE International Symposium on Information Theory*, 2001, p. 322.

[61] M. S. A. Mossaad, S. Hranilovic, and L. Lampe, "Visible light communications using OFDM and multiple LEDs," *IEEE Transactions on Communications*, vol. 63, no. 11, pp. 4304–4313, Nov 2015.

[62] "Lighting of indoor work places," *European Standard EN 12464-1*, 2003.

[63] J. Grubor, S. Randel, K.-D. Langer, and J. Walewski, "Broadband information broadcasting using LED-based interior lighting," *Journal of Lightwave Technology*, vol. 26, no. 24, pp. 3883–3892, Dec. 2008.

[64] P. H. Pathak, X. Feng, P. Hu, and P. Mohapatra, "Visible light communication,

networking, and sensing: A survey, potential and challenges," *IEEE Communications Surveys & Tutorials*, vol. 17, no. 4, pp. 2047–2077, 2015.

[65] M. S. A. Mossaad, S. Hranilovic, and L. Lampe, "Amplify-and-forward integration of power line and visible light communications," in *Proceedings of the 2015 IEEE Global Conference on Signal and Information Processing (GlobalSIP)*, 2015, pp. 1322–1326.

[66] M. Mossaad and S. Hranilovic, "Practical OFDM signalling for visible light communications using spatial summation," in *Proceedings of the 27th Biennial Symposium on Communications*, Jun. 2014, pp. 5–9.

[67] J. Armstrong, "OFDM for optical communications," *Journal of Lightwave Technology*, vol. 27, no. 3, pp. 189–204, Feb. 2009.

[68] H. Elgala, R. Mesleh, and H. Haas, "A study of LED nonlinearity effects on optical wireless transmission using OFDM," in *Proceedings of the 6th IEEE International Conference on Wireless Optical Communication Networks*, Apr. 2009, pp. 1–5.

[69] Z. Yu, R. Baxley, and G. Zhou, "Peak-to-average power ratio and illumination-to-communication efficiency considerations in visible light OFDM systems," in *IEEE International Conference on Acoustics, Speech and Signal Processing (ICASSP)*, May 2013, pp. 5397–5401.

[70] H. Elgala, R. Mesleh, and H. Haas, "Predistortion in optical wireless transmission using OFDM," in *Proceedings of the Ninth International Conference on Hybrid Intelligent Systems*, vol. 2, Aug. 2009, pp. 184–189.

[71] S. H. Han and J. H. Lee, "An overview of peak-to-average power ratio reduction techniques for multicarrier transmission," *IEEE Wireless Communications*, vol. 12, no. 2, pp. 56–65, Apr. 2005.

[72] S. Dimitrov, S. Sinanovic, and H. Haas, "Signal shaping and modulation for optical wireless communication," *Journal of Lightwave Technology*, vol. 30, no. 9, pp. 1319–1328, May 2012.

[73] H. Myung, J. Lim, and D. Goodman, "Single carrier FDMA for uplink wireless transmission," *IEEE Vehicular Technology Magazine*, vol. 1, no. 3, pp. 30–38, Sept. 2006.

[74] R. Lenk and C. Lenk, *Practical Lighting Design with LEDs*. Hoboken, New Jersey: John Wiley and Sons Inc., 2011.

[75] B. Serneels and M. Steyaert, *Design of High Voltage XDSL Line Drivers in Standard CMOS*. Springer Netherlands, 2008.

[76] N. Sokal, "Class E high-efficiency power amplifiers, from HF to microwave," in *IEEE MTT-S International Microwave Symposium Digest*, vol. 2, Jun. 1998, pp. 1109–1112 vol.2.

[77] T. Fath, C. Heller, and H. Haas, "Optical wireless transmitter employing discrete power level stepping," *Journal of Lightwave Technology*, vol. 31, no. 11, pp. 1734–1743, Jun. 2013.

[78] J. Armstrong, "Optical domain digital-to-analog converter for visible light communications using LED arrays," *Photonics Research*, vol. 1, no. 2, pp. 92–95, Aug. 2013.

[79] R. Mesleh, H. Elgala, and H. Haas, "LED nonlinearity mitigation techniques in optical wireless OFDM communication systems," *IEEE/OSA Journal of Optical Communications and Networking*, vol. 4, no. 11, pp. 865–875, Nov. 2012.

[80] W. Popoola, E. Poves, and H. Haas, "Spatial pulse position modulation for optical communications," *Journal of Lightwave Technology*, vol. 30, no. 18, pp. 2948–2954, Sept. 2012.

[81] X. Zhang, S. Dimitrov, S. Sinanovic, and H. Haas, "Optimal power allocation in spatial modulation OFDM for visible light communications," in *Proceedings of the IEEE Vehicular Technology Conference*, 2012, pp. 1–5.

[82] M. Noshad and M. Brandt-Pearce, "Can visible light communications provide Gb/s service?" *arXiv:1308.3217*, pp. 1–7, Aug. 2013.

[83] H. Dong, H. Zhang, K. Lang, B. Yu, and M. Yao, "OFDM visible light communication transmitter based on LED array," *Chinese Optics Letters*, vol. 12, no. 5, pp. 052 301–1–4, May 10, 2014.

[84] C. Wu, H. Zhang, and W. Xu, "On visible light communication using LED array with DFT-spread OFDM," in *IEEE International Conference on Communications*, Jun. 2014, pp. 3325–3330.

[85] J. Kahn and J. Barry, "Wireless infrared communications," *Proceedings of the IEEE*, vol. 85, no. 2, pp. 265–298, Feb. 1997.

[86] Philips Lumileds, "Power light source Luxeon Rebel," http://www.led-tech.de/produkt-pdf/luxeon/DS56_Rebel.pdf, Jul. 2007.

[87] P. Deng, M. Kavehrad, and M. A. Kashani, "Nonlinear modulation characteristics of white LEDs in visible light communications," in *Proceedings of the Optical Fiber Communication Conference*, 2015, p. W2A.64.

[88] D. Dardari, V. Tralli, and A. Vaccari, "A theoretical characterization of nonlinear distortion effects in OFDM systems," *IEEE Transactions on Communications*, vol. 48, no. 10, pp. 1755–1764, Oct. 2000.

[89] J. Bussgang, *Crosscorrelation Functions of Amplitude-distorted Gaussian Signals*, ser. Technical report. Research Laboratory of Electronics, Massachusetts Institute of Technology, 1952. [Online]. Available: http://books.google.ca/books?id=IWGLGwAACAAJ

[90] R. Mesleh, H. Elgala, and H. Haas, "On the performance of different OFDM based optical wireless communication systems," *IEEE/OSA Journal of Optical Communications and Networking*, vol. 3, no. 8, pp. 620–628, Aug. 2011.

[91] L. Franks, "Further results on Nyquist's problem in pulse transmission," *IEEE Transactions on Communication Technology*, vol. 16, no. 2, pp. 337–340, April 1968.

[92] M. Mohamed and S. Hranilovic, "Optical impulse modulation for indoor diffuse wireless communications," *IEEE Transactions on Communications*, vol. 57, no. 2, pp. 499–508, February 2009.

[93] "3GPP-The Mobile Broadband Standard," www.3gpp.org, [online]: 2014-11-06.

[94] C. Tellambura, "Computation of the continuous-time PAR of an OFDM signal

with BPSK subcarriers," *IEEE Communications Letters*, vol. 5, no. 5, pp. 185–187, May 2001.

[95] D. Jokanovic and M. Josipovic, "RF spectrum congestion: Resolving an interference case," in *Proceedings of the 2011 IEEE International Conference on Microwaves, Communications, Antennas and Electronics Systems (COMCAS)*, November 2011, pp. 1–4.

[96] N. Pavlidou, A. Vinck, J. Yazdani, and B. Honary, "Power line communications: state of the art and future trends," *IEEE Communications Magazine*, vol. 41, no. 4, pp. 34–40, April 2003.

[97] T. Komine and M. Nakagawa, "Integrated system of white LED visible-light communication and power-line communication," *IEEE Transactions on Consumer Electronics*, vol. 49, no. 1, pp. 71–79, February 2003.

[98] T. Komine, S. Haruyama, and M. Nakagawa, "Performance evaluation of narrowband OFDM on integrated system of power line communication and visible light wireless communication," in *Proceedings of the 2006 1st International Symposium on Wireless Pervasive Computing*, 2006, pp. 1–6.

[99] W. Ding, F. Yang, H. Yang, J. Wang, X. Wang, X. Zhang, and J. Song, "A hybrid power line and visible light communication system for indoor hospital applications," *Computers in Industry*, vol. 68, pp. 170 – 178, 2015. [Online]. Available: http://www.sciencedirect.com/science/article/pii/S0166361515000160

[100] H. Elgala, R. Mesleh, and H. Haas, "Indoor optical wireless communication:

potential and state-of-the-art," *IEEE Communications Magazine*, vol. 49, no. 9, pp. 56–62, September 2011.

[101] H. Ferreira, L. Lampe, J. Newbury, and T. Swart, *Power Line Communications: Theory and Applications for Narrowband and Broadband Communications over Power Lines, 1st ed.* New York, NY: John Wiley & Sons, 2010.

[102] "IEEE standard for broadband over power line networks: Medium access control and physical layer specifications," *IEEE Std 1901-2010*, pp. 1–1586, Dec 2010.

[103] I. T. U. (ITU), "ITU-T Recommendation G.9960, Unified high-speed wire-line based home networking transceivers - System architecture and physical layer specification," 2010. [Online]. Available: https://www.itu.int/rec/T-REC-G.9960

[104] ——, "ITU-T Recommendation G.9961, Data link layer (DLL) for unified high-speed wire-line based home networking transceivers," 2010. [Online]. Available: http://www.itu.int/rec/T-REC-G.9961

[105] J. Armstrong and B. Schmidt, "Comparison of asymmetrically clipped optical OFDM and DC-biased optical OFDM in AWGN," *IEEE Communications Letters*, vol. 12, no. 5, pp. 343–345, May 2008.

[106] H. Elgala, R. Mesleh, H. Haas, and B. Pricope, "OFDM visible light wireless communication based on white LEDs," in *Proceedings of the 65th IEEE Vehicular Technology Conference*, 2007, pp. 2185–2189.

[107] D. Weaver, "A third method of generation and detection of single-sideband signals," *Proceedings of the IRE*, vol. 44, no. 12, pp. 1703–1705, Dec 1956.

[108] F. Corripio, J. Arrabal, L. del Rio, and J. Munoz, "Analysis of the cyclic short-term variation of indoor power line channels," *IEEE Journal on Selected Areas in Communications*, vol. 24, no. 7, pp. 1327–1338, July 2006.

[109] "Website of the PLC group, ingeniería de comunicaciones department, universidad de málaga." http://www.plc.uma.es.

[110] L. Grobe, A. Paraskevopoulos, J. Hilt, D. Schulz, F. Lassak, F. Hartlieb, C. Kottke, V. Jungnickel, and K.-D. Langer, "High-speed visible light communication systems," *IEEE Communications Magazine*, vol. 51, no. 12, pp. 60–66, December 2013.

[111] I. Azevedo, M. Morgan, and F. Morgan, "The transition to solid-state lighting," *Proceedings of the IEEE*, vol. 97, no. 3, pp. 481–510, March 2009.

[112] T. Cevik and S. Yilmaz, "An overview of visible light communication systems," *ArXiv*, vol. abs/1512.03568, 2015.

[113] R. Mesleh, R. Mehmood, H. Elgala, and H. Haas, "Indoor MIMO optical wireless communication using spatial modulation," in *Proceedings of the 2010 IEEE International Conference on Communications*, 2010, pp. 1–5.

[114] Z. Yu, R. J. Baxley, and G. T. Zhou, "Distributions of upper PAPR and lower PAPR of OFDM signals in visible light communications," in *Proceedings of the 2014 IEEE International Conference on Acoustics, Speech and Signal Processing (ICASSP)*, 2014, pp. 355–359.

[115] J. Sheu, B. Li, and J. Lain, "LED non-linearity mitigation techniques for optical

OFDM-based visible light communications," *IET Optoelectronics*, vol. 11, no. 6, pp. 259–264, 2017.

[116] G. del Campo-Jimenez, F. J. Lopez-Hernandez, and R. Perez-Jimenez, "Modulation schemes effect on the driver efficiency and the global VLC transmitter energy consumption," in *Proceedings of the 2016 10th International Symposium on Communication Systems, Networks and Digital Signal Processing (CSNDSP)*, 2016, pp. 1–6.

[117] A. F. Hussein and H. Elgala, "Lightweight multi-carrier modulation for IoT," in *Broadband Access Communication Technologies XII*, B. B. Dingel, K. Tsukamoto, and S. Mikroulis, Eds., vol. 10559, International Society for Optics and Photonics. SPIE, 2018, pp. 183 – 192. [Online]. Available: https://doi.org/10.1117/12.2290602

[118] F. B. Ogunkoya, W. O. Popoola, and S. Sinanović, "Pilot-assisted PAPR reduction technique for O-OFDM using multiple LEDs in VLC systems," in *Proceedings of the 2016 IEEE International Conference on Communications Workshops (ICC)*, 2016, pp. 309–314.

[119] J. Du, W. Xu, H. Zhang, and C. Zhao, "Visible light communications using spatial summing PAM with LED array," in *Proceedings of the 2017 IEEE Wireless Communications and Networking Conference (WCNC)*, March 2017, pp. 1–6.

[120] M. Kong, Y. Chen, R. Sarwar, B. Sun, Z. Xu, J. Han, J. Chen, H. Qin, and J. Xu, "Underwater wireless optical communication using an arrayed transmitter/receiver and optical superimposition-based PAM-4 signal," *Optics*

Express, vol. 26, no. 3, pp. 3087–3097, February 2018. [Online]. Available: http://www.opticsexpress.org/abstract.cfm?URI=oe-26-3-3087

[121] Z. Ghassemlooy, F. Ebrahimi, S. Rajbhandari, S. Olyaee, X. Tang, and S. Zvanovec, "Visible light communications with hybrid OFDM-PTM," in *Proceedings of the 13th International Wireless Communications and Mobile Computing Conference (IWCMC)*, June 2017, pp. 894–898.

[122] L. Deniel, M. Gay, D. P. Galacho, C. Baudot, L. Bramerie, O. Ozolins, F. Boeuf, L. Vivien, C. Peucheret, and D. Marris-Morini, "DAC-less PAM-4 generation in the O-band using a silicon Mach-Zehnder modulator," *Optics Express*, vol. 27, pp. 9740–9748, 2019.

[123] Y. Yang, C. Chen, P. Du, X. Deng, J. Luo, W.-D. Zhong, and L. Chen, "Low complexity OFDM VLC system enabled by spatial summing modulation," *Optics Express*, vol. 27, no. 21, pp. 30 788–30 795, October 2019. [Online]. Available: http://www.opticsexpress.org/abstract.cfm?URI=oe-27-21-30788

[124] A. Narasimhamurthy, M. Banavar, and C. Tepedelenliouglu, *OFDM Systems for Wireless Communications*. Morgan & Claypool, 2010.

[125] "IEEE 802.11bb task group on light communications," https://www.ieee802.org/11/Reports/tgbb_update.htm, accessed: 2021-02-12.

[126] O. Kükrer, "Modulation techniques," in *Modern Electrical Drives*, H. B. Ertan, M. Y. Üçtug, R. Colyer, and A. Consoli, Eds. Springer Netherlands, 2000, ch. 13, pp. 289–309.

[127] H.-P. Chen, S.-H. Fang, S.-H. Feng, and C.-J. Shen, "Method and apparatus for providing a power factor correction (PFC) compatible solution for nonsinusoidal uninterruptible power supply (UPS)," November 2013.

[128] J. G. Proakis, *Digital Communications 5th Edition*. McGraw Hill, 2007.

[129] C. Yang, X. Li, W. Liu, S. You, M. Chen, Y. Wang, Z. Wang, S. Bian, H. Chen, J. Ding, H. Wu, Q. Yang, and C. Yu, "Successive interference cancellation in practical indoor interfered visible light communication," in *Advanced Photonics 2016 (IPR, NOMA, Sensors, Networks, SPPCom, SOF)*. Optical Society of America, 2016, p. SpTu2F.5. [Online]. Available: http://www.osapublishing.org/abstract.cfm?URI=SPPCom-2016-SpTu2F.5

[130] *MATLAB version 9.8.0.1323502 (R2020a)*, The Mathworks, Inc., Natick, Massachusetts, 2020.

[131] H. Ma, "Coordinated transmission for visible light communication systems," Ph.D. dissertation, University of British Columbia, 2017.

[132] S. Nobakhtian and M. R. Pouryayevali, "KKT optimality conditions and nonsmooth continuous time optimization problems," *Numerical Functional Analysis and Optimization*, vol. 32, no. 11, pp. 1175–1189, 2011. [Online]. Available: https://doi.org/10.1080/01630563.2011.592961

[133] M. A. Rojas-Medar, A. J. V. Brandão, and G. N. Silva, "Nonsmooth continuous-time optimization problems: Sufficient conditions," *Journal of Mathematical Analysis and Applications*, vol. 227, no. 2, pp. 305 – 318,

1998. [Online]. Available: http://www.sciencedirect.com/science/article/pii/S0022247X98960243

[134] A. J. V. Brando, M. A. Rojas-Medar, and G. N. Silva, "Nonsmooth continuous-time optimization problems: necessary conditions," *Computers Mathematics with Applications*, vol. 41, no. 12, pp. 1477 – 1486, 2001. [Online]. Available: http://www.sciencedirect.com/science/article/pii/S0898122101001122

[135] V. de Oliveira, M. Medar, and B. Adilson, "A note on KKT-invexity in nonsmooth continuous-time optimization," *Proyecciones (Antofagasta)*, vol. 26, 12 2007.

[136] G. J. Zalmai, "Optimality conditions and Lagrangian duality in continuous-time nonlinear programming," *Journal of Mathematical Analysis and Applications*, vol. 109, no. 2, pp. 426 – 452, 1985. [Online]. Available: http://www.sciencedirect.com/science/article/pii/0022247X8590160X

[137] ——, "The Fritz John and Kuhn-Tucker optimality conditions in continuous-time nonlinear programming," *Journal of Mathematical Analysis and Applications*, vol. 110, no. 2, pp. 503 – 518, 1985. [Online]. Available: http://www.sciencedirect.com/science/article/pii/0022247X85903129